

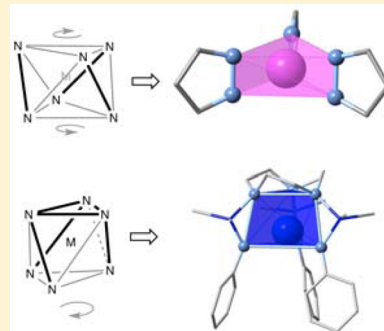
Distortion Pathways of Transition Metal Coordination Polyhedra Induced by Chelating Topology

Santiago Alvarez*

Departament de Química Inorgànica and Institut de Química Teòrica i Computacional, Universitat de Barcelona, Martí i Franquès 1-11, 08028 Barcelona, Spain

 Supporting Information

ABSTRACT: A continuous shape measures analysis of the coordination polyhedra of a host of transition metal complexes with bi- and multidentate ligands discloses the distortion pathway associated with each particular topology of the chelate rings formed. The basic parameter that controls the degree of distortion is the metal–donor atom bond distance that induces nonideal bond angles due to the rigidity of the ligands. Thus, the degree of distortion within each family of complexes depends on the atomic size, on which the high- or low-spin state has a large effect. Special attention is therefore paid to several spin-crossover systems and to the enhanced distortions that go along with the transition from low- to high-spin state affected by temperature, light, or pressure. Several families of complexes show deviations from the expected distortion pathways in the high-spin state that can be associated to the onset of intermolecular interactions such as secondary coordination of counterions or solvent molecules. Also, significant displacement of counterions in an extended solid may result from the changes in metal–ligand bond distances when ligands are involved in intermolecular hydrogen bonding.



CONTENTS

1. Introduction	13447	24. Conclusions	13473
2. Continuous Shape Measures: Concepts and Tools	13448	25. Methodological Aspects	13476
3. Monodentate Ligands: Isotropic Expansion of the Coordination Sphere	13449	Associated Content	13476
4. Trischelate Complexes: Bailar Twist, Flattening Distortion, and Anti-Bailar Twist	13450	Supporting Information	13476
5. Size of the Chelate Ring	13453	Author Information	13476
6. Bischelate Complexes	13454	Corresponding Author	13476
7. Monochelated Complexes	13456	Notes	13476
8. Extended Tripod Ligands	13456	Biography	13476
9. Macroyclic Pentadentate Ligands	13459	Acknowledgments	13477
10. Complexes with Two Macroyclic Tridentate Ligands	13460	References	13477
11. One Tridentate Macroyclic and Three Monodentate Ligands	13461		
12. <i>fac</i> -Coordinated Open-Chain Tridentate Ligands	13461		
13. Scorpionates and Related Claw-Type Ligands	13462		
14. Clamp (or Pincer) Ligands: Terpyridine and Bis(pyrazolyl)pyridine	13463	1. INTRODUCTION	
15. Sawhorse Hexadentate Ligands	13465	The aim of this review is to analyze how differences in metal–ligand bond distances in a coordination complex, combined with chelating ligands of varying topologies, induce angular distortion modes of the coordination sphere. A wide variety of bond distances for several families of ligands with all transition metals provides us with significantly large data sets and allows us to establish general trends. The basic observation ^{1,2} is that most bidentate ligands are relatively rigid, and their bite (the distance <i>d</i> between the two donor atoms, see 1) can be considered approximately constant throughout a wide sample of its compounds with different metal atoms, while its flexibility is indicated by the standard deviation of the bite for the sample. As an immediate consequence of a ligand’s rigidity, the bite angle of the chelate ring (α in 1) is sensitive to the metal–	
16. Equatorially Coordinated Open-Chain Tetradentate Ligands	13465		
17. Macroyclic Tetradeятate Ligands	13466		
18. Open-Chain Pentadentate Ligands	13467		
19. Macroyclic Hexadentate Ligands	13468		
20. Open-Chain Hexadentate Ligands	13468		
21. Paneling Ligands	13470		
22. Claw Ligands in Four-Coordinated Complexes	13470		
23. Bis(bidentate) Four-Coordinate Complexes	13472		

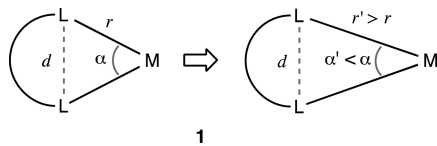
1. INTRODUCTION

The aim of this review is to analyze how differences in metal–ligand bond distances in a coordination complex, combined with chelating ligands of varying topologies, induce angular distortion modes of the coordination sphere. A wide variety of bond distances for several families of ligands with all transition metals provides us with significantly large data sets and allows us to establish general trends. The basic observation^{1,2} is that most bidentate ligands are relatively rigid, and their bite (the distance *d* between the two donor atoms, see 1) can be considered approximately constant throughout a wide sample of its compounds with different metal atoms, while its flexibility is indicated by the standard deviation of the bite for the sample. As an immediate consequence of a ligand’s rigidity, the bite angle of the chelate ring (α in 1) is sensitive to the metal–

Received: September 15, 2015

Published: November 17, 2015

ligand distance: the longer the bond distance, the smaller is the bite angle. Alternatively to the bite angle, one may use the normalized bite, $b = d/r$, with both parameters being related through a simple trigonometric expression.



Because a chelate ring occupies an edge of the coordination polyhedron, as the metal–ligand distances increase the edges occupied by chelate rings are roughly invariable, whereas the nonchelated edges are stretched. As a result, important distortions of the coordination polyhedron are to be expected upon changes in bond distances. In the case of multidentate ligands, their denticity and topology are therefore important in determining the distortion mode that accompanies bond distance changes.

What can affect metal–ligand bond lengths? To what extent may a bond lengthening induce relevant distortions of the coordination polyhedra? First of all, the nature of the metal and donor atoms determines those bond lengths, according to their covalent radii.³ The periodic trends of the covalent radii for the transition metal series are shown in Figure 1. The most

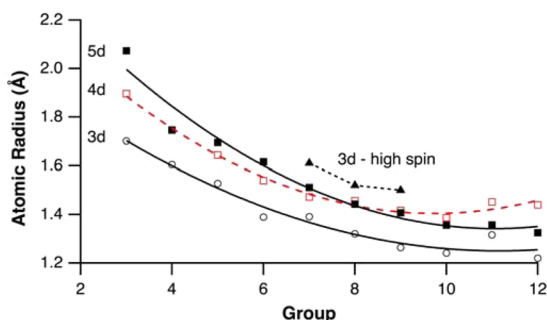


Figure 1. Periodic trends of the atomic radii of the transition metals. Adapted with permission from ref 3. Copyright 2008 The Royal Society of Chemistry.

important atom size changes are those that occur along a period, especially from group 3 to group 8, as can be seen by comparing, e.g., the radius of Ti (1.60 Å) with that for Zn (1.22 Å). Moderate variations in atomic size also occur when we descend down a group, from a 3d to the corresponding 4d metal, while the sizes of the 4d and 5d metals of the same group are very similar. Although the oxidation state and the coordination number of the metal atom are expected to affect the metal–ligand distances, the differences found for mean distances are in general within two standard deviations and are therefore not significant.

Another factor that results in important changes in metal–ligand distances is the spin state, with the metal ions in a high-spin state being significantly larger than those in the low-spin state (Figure 1). Notice that a 3d metal in a high-spin state is even larger than the 4d and 5d metals of the same group. Therefore, spin-crossover (SCO) compounds^{4–6} will provide us with optimal examples for analyzing the effect of bond distances on molecular stereochemistry, because the low- and high-spin states have exactly the same molecular composition and all geometry changes that accompany the SCO transition

must be attached to the variations of metal–ligand bond distances. Spin-crossover behavior has been observed for several transition metal ions,^{7–9} but by far the most common ones are those of Fe(II), Fe(III), and Co(II), to which this paper will pay special attention.

2. CONTINUOUS SHAPE MEASURES: CONCEPTS AND TOOLS

The stereochemistry of the coordination sphere will be characterized in this work by continuous shape measures and derived parameters.¹⁰ In essence, a continuous shape measure calibrates the deviation of a given structure from an ideal shape,^{11,12} such as the octahedron or the trigonal prism, to take the most common case. In essence, the octahedral shape measure of a coordination polyhedron, $S(\text{OC-}6)$, will be zero if it is perfectly octahedral and will adopt progressively higher positive values as the structure deviates from ideality. Similarly, a zero trigonal prismatic shape measure, $S(\text{TPR-}6)$, indicates a perfect trigonal prism with all edges of the same length.

Many of the structures to be studied present geometries intermediate between two idealized polyhedra such as the octahedron (OC) and the trigonal prism (TPR), and it will be useful to describe the stereochemistry of each molecule by its position relative to the minimal distortion interconversion path between those two ideal polyhedra, by means of two parameters. On one hand, the path-deviation function, $\Delta_{\text{OC},\text{TPR}}(Q)$, measures the distance of a structure Q to the minimal distortion pathway between OC and TPR (in percentage of the path length).¹³ On the other hand, for structures Q along the minimal distortion path, we can measure the percentage of conversion from one ideal polyhedron to the other one, by means of the generalized interconversion coordinate, $\varphi_{\text{OC}\rightarrow\text{TPR}}(Q)$.¹⁴ As defined, a generalized coordinate only applies to polyhedra Q that are on the minimal distortion (Bailar) path or, in an approximate way, to those that deviate slightly from it. It can adopt values from 0 for the perfect octahedron to 100% for the ideal trigonal prism. It can be shown that the usually employed twist angle θ and the generalized coordinate $\varphi_{\text{OC}\rightarrow\text{TPR}}$ are equivalent and linearly related (eq 1). Although the latter provides us with a comparable parameter for all conceivable distortion pathways, because this review will refer to distortion coordinates mostly for trigonal twist paths, the twist angle θ will be used in many instances assuming that the readers are more familiar with such a parameter than with generalized coordinates.

$$\theta = 60 - \frac{2}{3}\varphi_{\text{OC}\rightarrow\text{TPR}} \quad (1)$$

The relative path-deviation function used so far in our previous stereochemical studies is very useful when one analyzes different structures that may appear all along a given path, as for the Bailar, Berry, and planarization pathways that relate the octahedron with the trigonal prism, the square pyramid with the trigonal bipyramidal, and the tetrahedron with the square, respectively. However, when we wish to compare different distortion modes of the same ideal polyhedron, which may have very different path lengths, comparison of the values of the path-deviation functions for two paths may not give us correct information on which of the two paths best describes the distortion of our problem structure from an ideal shape T that represents, e.g., a highly distorted octahedron. This is especially true when one of the paths has an extreme shape T that is physically unachievable, and for which we may find

molecular structures that cover at most the initial 30 or 40% of the path. This issue is discussed in more detail in the *Methodological Aspects* section, but it is important to state here that throughout this work the choice of the best distortion path to describe a family of structures is based on the comparison of both absolute and relative path deviations for alternative pathways.

In specific cases in which ligands coordinated to a metal atom present quite different metal–ligand bond distances, we may disregard the deviations from ideal geometries due to differences in bond distances by using normalized coordination polyhedra that calibrate only the angular distortions, as discussed elsewhere.¹⁵ Such an approach will be explicitly stated by making reference to the use of normalized coordination polyhedra instead of the experimental X-ray coordination polyhedra. All shape parameters have been calculated with the *SHAPE* 2.1 program.¹⁶

3. MONODENTATE LIGANDS: ISOTROPIC EXPANSION OF THE COORDINATION SPHERE

The metal–ligand bond distances in metal complexes can increase or decrease according to (a) the size of the donor atoms, (b) the position of the metal atom in the periodic table, (c) the metal oxidation state, (d) the spin state of the metal, and (e) the metal–ligand bond order. In the absence of geometrical constraints imposed by bi- or multidentate ligands, complexes with only monodentate ligands react to, e.g., the occupation of the antibonding e_g orbitals in the high-spin state of an octahedral ML_6 complex by elongating all metal–ligand bond distances without angular distortions. In other words, the result of bond elongation induced by spin crossover is just an isotropic expansion of the coordination sphere upon low- to high-spin crossover, although some Jahn–Teller induced anisotropy may appear for specific electron configurations.

In a broad perspective, this behavior can be illustrated by comparing the structures of six-coordinate complexes or all transition metals with monodentate ligands only (normalized coordination polyhedra, 16 597 crystallographically independent molecules) with those bearing two or more chelate rings (normalized polyhedra, 80 392 structural data). In the histograms shown in Figure 2, we can see that an overwhelming majority of the metals coordinated by only monodentate ligands concentrate very close to the octahedral end of the Bailar path, as shown by the distribution of the path-deviation function, whereas the presence of chelate rings produces much larger deviations from the octahedron and from the Bailar pathway. The subset of iron(II) complexes with monodentate ligands follows the same trend, with deviations from the Bailar path of <15.8% (average 4.2%), and similar values are found for Fe(III), with both ions susceptible of being in low- or high-spin alternative states.

Let us take a closer look and focus on the specific example of the $\text{Fe}^{\text{II}}(\text{tetrazole})_6$ units in a polymeric spin-crossover compound.¹⁷ Even if it experiences incomplete spin crossover, the changes in the Fe–N bond distances with temperature (2.01 to 2.20 Å from 90 to 330 K) are large enough as to make any associated distortion of the coordination sphere evident, yet the FeN_6 core is perfectly octahedral at all temperatures (octahedral shape measures of at most 0.06). A similar situation is found for Fe^{II} complexes with monodentate ligands, such as the diazenebisnitrile coordination polymers,¹⁸ a tetrazole coordination polymer,¹⁹ or homoleptic complexes with diversely substituted tetrazoles.^{20–27} A nice example is also

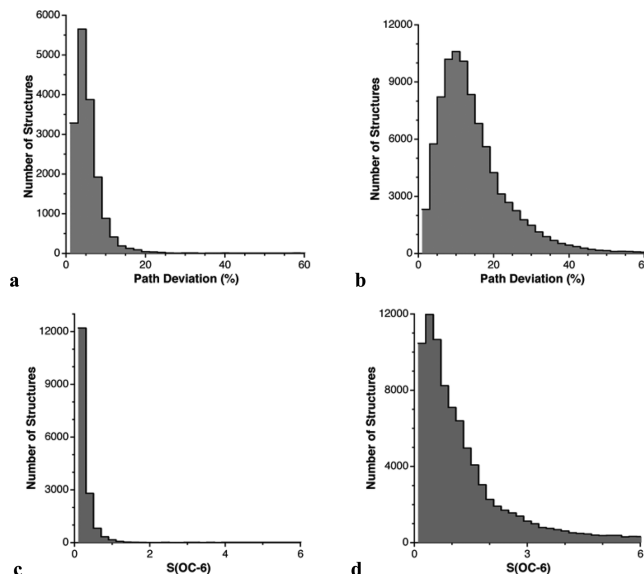
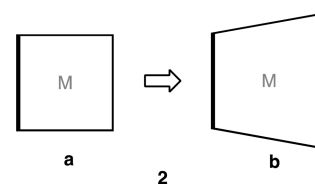


Figure 2. Distribution of the deviation from the Bailar path for six-coordinate transition metal complexes with only monodentate ligands (a) and with two or more chelate rings (b), and the corresponding distribution of octahedral shape measures (c and d).

found in the high- and low-spin cationic complexes present in the structure of $[\text{Fe(isoxazole)}_6](\text{BF}_4)_2$ at 130 K, with both equally octahedral (octahedral shape measures of 0.02 and 0.03, respectively) only with quite different sizes: average Fe–N distances of 1.98 and 2.17 Å for the low- and high-spin molecules, respectively.²⁸

Bi- or multidentate ligands forming chelate rings occupy the edges of the coordination polyhedron or polygon, with an approximately constant length, given the rigidity of most chelating ligands.^{1,2} Therefore, only the unconstrained edges can lengthen to allow for an expansion of the coordination sphere as we move to longer metal–donor distances, and specific distortions from the ideal coordination polyhedron result for each topological distribution of chelate rings. To facilitate the visualization of the distortions of the coordination polyhedron that go along with the elongation of metal–ligand bonds in the presence of chelate rings, from here on I will represent the edges spanned by chelate rings by bold lines. As a simple example, consider an octahedral complex with one bidentate ligand represented schematically in 2a, where two axial ligands are omitted for clarity. If the metal–ligand distances increase, only the non chelated edges can expand and the arrangement of the equatorial ligands distorts from a regular square to a trapezoid 2b. A real example of such a distortion will be disclosed below, in the *Monochelated Complexes* section.



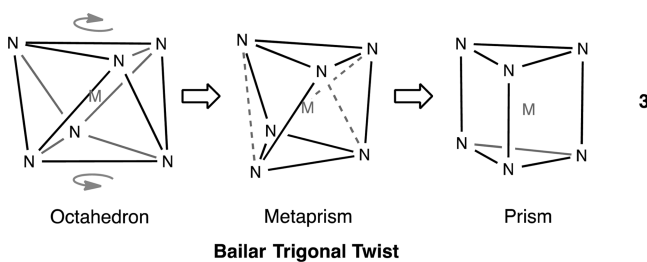
A basic assumption can be made here, that three factors concur to determine the stereochemistry of a transition metal complex: (i) the electronic preference for a given coordination polyhedron (e.g., the octahedron for d^6 but the trigonal prism for d^0 complexes, or the tetrahedron for a d^{10} but the square

planar for a d^8 complex); (ii) a tendency to form metal–ligand bonds in all directions of space, to maximize the use of its valence atomic orbitals (here the exceptions correspond to metals with stereochemically active lone pairs, including the z^2 electron pair in d^8 square planar compounds); (iii) the geometrical and steric constraints imposed by the ligands.

Upon elongation of the bond distances between a metal and the donor atoms in a spherical polyhedron such as the octahedron, all the edges also should be elongated to retain the spherical shape. However, in the presence of rigid chelating ligands, some edges are constrained to remain frozen as the M–L bond distances increase, and sphericity may be lost as the bite angle α decreases (**1**). A possible way of retaining a ligand distribution as spherical as possible consists of forming an alternative polyhedron with smaller ideal bond angles. In the case of the octahedron, an alternative polyhedron is the trigonal prism, whose ideal bond angles are 81.8° along the edges or 135.6° in a diagonal across a square face. Intermediate metaprisms, generated by a trigonal twist of the octahedron, can adapt to intermediate angles.

4. TRISCHELATE COMPLEXES: BAILAR TWIST, FLATTENING DISTORTION, AND ANTI-BAILAR TWIST

Before discussing the structural features of the compounds in the trischelate families, let us make a brief reminder of the Bailar trigonal twist (**3**) and establish the way in which we will refer to structures that fall along that path. A rotation of two opposing triangular faces of the octahedron (O_h symmetry) can transform it into a trigonal prism (D_{3h} symmetry), passing through intermediate geometries (D_3 symmetry) called metaprisms. The Bailar path is the trigonal twist that takes the octahedron to a trigonal prism with square faces,²⁹ our ideal trigonal prism, and it has been shown to be a minimal distortion pathway.¹³ We thus call Bailar twist the one in which the full D_3 symmetry is retained throughout the path, while the lengths of the edges within the two triangular faces and those that link them remain identical.



The polyhedral edges thus represent distances between neighboring donor atoms, and those that are forming a chelate ring will be highlighted as bold lines. As longer M–L bond distances make those edges shorter than the unchelated ones, it is easy to visualize with a schematic representation (Figure 3) the distortions from the octahedron by freezing the length of the bold edges and lengthening the regular ones. This visual approach suggests that for the case of trischelate complexes a flattening Bailar twist may result, which would ultimately yield a compressed trigonal prism rather than the regular prism achieved through the canonical Bailar twist **3**.

For relatively rigid bidentate ligands, the formation of a chelate ring often results in a small bite angle, and practically all N- and O- donor bidentate ligands that form five-member

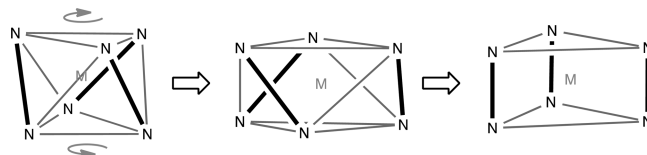
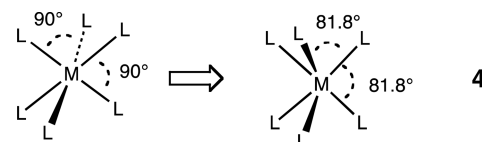


Figure 3. Schematic depiction of the flattening twist of the coordination octahedron of a trischelate complex as the bite angle decreases, which would ultimately lead to a compressed trigonal prism. The bold lines represent the edges occupied by the bidentate ligands.

chelate rings or smaller have bite angles of $<90^\circ$.¹ The decreased bond angle is followed by the rest of the coordination sphere by means of a twist toward the trigonal prism that requires smaller bond angles than the octahedron (**4**), as confirmed by means of shape analyses of trischelate complexes.^{11,30} In the case of spin-crossover complexes, the transition from low- to high-spin configuration implies a metal–ligand bond lengthening that imposes a decrease in the bite angle, which is in turn responsible for a significant Bailar twist in the high-spin state.³¹



The general geometric behavior of trichelate complexes was analyzed earlier by Kepert³⁰ and later expanded by us.¹¹ An updated version of such an analysis with the much larger number of structural data points currently available is shown in Figure 4. Each family of ligands seems to follow a specific path

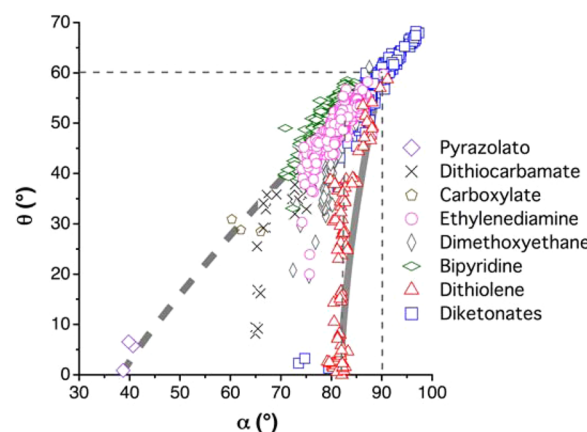
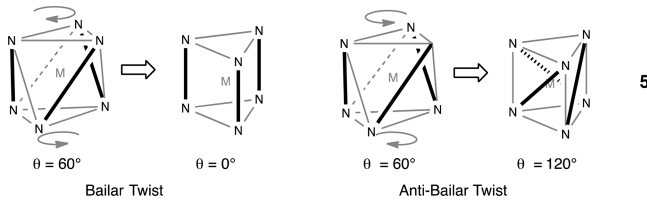


Figure 4. Trigonal twist angle θ in tris(chelate) transition metal complexes as a function of the bite angle of the bidentate ligands. The thick solid and dashed lines represent the Bailar and flattened twist pathways, respectively.

that reaches the eclipsed conformation of the two trigonal faces ($\theta = 0^\circ$) at different values of the bite angle α . Thus, the large bite dithiolenes ($\alpha_s = 91^\circ$) follow nicely the Bailar path that ends in the regular trigonal prism ($\theta = 0^\circ$, $\alpha = 82^\circ$). In contrast, the very small bite pyrazolato ligand ($\alpha_s = 40^\circ$) forms trigonal prisms with such small bond angles. An anti-Bailar torsion toward a trigonal prism with the bidentate ligands occupying diagonals of the square faces (**5**, $\theta = 120^\circ$) is favored by ligands with larger bites, exemplified by β -diketonate ($\alpha_s = 90^\circ$) and propanediamine (91°) complexes (the latter are not shown in

Figure 4 for clarity). For all families, the first portion of the path ($\theta \approx 60^\circ$) is covered by complexes with an electronic preference for the octahedron, with a twist induced by long metal–ligand distances and the corresponding small bite angles, whereas the final section of the path ($\theta \approx 0^\circ$) is occupied by complexes with an electronic preference for a trigonal prism.



It must be noted that the complexes that appear most twisted toward trigonal prisms are those of metal ions with d^0 , d^1 , d^2 , d^5 , or d^{10} electron configurations, which are known to have an electronic preference for the trigonal prismatic geometry.³² Thus, the most twisted coordination polyhedron with ligands containing the dimethoxyethane skeleton belongs to a Zn(II) malato complex that has $\theta < 30^\circ$,³³ while with ethylenediamine two Cd(II) complexes are nearly trigonal prismatic.^{34,35} Cd(II) is also present in the most trigonal prismatic dithiocarbamate complexes,^{36–38} a trigonal prismatic complex with nitrate ligands has Ag(I) as its central ion,³⁹ and Fe(III)⁴⁰ and Sc(III)⁴¹ are present in trigonal prismatic pyrazolato complexes. Even complexes with a large bite angle ligand such as the diketonates can appear in a trigonal prismatic geometry with the appropriate electron configuration, as in Cd(II)⁴² and Y(III)⁴³ compounds. In summary, the coordination sphere of tris(chelate) complexes departs from the octahedral geometry through a trigonal twist, whose extent depends on geometrical (the bite angle) and electronic (electron configuration) factors.

The representation of the structural data for trischelate complexes by their twist and bite angles θ and α offers us a simple and efficient description of their stereochemistries. However, to compare on the same footing those distortions with the ones that appear in compounds with varying numbers of chelate rings in a host of topologies, it is more appropriate to use shape maps that offer us a common language and methodology for all possible distortions. We may therefore start by translating the data just discussed to the context of those shape maps. Let us take as an example the $[M(\text{bipy})_3]$

complexes and analyze their shape measures relative to the octahedron and the trigonal prism. We observe (Figure 5a) that the Bailar twist does not fully explain the distortion of the coordination octahedron, because most of the structures deviate significantly from that path. Considering the expected changes in the relative edge lengths that go along with a trigonal twist in a trischelate complex (Figure 3), we can define an alternative distortion pathway, a trigonal twist that takes the octahedron to a flattened trigonal prism (fTPR-6). After an analysis of the experimental structures of all trischelate complexes and all trigonal prismatic complexes, it was found reasonable to define as a reference flattened trigonal prism the one shown in Figure 6, characterized by having an edge length

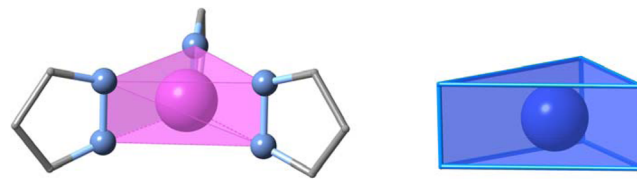


Figure 6. Most flattened trigonal prismatic structure found in a trispypyridyl scandium(III) complex⁴⁰ and ideal reference flattened trigonal prism with an edge length ratio of 2.50.

ratio of 2.50, as in the most flattened trigonal prismatic structure found, that of a Sc(III) pyrazolato complex.⁴⁰ The bipyridine complexes are seen to be closely aligned along the newly defined path (Figure 5b). The most twisted structure (i.e., the one with the lowest S(fTPR-6) value) belongs to the unusual Zr(IV) complex $[\text{Zr}(\text{bipy})_3]^{2-}$, in which the bipyridine ligands are dianionic and nonaromatic,⁴⁴ and whose formal d^0 electron configuration should favor a nearly trigonal prismatic coordination geometry.³²

In Figure 4 it can be seen that most trischelate complexes are within the regions defined by the Bailar and flattening trigonal twists. It is no surprise therefore that the stereochemistries of a number of families of trischelate complexes can be well described by either the Bailar or the flattening twist distortion. Many such structures are plotted in the corresponding shape maps in Figure 7, where the complexes of ligands with large average bite angles¹ are compared to the canonical Bailar path (Figure 7a) and those with small bite angles are plotted

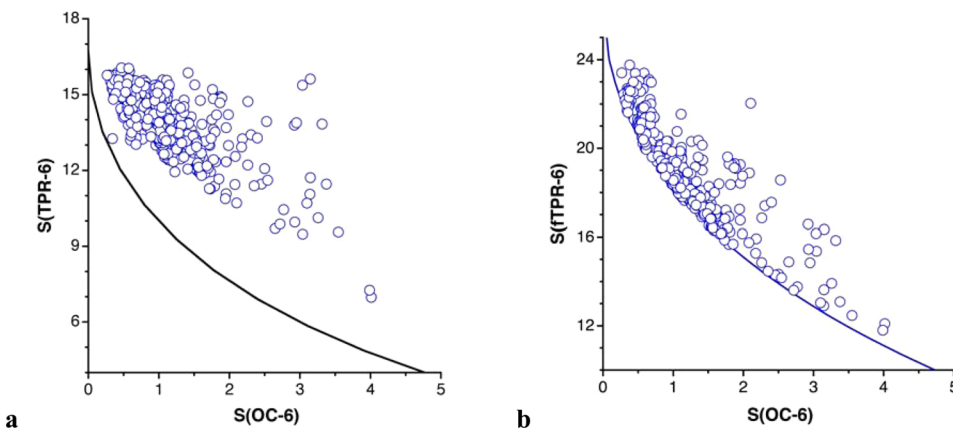


Figure 5. Shape maps for tris(bipyridine) complexes of groups 3–10 transition metals in the octahedron–trigonal prism (a) and octahedron–flattened trigonal prism (b) spaces. The continuous lines represent the minimal distortion paths, and the circles represent the experimental structures.

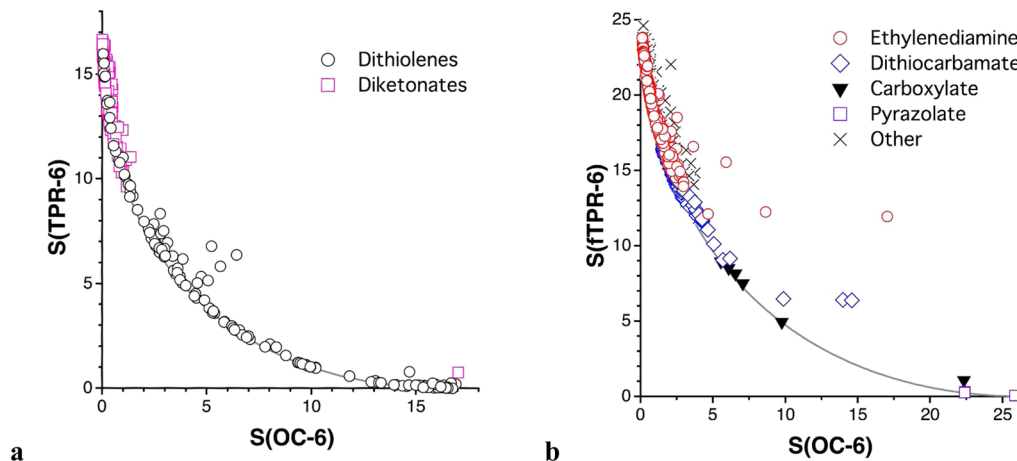


Figure 7. (a) Shape measures of trischelate complexes with large bite angles (dithiolenes and diketonates) relative to the Bailar path and (b) for trischelate complexes with small bite bidentate ligands (crosses for bipyridine, dimethoxyethane, oxalate, nitrate, and dithiophosphinate; other symbols as indicated in the inset), relative to the flattening trigonal twist.

alongside the flattening Bailar path (Figure 7b), taking into account the average absolute path deviations for each ligand family (Table 1). In agreement with Figure 4, those ligands

Table 1. Mean Absolute Deviations from the Bailar and Flattened Trigonal Twist Pathways for Trischelate Complexes with Different Families of Ligands and Their Average Bite Angles α

	α	Bailar	flattening
pyrazolate	40 (1)	30 (2)	0.06 (4)
nitrate	54 (5)	23 (8)	8 (5)
carboxylate	57 (4)	15.6 (3)	2 (3)
Dtc	74 (3)	4 (1)	0.4 (8)
bipyridine	78 (3)	4 (1)	0.9 (1)
Dme	80 (2) ^a	1.2 (8)	1.3 (6)
dtp	82 (1)	1.1 (8)	0.4 (4)
oxalate	83 (2)	6 (3)	0.7 (6)
en	83 (3)	2 (1)	0.4 (9)
diketonate	90 (4)	0.8 (8)	1 (1)
pn	91 (4)	0.7 (3)	0.7 (3)
dithiolene	91 (2)	0.6 (7)	8 (5)

^aAverage bite angle from this work, other bite angles from ref 1.

with average bite angles of 83° or less are best adapted to the flattening trigonal twist, whereas those with bite angles of 90° or larger follow more closely the Bailar twist. Regarding the mean absolute path-deviation values given in Table 1, it must be noticed that some families of complexes seem to present similar deviations from both extreme pathways, but this is mainly due to the absence of highly twisted compounds among them, because the two paths are pretty close to each other at the octahedral extreme and diverge as we approach the trigonal (or flattened trigonal) prism.

In spite of the good general agreement of the structural data of most trischelate complexes with either the Bailar or the flattening twist distortion paths, there are some outliers that deserve a closer look. The deviation from the established paths of such complexes with dithiolene,^{45–47} ethylenediamine,^{48,49} or dithiocarbamate^{36,37} ligands can be attributed to distortions of their coordination spheres along a Rây–Dutt path (Figure 8). The Rây–Dutt twist is a mechanism proposed⁵⁰ for the racemization of octahedral trischelate complexes through a

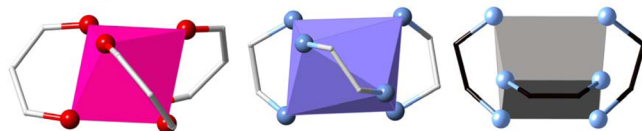


Figure 8. Three structures that correspond to the Rây–Dutt pathway from the octahedron⁵² to the trigonal prism,⁴⁹ passing through an intermediate twisted geometry.⁴⁸

trigonal prismatic intermediate of structure **6**, and indeed Rây–Dutt structures **6** have been identified as transition states in computational studies.⁵¹ However, there is a scarcity of information on the existence of such coordination geometries in the crystal state, and they have not been identified computationally as ground states. Structurally, geometries along the Rây–Dutt distortion of the octahedron to a trigonal prism with the chelate rings arranged as in **6** can be described by a variation of the angles between the three chelated edges, τ_1 , τ_2 , and τ_3 from $(60^\circ, 60^\circ, 60^\circ)$ in the ideal octahedron to $(0^\circ, 90^\circ, 90^\circ)$ in the Rây–Dutt trigonal prism through intermediates characterized by angles $(\tau_1 < 60^\circ, \tau_2, \tau_3 > 60^\circ)$. In contrast, in both the Bailar and flattening trigonal twists, those angles vary simultaneously all the way to trigonal prisms $(0^\circ, 0^\circ, 0^\circ)$ via structures with angles $(60^\circ > \tau_1, \tau_2, \tau_3 > 0^\circ)$. A few complexes that illustrate these two different ways to go from an octahedron to a trigonal prism are listed in Table 2. An outstanding example of a complex with a Rây–Dutt trigonal prismatic structure is that of the $[\text{Hg}(\text{en})_3]^{2+}$ cation,⁴⁹ as noted earlier by Cremades et al.³² The structures that deviate from trigonal twist paths, however, seem to correspond to a path for the interconversion between trigonal and Rây–Dutt prisms, characterized by angles $(\tau_1 = 60^\circ, \tau_2, \tau_3 < 90^\circ)$.

If we focus now on the family of Fe(II) tris(chelate) complexes with the bidentate pycolylamine ligand **7a**, which can switch from high^{63–71} to low spin^{63–68} at low temperatures, we can see in Figure 9a how the shape map neatly discriminates the two spin states, with the high-spin structures appearing more distorted toward the flattened trigonal prism. It is interesting to compare the stereochemical behavior of the topologically related complex with the 2,2'-pyridylquinoline ligand (**7b**).⁷² This molecule is prevented to adopt the flattened Bailar geometry because of the presence of a benzo ring fused

Table 2. Examples of Trischelate Complexes That Represent Snapshots along the Trigonal ($\tau_1 = \tau_2 = \tau_3$) and Rây–Dutt ($\tau_1 < \tau_2 = \tau_3$) Twists

refcode	M	ligand	τ_1	τ_2	τ_3	ref
trigonal twist paths						
fecwal02-Cr1	Cr(III)	diketonate	60	60	60	52
birsu0	Co(III)	ethylenediamine	59	59	59	53
laqqup	Ru(III)	dithiolene	51	51	51	54
cexxim	Fe(III)	dithiocarbamate	43	43	43	55
vibjas	Ti(IV)	dithiolene	38	38	38	56
dognet	Mo(IV)	dithiolene	23	23	23	57
quqba0	W(IV)	dithiolene	16	16	17	58
bzdtbn10	Nb(V)	dithiolene	2	2	3	59
huksah	W(VI)	dithiolene	0	0	0	60
Rây–Dutt path						
fecwal02-Cr1	Cr(III)	diketonate	60	60	60	52
kaxtin	Cd(II)	ethylenediamine	40	67	68	49
tawduq	Ru(IV)	ethylenediamine	39	60	60	61
hamkem	Cd(II)	ethylenediamine	25	64	64	48
kiylua	Cd(II)	ethylenediamine	19	69	70	62
kaxtot	Hg(II)	ethylenediamine	9	86	86	49
prism-to-prism twist path						
dassul	Cd(II)	dithiocarbamate	6	13	17	36
juscef	Cd(II)	dithiocarbamate	8	14	19	37
pabzta	Ta(V)	dithiolate	18	42	42	45
kaxmurr	Nb(V)	dithiolate	15	44	44	46
selkoj	Ti(IV)	dithiolate	19	51	51	47
kaxtot	Hg(II)	ethylenediamine	9	86	86	49

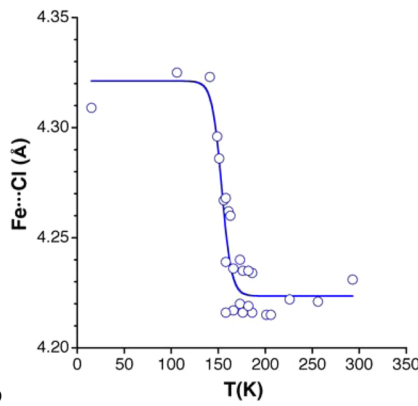
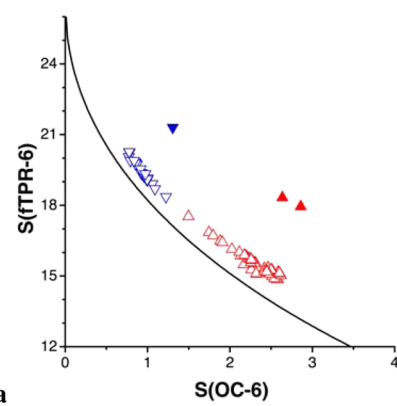
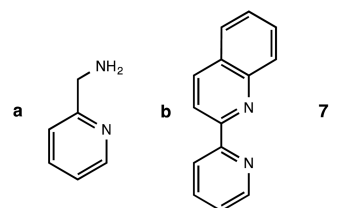
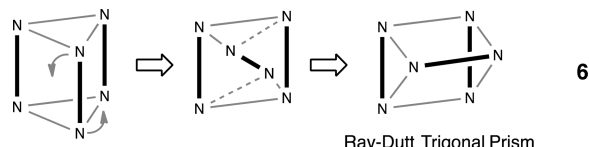


Figure 9. (a) Tris(chelate) Fe(II) complexes with pycolylamine ligands **7a** (empty triangles) in their high- (upward triangles) and low-spin (downward triangles) states, compared with the flattening Bailar distortion (continuous line). The behavior of the complexes with the topologically related pyridylquinoline ligand **7b** (solid triangles) is also plotted for comparison. (b) Shortest Fe...Cl contact in the spin-crossover isopropanol solvate of $[\text{Fe}(\text{pycolylamine})_3]\text{Cl}_2$ ⁶⁷ plotted as a function of the temperature.

to a bipyridine skeleton and therefore follows a parallel distortion pathway, but again clearly discriminating the high- and low-spin states. Other Fe(II) bipyridine complexes free of that steric constraint^{73–75} are found to follow very closely the flattened Bailar path.

A remarkable feature of the chloride of the pycolylamine Fe(II) complex ion in its isopropanol,⁶⁷ ethanol,^{63–66,70} and methanol^{63,69,71} solvates is the apparent effect that the spin crossover has on the supramolecular interactions. The transition from low to high spin at ~ 150 K is associated with a sharp approach of the closest chloride anion to the iron atom, with a decrease in the $\text{Fe}\cdots\text{Cl}$ distance of 0.10 Å (Figure 9b). It must be noticed that the short contact distance present in the high-spin structures, of ~ 4.22 Å, is similar to the sum of the van der Waals radii of 4.26 Å.⁷⁶ In this case each chloride ion forms hydrogen bonds with the amino groups of two ligands and, as these groups are separated (from 2.96 to 3.36 Å) due to the expansion of the coordination sphere in the high-spin state, the chlorides are pulled toward the metal atom.

5. SIZE OF THE CHELATE RING

In this section we will take a look at trischelate complexes with relatively flexible ligands, to analyze in more detail the effect of the size of the chelate ring. To that end we consider bidentate ligands with ethylenediamine and propanediamine skeletons. The former complexes, $[\text{M}(\text{en})_3]$, behave essentially in the same way as the bipyridine analogues just discussed, with most of them aligned along the flattening Bailar distortion (Figure 10a), while those that present important deviations from the idealized path (with $S(\text{OC-6}) \approx 17$) correspond mostly to disordered structures (excluded from Figure 10). The non-disordered structure that shows the highest deviation from that pathway belongs to a Cd(II) complex⁴⁹ with a Rây–Dutt trigonal prismatic structure, in which two of the bidentate ligands span edges perpendicular to the trigonal axis of the prism (**6**). In this case, the shorter edges associated with the chelate rings induce an important distortion from the ideal trigonal prismatic structure of that molecule in a non Bailar mode.

The propanediamine complexes, $[\text{M}(\text{pn})_3]$, present a different stereochemical behavior than the ethylenediamine analogues (Figure 10a and b), showing much lesser degrees of distortion of the coordination octahedron. Such a result can be

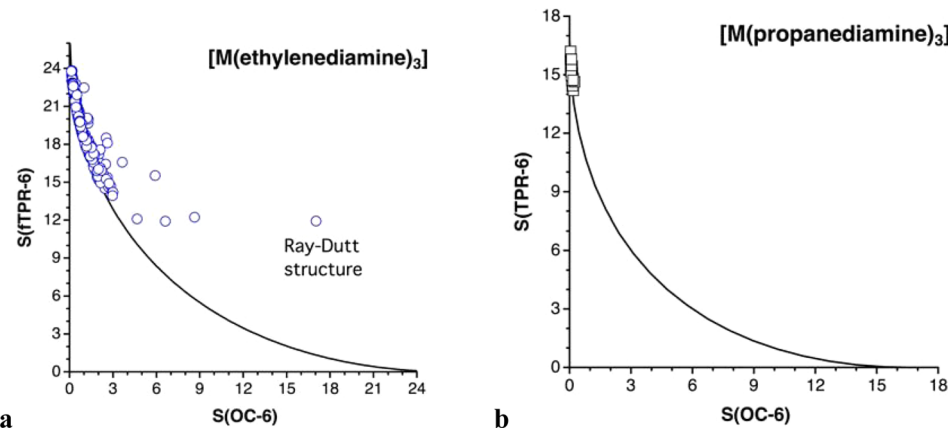


Figure 10. (a) Shape measures of the $[M(\text{ethylenediamine})_3]$ complexes (circles, disordered structures excluded) compared to the octahedron–flattened trigonal prism pathway (continuous line); (b) shape measures of the $[M(\text{propanediamine})_3]$ complexes (squares) compared to the Bailar path (continuous line).

traced back to the different bite angles of the two bidentate ligands,¹ which are on average for most 3d transition metals 83(3) and 91(4) $^\circ$ for ethylenediamine and propanediamine, respectively. Thus, the ethylenediamine complexes have bite angles between 74 and 90 $^\circ$, and the smaller the bite the more favored is the twist of the octahedron toward a trigonal prism³¹ (Figure 10a). Because propanediamine is a bidentate ligand with a wider bite angle (between 87 and 94 $^\circ$), it can favor trigonal twists both in Bailar ($\alpha < 90^\circ$ and $\theta < 60^\circ$) and anti-Bailar ($\alpha > 90^\circ$ and $\theta > 60^\circ$) modes (5), but with minor deviations from the octahedron (Figure 9b). The nearly linear dependence between these two angles at geometries close to octahedral, and the drop in the torsion angle below a threshold bite angle, have been discussed earlier.¹¹

The trischelate complexes with diketonato ligands also cover torsion angles around the octahedron in both Bailar and anti-Bailar distortion modes that correlate well with the bite angles and the normalized bites (Figure 4). A fascinating result for this family of compounds is that they follow closely the minimal distortion pathway (a maximum path-deviation function of 23%) all the way from the anti-Bailar twisted structures with torsion angles of up to 68 $^\circ$ to the trigonal prismatic structures with twist angles close to 0 $^\circ$ (Figure 7). The only two structures within this family that present trigonal prismatic coordination correspond to Cd(II)⁴² and Y(III)⁴³ complexes. Notice that the shape map does not distinguish Bailar from anti-Bailar twists, because these two modes differ in the arrangement of the chelate rings around the coordination polyhedron, whereas the shape measures analyze only the coordination polyhedron itself, formed by the central metal and donor atoms. Therefore, a better description of the Bailar and anti-Bailar structures in the family of tris(diketonato) complexes can be obtained by plotting their octahedral and trigonal prismatic shape measures as a function of the twist angle θ (Figure 11). Such a plot shows how the $S(\text{OC-}6)$ values become zero for a number of compounds at $\theta = 60^\circ$, whereas one complex presents a zero value of $S(\text{TPR-}6)$ at $\theta = 0^\circ$, stressing the ability of this family of ligands to adapt to both perfect octahedral and perfect trigonal prismatic coordination spheres, in spite of the formation of chelate rings. Moreover, we can see how twist angles larger than 60 $^\circ$ take it back toward the trigonal prism.

The trends found for the families of tris(chelate) complexes analyzed allow us to conclude that when the bidentate ligand

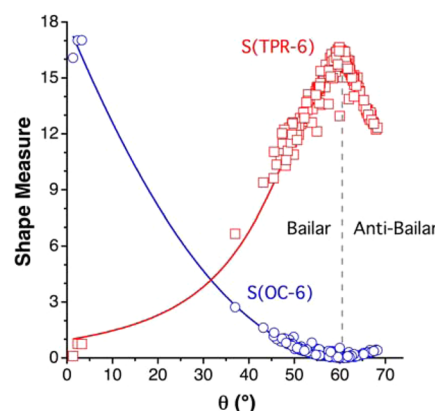


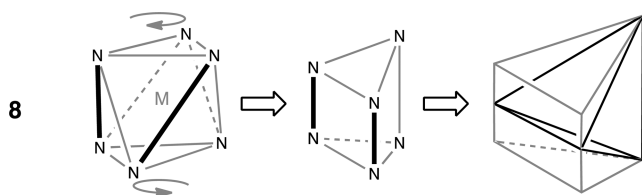
Figure 11. Variation of the octahedral and trigonal prismatic shape measures as a function of the torsion angle θ for the Bailar ($0 \leq \theta \leq 60^\circ$) and anti-Bailar ($\theta \geq 60^\circ$) regimes in the case of $[M(\text{diketonato})_3]$ complexes. The continuous lines are given as a guide to the eye.

has a small bite angle¹ (57–80 $^\circ$) the coordination sphere follows more closely the flattening Bailar twist, as found for ligands such as triazenes, amidines, dithiocarbamates (including dithiocarbonates, dithiophosphinates, and dithiophosphates), dimethoxyethane (including oxalate), bipyridine, pycolyamine, and ethylenediamine. In contrast, for ligands with larger bite angles (81–97 $^\circ$), the trischelate complexes follow the Bailar path, as found for complexes with β -diketonates, propanediamine, malonato, and dithiolene ligands.

6. BISCHELATE COMPLEXES

The *cis*-[Fe(bipy)₂(NCS)₂] complex is without doubt one of the most studied spin-crossover systems, and in this section we consider analogous complexes with bipyridine- and phenanthroline-based bidentate ligands complemented by two monodentate ligands, of general formula *cis*-[M(bipy)₂XY].⁷⁷ The fact that only two edges are constrained by the formation of chelate rings results in two short edges and one long edge as the metal–ligand distances increase (8), and the structures of these compounds do not follow the Bailar twist, as expected from visual inspection of 8. The simultaneous changes in the torsion angles and the asymmetrization of the faces of the octahedron result in a path that, taken to its extreme, can be idealized as a tetrahedron in which the centroids of each pair of

donor atoms of the bidentate ligands jointly occupy a vertex of the tetrahedron (**8**), represented from here on by the symbol t-6.



A plot of the *cis*-[M(bipy)₂XY] complexes in a shape map relative to the octahedron and the tetrahedron with two doubled vertices (Figure 12) shows most of the structures to be

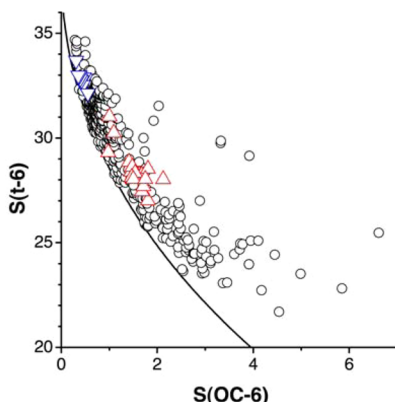


Figure 12. Bischelate complexes of the *cis*-[M(bipy)₂XY] family (normalized polyhedra, circles), highlighting the Fe members of these families with two N-donor monodentate ligands in their high-spin (upward triangles) and low-spin (downward triangles) states, in the shape map relative to the octahedron (OC-6) and the tetrahedron with two doubled vertices (t-6).

aligned very close to the minimal distortion pathway. The complexes that deviate most from that path are essentially those with an incipient metal–ligand bond involving the second oxygen atom of potentially bidentate groups such as carboxylates, nitrate, sulfonates, perchlorate, chromate, or polyoxometallates. In the case of the [Fe^{II}L₂X₂] complexes, for which X is NCS[−], NCSe[−], N₃[−], or NC[−], as the molecule transits from low- to high-spin (i.e., as the Fe–N distances increase), the stretching of the Fe–N bond implies that, even if the metal atom, its oxidation state, and the bidentate ligand are the same in both spin states, they span a wide portion of the distortion path to the doubled tetrahedron. This can be seen in Figure 12, where the low-spin molecules occupy the early stages of the distortion pathway and the high-spin ones appear farther away from the octahedron (at smaller values of the t-6 measure). The complex of this family that deviates most from the path under consideration has a benzo group attached to a bipyridine skeleton (**7b**).⁷⁸

The *trans*-bischelate complexes behave quite differently to their *cis* isomers. Consider, for instance, the family of [Cr(diphosphine)₂XY] complexes (X, Y = Cl, Br, I, CN), most of which have a low-spin configuration, with the exception of *trans*-[Cr(dppe)₂I₂], which presents spin crossover.⁷⁹ For those complexes, one would expect a metal–ligand bond lengthening to distort the octahedron to a rectangular bipyramidal, as in **9**. The most distorted octahedron in this family is precisely the high-spin form of [Cr(dppe)₂I₂].

Although one would expect it to follow a larger rectangular distortion than the low-spin molecules, its deviation from the rectangular path is non-negligible (7%). The different axial and equatorial bond distances might account for such deviations: 2.39 and 2.71 Å for Cr–P and Cr–I in the low-spin state⁸⁰ but 2.52 and 3.07 Å in the high-spin state, respectively.⁷⁹ Therefore, a strong bond distance difference between the equatorial and axial bonds (0.32 Å) in the low-spin state is due simply to the different covalent radii of the P and I atoms (1.07 and 1.39 Å, respectively),³ but such a difference is significantly enhanced in the high-spin state (2.52 and 3.07 Å for the Cr–P and Cr–I bonds, respectively) due to a Jahn–Teller effect. If the bond distance effects are disregarded, by looking at the normalized coordination polyhedra¹⁵ in which all distances are equalized while keeping the same bond angles as in the experimental structure, the high-spin complex appears very close to the rectangular path (Figure 13), with a marginal deviation of 2%

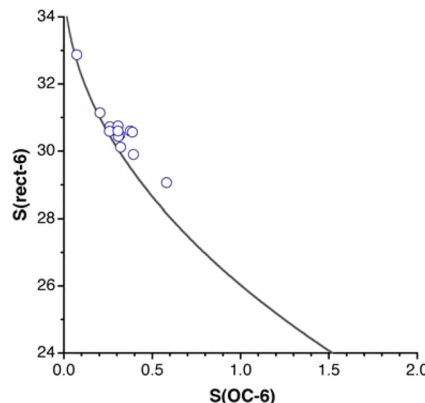
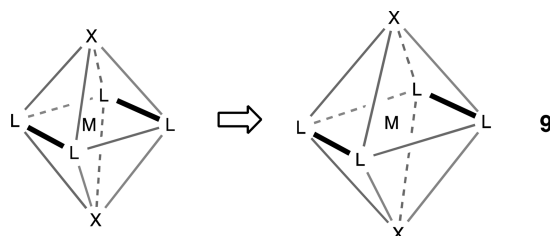


Figure 13. Shape map showing the rectangular distortion pathway of the octahedron (continuous line) and the position of the normalized coordination polyhedra of [Cr(diphosphine)₂XY] complexes (X, Y = Cl, Br, I, CN).

associated with a slight tilting of the two iodides from the purported symmetry axis. Similarly, the other low-spin complexes from this family appear to strongly deviate from the rectangular pathway expected for *trans*-bischelate complexes, but this deviation is due to differences between axial Cr–C and equatorial Cr–P bond lengths, and the use of normalized polyhedra clearly show that most of them present some degree of rectangular distortion imposed by the bidentate ligands (Figure 13).



A topologically related family is that of the *trans*-Fe(II) complexes, with two bidentate pyridyltriazole and two thiocyanate ligands (**10**), which show a similar stereochemical behavior. One of the members of this family (R = NH₂, R' = pyridyl) presents spin crossover (Figure 14).⁸¹ Only a few high-spin complexes deviate significantly from the rectangular path

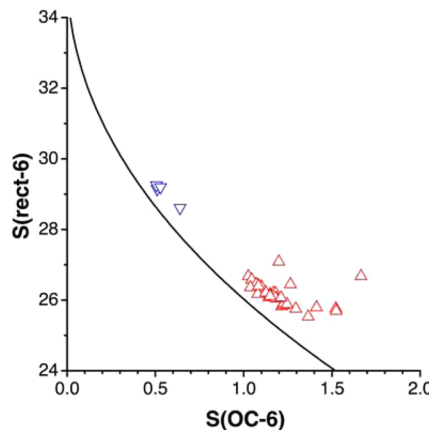
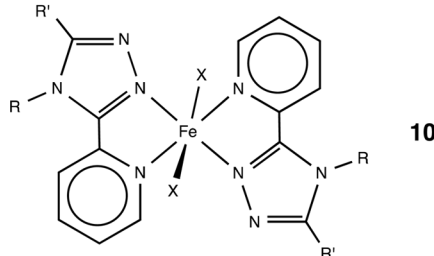


Figure 14. Shape map showing the pathway for the rectangular distortion of the octahedron (continuous line) and the position therein of the normalized coordination polyhedra of iron complexes **10** in their high-spin (downward triangles) and low-spin (upward triangles) states.

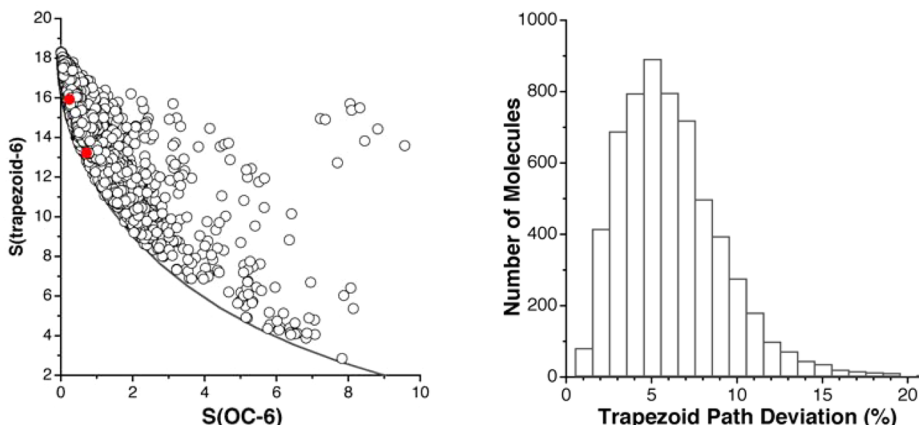


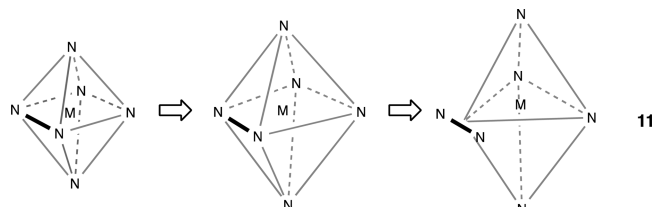
Figure 15. (a) Shape map for monochelated complexes showing the trapezoidal distortion pathway from the octahedron (continuous line) of their normalized (squares) coordination polyhedra. The two spinomers of $[\text{Fe}(\text{Medpq})\text{py}_2(\text{NCSe})_2]$ ⁸² are represented by filled circles. (b) Distribution of the path deviations for the same monochelated complexes.

because of the simultaneous shift of the two thiocyanate ligands from the axial directions.

7. MONOCHELATED COMPLEXES

In six-coordinate complexes with only one bidentate ligand, the expansion of all the edges except for that occupied by the chelate ring results in a distortion of the octahedron to a trapezoidal bipyramidal (**11**). Taking such a distortion to the extreme, we would arrive at a trigonal bipyramidal with a doubly occupied equatorial vertex, a shape that we take as our reference for the trapezoidal distortion pathway. The behavior of all monochelate metal complexes (6 140 structural data points, $R \leq 7.5\%$, no disorder, not polymeric) can be reasonably described by that pathway. Figure 15a shows a shape map in which most of the monochelate structures are grouped close to the trapezoid path. Although there are some compounds that present significant deviations from that path, they are not statistically significant, as shown by the distribution of the path-deviation functions for these structures (Figure 15b), because most of the structures deviate $<10\%$ from the pathway.

Among the relatively small family of FeN_6 complexes with only one bidentate ligand, we can focus on the spin-crossover system reported by Tao et al.,⁸² $[\text{Fe}(\text{Medpq})\text{py}_2(\text{NCSe})_2]$, where Medpq is a bidentate ligand with a phenanthroline



skeleton. The significant decrease of the bite angle on going from the low-spin to the high-spin state (from 81.3 to 72.5°) is accompanied by an increase in the angle between the coplanar monodentate ligands (90.5 – 98.3°), thus forming a trapezoidal bipyramidal, nicely reflected by the position of the two spin isomers highlighted in the shape map (Figure 15a) and whose equatorial plane is shown in Figure 16 for the two spin states.

8. EXTENDED TRIPOD LIGANDS

We consider in this section a broad family of ligands that bear three bidentate units linked at one end, forming what we might call extended tripods (**12**). In a quite common case, the pivotal position is occupied by a potentially coordinating atom, mostly nitrogen, a fact that may introduce a differential stereochemical behavior upon changes in the spin state. These ligands have three chelate rings in the same arrangement as the trischelates discussed above, but because the upper ends of those rings are

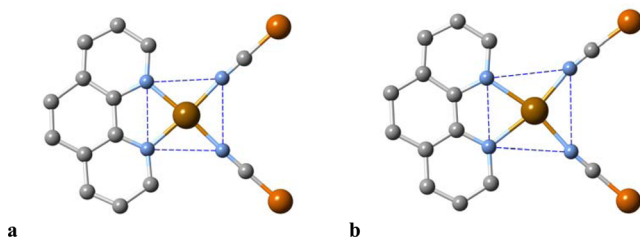


Figure 16. Trapezoidal distortion of the equatorial coordination plane in $[\text{Fe}(\text{Medpq})\text{py}_2(\text{NCSe})_2]$ on going from the low-spin (a) to the high-spin state (b). Only the phenanthroline skeleton of the bidentate ligand is shown, and the axial pyridine ligands are omitted for clarity.

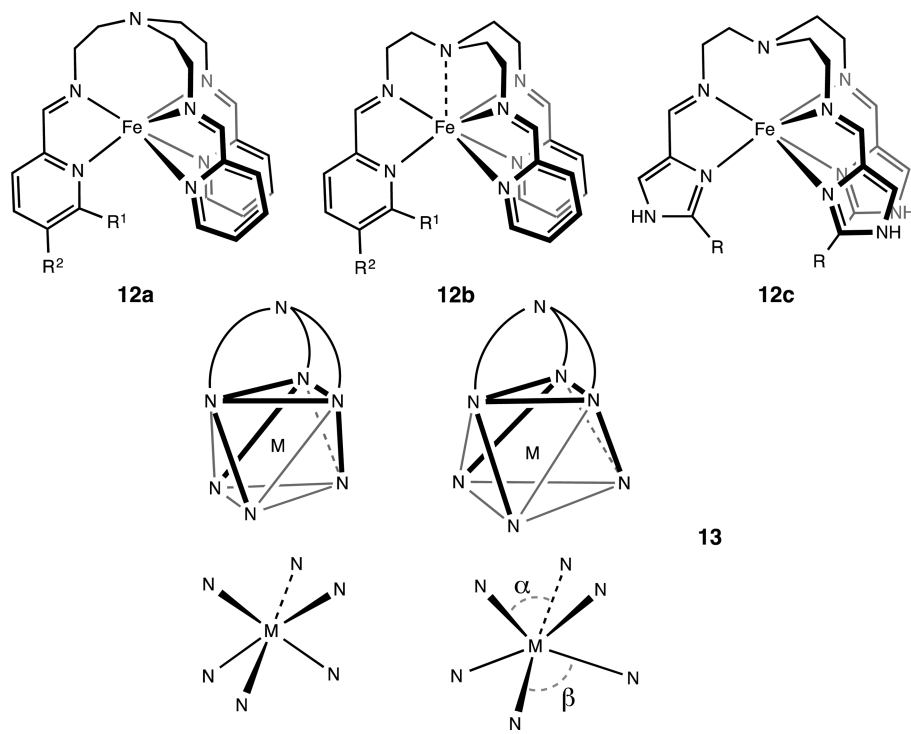
linked to a pivotal atom, they form three additional chelate rings that cover a face of the octahedron (compare 13 with Figure 3).

With the constrained edges shown in 13, an increase in the M–N bond distances should induce a distortion of the coordination sphere in which the three legs open. As a result, the three upper N–M–N bond angles (α) decrease and the lower three angles (β) increase. In addition, there is some degree of Bailar distortion due to the presence of the three chelate rings along the legs, so the twist angles found between the trigonal faces are in the range 40–58°, compared to 60° for the ideal octahedron and 0° for the trigonal prism. A plot of the structural data for the complexes with extended pyridine tripodal ligands on a Bailar shape map (not shown) tells us how the coordination spheres of complexes with unsubstituted ligands at the ortho position ($R^1 = H$) somewhat deviate from the flattening Bailar distortion expected for three independent chelate rings, as in the $[\text{M}(\text{bipy})_3]$ complexes (Figure 5). Such a deviation is due to the leg-opening distortion just commented upon and is a consequence of the existence of three chelate rings spanning the edges of the upper face. Therefore, these data are better represented (Figure 17) by the truncated trigonal pyramid path defined below.

Among the analyzed structures of complexes with extended tripods, we point to a set of salts of Fe(II) complexes with ligand 12c ($R = \text{Me}$) and different counteranions,⁸³ whose high- and low-spin versions appear in well-separated regions of the shape map (Figure 17c). A related Mn(III) complex in low- and high-spin versions⁸⁴ presents distortions intermediate between those of the iron complexes just commented upon, spanning a narrower range of distortions consistent with the lesser Mn–N distance variations (2.00–2.10 Å compared with 1.97–2.20 Å for the Fe complexes). Ultimately, the degree of distortion from the octahedron of complexes with ligands 12a is nicely correlated to the average M–N bond distance (Figure 18a), which clearly differentiates the low- and high-spin Fe(II) complexes.

It must be noted that, when the pyridyl legs have a substituent at the ortho positions, even a small methyl group, the legs are wide open and barely sensitive to the M–N distance: β has values between 99 and 106°, to be compared with angles of 81–96° for the unsubstituted analogues. The larger β values are associated with smaller values of α , although the latter show a similar dependence on the average M–N bond distance as in the unsubstituted compounds. After all, however, these angle variations seem to be relatively small compared to the trigonal twist, given the proximity of most of the structures to the path between the octahedron and the truncated trigonal pyramid, a fact that must be attributed to a higher flexibility of the upper portion of the ligand that forms eight-member chelate rings, while the legs of the ligand form five-member rings with less flexible sp^2 carbon and nitrogen atoms.

We note that the structures that are most distorted toward the truncated trigonal pyramid belong to Mn(II)^{85–88} and Cd(II)⁸⁹ complexes, which are known to have an electronic preference for the trigonal prism.³² An interesting feature of this family of complexes is the possibility of a coordinative bond from the pivotal nitrogen atom (12b). Such an extra bonding interaction produces an expansion of the upper face and a



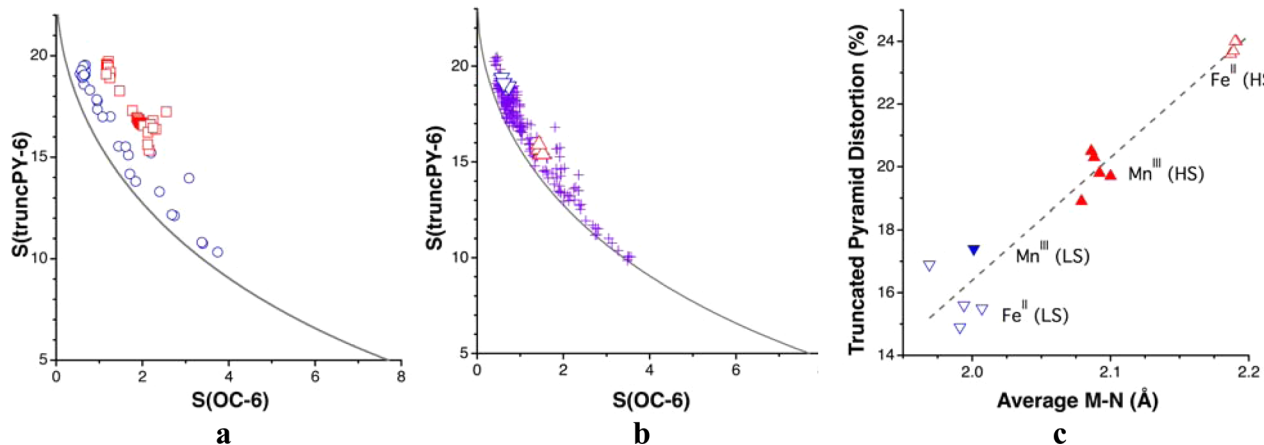


Figure 17. Transition metal complexes with extended tripod pyridyl ligands **12a** (a) and with five-member N-donor rings (e.g., pyrrol or imidazol) of type **12c** (b) in a shape map relative to the octahedron (**OC-6**) and the truncated trigonal pyramid (**truncPY-6**). The compounds with substituted ortho positions in the pyridyl rings (R^1 in **12a**) are represented by squares, unsubstituted ones are represented by circles, and the high- and low-spin centers of the Fe(II) complex cation with ligand **12c** ($R = \text{Me}$) and different counterions⁸³ are represented by upward and downward triangles, respectively. (c) Degree of distortion (generalized coordinate) of some Fe(II) and Mn(III) complexes in high- and low-spin states as a function of the M–N distance.

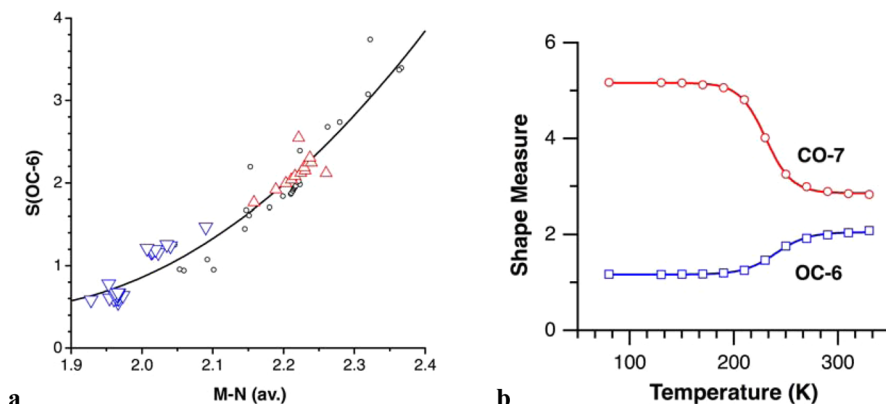
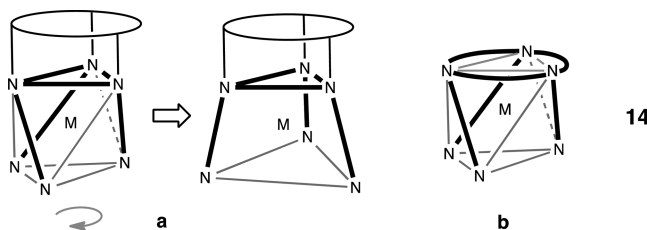


Figure 18. (a) Dependence of the octahedral shape measure on the average M–N bond distance for Fe complexes with extended pyridyl ligands **12a** in their low-spin (downward triangles) and high-spin (upward triangles) states and for complexes with other metal ions (circles). A least-squares fitting line is provided as a guide to the eye. (b) Shape measures of $[\text{Fe}^{\text{II}}(\text{12a})](\text{ClO}_4)_2$ ($R^1 = \text{Me}$, $R^2 = \text{H}$)⁸⁵ relative to the octahedron (**OC-6**) and the capped octahedron (**CO-7**) as a function of the temperature. Reproduced with permission from ref 97. Copyright 2010 Wiley.

significant deviation from the flattening Bailar twist, en route to a capped octahedron: four compounds with $M-\text{N}_{\text{apical}}$ distances shorter than 2.70 Å^{86,87,90} are the ones that deviate 8% or more from the flattened trigonal prism pathway. The onset of this extra bond may even be associated with a change in spin state, as shown in Figure 18b for $[\text{Fe}^{\text{II}}(\text{12a})](\text{ClO}_4)_2$ ($R^1 = \text{Me}$, $R^2 = \text{H}$)⁸⁵ where the coordination sphere is seen to switch at the spin-crossover temperature (240 K) from nearly octahedral in its low-spin state to intermediate between octahedral and capped octahedral in the high-spin state.



We may wonder whether a substitution of the flexible pivotal skeleton of ligands **12** by a more rigid ring system (**14**) may

result in a more pronounced difference in the sizes of the two basal triangles. To try to answer this question, two families of compounds have been analyzed with triazacyclononane (tacn) and cyclohexanetriamine (chta) as cyclic linkers (**15**). From the topology of the chelate rings formed by these ligands, one would expect a trigonal twist upon increasing the metal–ligand distances, as in the tris(chelate) complexes, but also a pyramidalization of the resulting coordination polyhedron, because one of its trigonal bases cannot significantly change its size, constrained as it is by three chelate rings (**14a**). We therefore define a truncated trigonal pyramid (**Figure 19a**) as the ideal shape for such a distortion. It must be noted that the choice of that reference polyhedron is not unique, and the one we adopt is but one possible choice, and therefore our shape and path analysis are intended in this case to provide only qualitative information on trends and relative degrees of distortion. Our reference truncated trigonal pyramid is characterized by a ratio of 1.25 between the sides of the nonchelated and chelated triangular bases, as well as by a height/short edge ratio of 1.00. The latter ratio is, in the

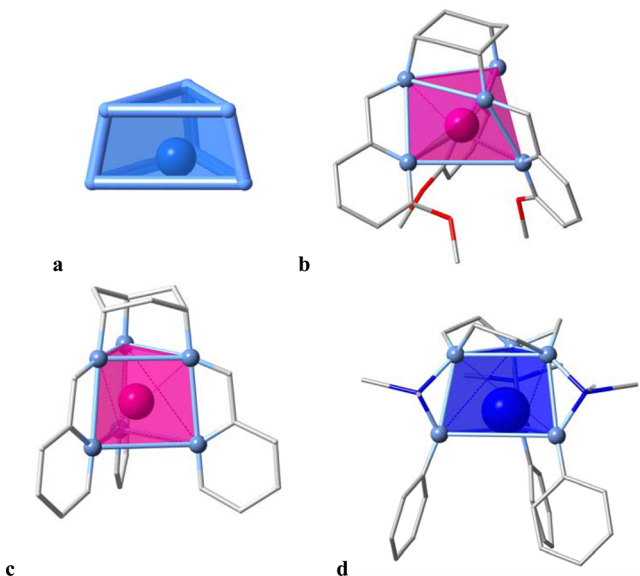
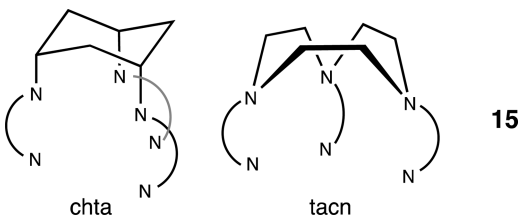


Figure 19. (a) Reference shape for a truncated trigonal pyramidal coordination sphere. (b, c) Structures of two Mn complexes with cyclohexyl-supported hexadentate ligands,^{91,92} and (d) an yttrium complex with a triazacyclononane-based hexadentate ligand having shorter arms,⁹³ showing their varying degrees of twisting toward truncated trigonal pyramidal coordination spheres.

molecular structures, dependent on the length of the arms that hold the terminal donor atoms.



For the chta complexes, the truncated pyramidal path seems to reasonably describe the distortions from the octahedron (Figure 20a). Two of the three most distorted structures are shown in Figure 19 (b, c), where the varying degrees of trigonal twist and the truncated pyramidal shape can be clearly

appreciated. If we turn to complexes with ligands formed by a tacn macrocycle appended with three coordinating arms, the truncated pyramidal distortion pathway also represents well those structures in which one or two spacers separate the two types of donor atoms (Figure 20b) but appears to provide a poorer description of those with three spacers. Plotting the latter structures in the octahedron–trigonal prism map (Figure 20c) indicates that these structures follow very closely the Bailer path, because the arms now have enough flexibility as to adapt to the trigonal prism. The three most rotated structures are the Zn, Cd, and Hg complexes of a tacn ligand with aminobenzyl arms,⁹⁴ with the former appearing right on the Bailer path, midway from the octahedron to the trigonal prism.

9. MACROCYCLIC PENTADENTATE LIGANDS

A family of N- or O-donor pentadentate macrocyclic ligands have the skeleton **16**, with several distributions of single, double, and aromatic C–C and C–X bonds. We will analyze the structures in which two additional monodentate ligands are in trans, because only two cis structures have been found.^{95,96} Among this family we will pay particular attention to the ligands with skeletons similar to **16**, with either single or double C–N bonds, and having X = O or NH. Those ligands appear commonly in seven-coordinate complexes with two extra monodentate ligands, and a shape analysis (Figure 21a) shows them to adopt essentially a pentagonal bipyramidal geometry (PBPY-7), with some degree of distortion along the path to the capped octahedron (COC-7) due to the nonplanarity of the macrocyclic rings. The effect of nonplanarity is supported by a nice correlation of those shape measures with the average deviation of the five donor atoms of the macrocycle from the mean plane: as the nonplanarity increases, S(PBPY-7) increases and S(COC-7) decreases.

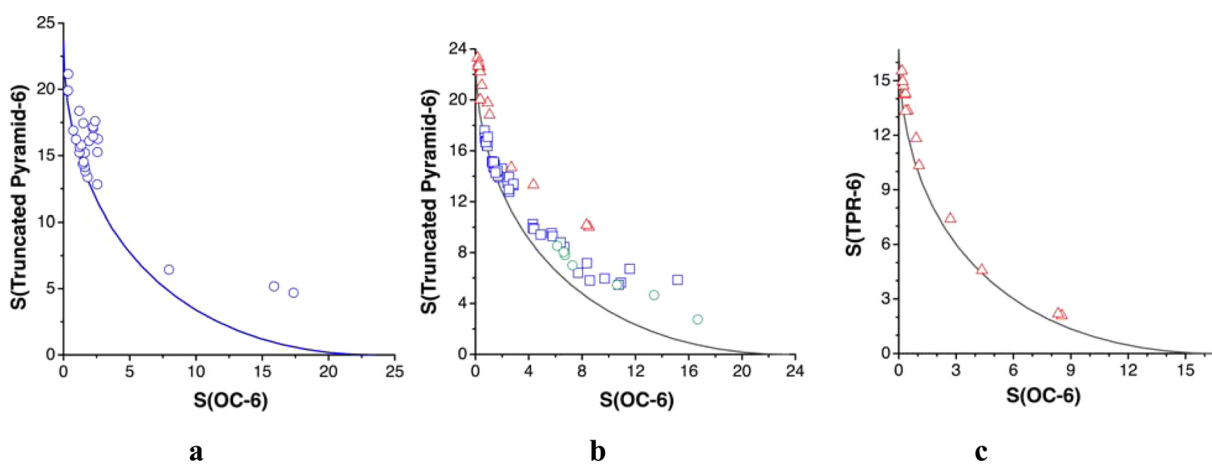
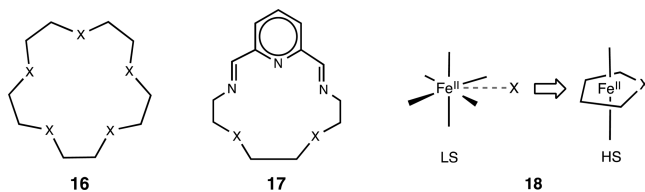


Figure 20. Shape map relative to the octahedron and a truncated trigonal pyramid for (a) $[M(\text{chta}-\text{L}_3)]$ and (b) $[M(\text{tacn}-\text{L}_3)]$ complexes with one (circles), two (squares), or three spacers (triangles) between N-donor atoms. (c) Shape map for the $[M(\text{tacn}-\text{L}_3)]$ complexes with three spacers relative to the octahedron and the trigonal prism.

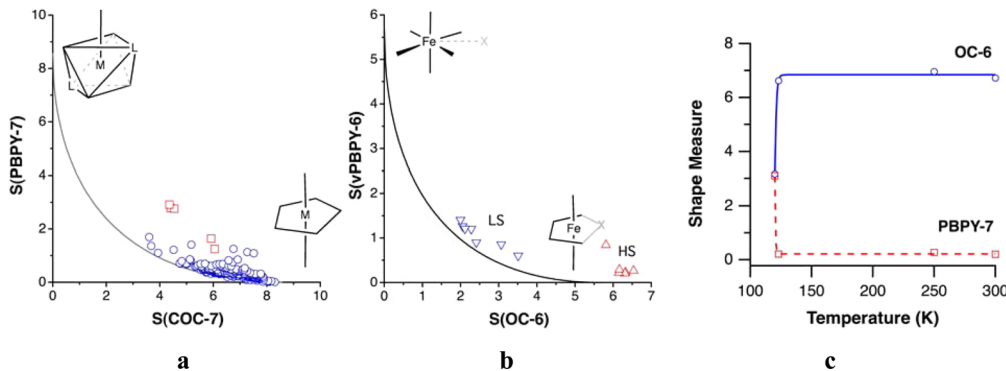


Figure 21. (a) Shape measures relative to the pentagonal bipyramid (PBPY-7) and the capped octahedron (COC-7) for the normalized coordination polyhedra of heptacoordinated metal complexes with one pentadentate macrocyclic ligand and two monodentate ligands (circles). The squares correspond to compounds with ligands of type **16**, which are effectively six-coordinate with one of the M–X distances at least 1.0 Å longer than the other one. (b) Shape map for the normalized coordination polyhedra of Fe compounds with ligands **17** and one long Fe–X distance, relative to the octahedron and the equatorially vacant pentagonal bipyramidal (vPBPY-6), corresponding to low-spin complexes (downward triangles), with the corresponding seven-coordinate high-spin structures shown for comparison (upward triangles). (c) Representation of the shape measures of a spin-crossover Fe(II) complex of this family^{99–102} as a function of the temperature.

Some of the structures that deviate most from the minimal distortion pathway between the pentagonal bipyramid and the capped octahedron correspond in fact to Fe complexes in which one of the two X atoms of a ligand **17** is at a much longer distance (1.0 Å or more) than the other, making the metal atom practically six-coordinated. A shape analysis of the resulting six-vertex coordination polyhedra (Figure 21b) indicates that those structures are along the ligand association/dissociation pathway⁹⁷ that links the pentagonal bipyramid with the octahedron (**18**). These structures belong to low-spin (LS) states of Fe(II) complexes^{98–103} that undergo spin crossover, and the corresponding high-spin (HS) states are plotted also in Figure 21b for comparison. We can thus see that the HS structures are practically pentagonal bipyramidal, whereas the LS ones are intermediate between the pentagonal bipyramid and the octahedron. A plot of the shape measures as a function of the temperature for one of those compounds (Figure 21c) nicely shows how the spin transition at 120 K is accompanied by a sudden change of the coordination polyhedron from a pentagonal bipyramidal (HS, high temperature) to a geometry intermediate between that bipyramid and the octahedron (LS, low temperature).

10. COMPLEXES WITH TWO MACROCYCLIC TRIDENTATE LIGANDS

In this section we examine first the bis(macrocylic) complexes with two independent triazacyclononane ligands (tacn, **19**), and then we will analyze the effect of connecting the two macrocycles with alkyl bridges (**20**). The topology of the complexes with two independent macrocyclic ligands must favor an elongation of the metaprism resulting from a Bailar twist (**21**). The target reference shape for such a pathway has been defined in this work as an elongated trigonal prism with an edge ratio of 0.80 (abbreviated eTPR-6).

A shape map relative to the octahedron and the elongated trigonal prism is shown in Figure 22, on which the structural data for the families of metal complexes with two independent or two strapped tacn ligands are plotted. It can be seen that the elongated Bailar path describes well the distribution of molecular geometries, despite the arbitrariness of the choice of a specific elongated prism as a reference shape. Thus, we can see that most of the structures present moderate deviations

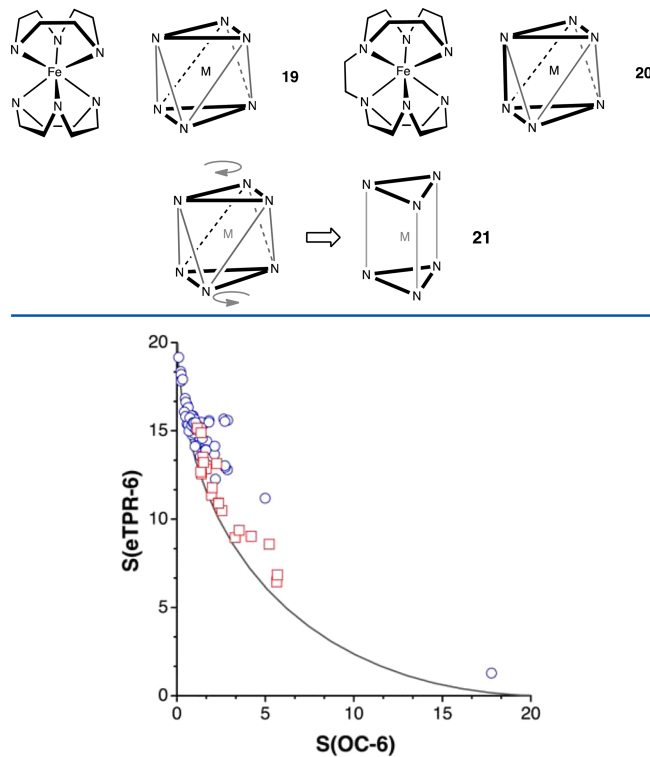


Figure 22. Structures of $[M(\text{tacn})_2]$ complexes with two independent (**18**, circles) or two strapped (**19**, squares) macrocyclic ligands, represented in the elongating Bailar shape map.

from the octahedron, with $S(\text{OC-6}) < 3.0$, except for a Hg(II) complex¹⁰⁴ at $S(\text{OC-6}) \approx 18$ with a clear elongated trigonal prismatic structure. It must be noted, though, that the outlier at $S(\text{OC-6}) \approx 5.0$ represents a silver complex¹⁰⁵ with the shape of an elongated untwisted octahedron. We must remember that, different from the Bailar twist, the minimal distortion path that leads from a regular octahedron to an elongated trigonal prism implies the coexistence of two distortion modes: a rigid twist and a pure elongation. Therefore, any structure that undergoes only one of those two distortion modes is away from the octahedron but quite separated from the minimal distortion path, as exemplified by this particular Ag compound. When the

two macrocycles are linked by a strap, the new chelate ring formed forces larger degrees of trigonal twist (Figure 22), although no correlation has been found between the length of the strap (2, 3, or 4 intervening atoms) and the extent of the twist.

11. ONE TRIDENTATE MACROCYCLIC AND THREE MONODENTATE LIGANDS

When one of the cyclic tridentate ligands considered in the previous section is combined with three monodentate ligands, we expect one face of the coordination octahedron to remain practically unchanged in size in spite of changes in the metal–ligand bond lengths, while the opposite face is free to adapt to the varying distances (22). A shape analysis of the family of $[M(\text{tacn})L_3]$ complexes indicates that the path that best describes the normalized coordination polyhedra is that of a Bajilar twist to an elongated trigonal prism (Figure 23),

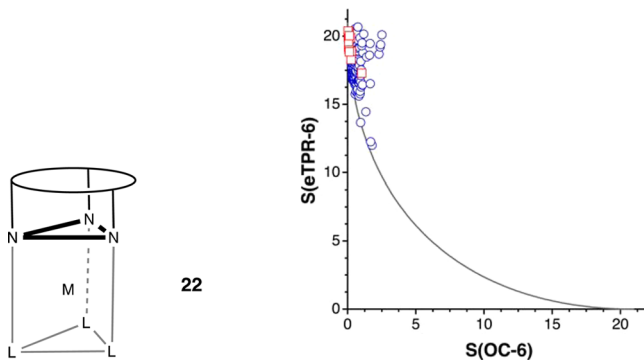


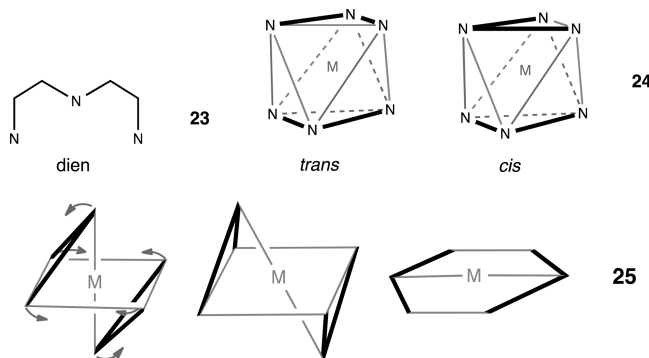
Figure 23. Normalized coordination polyhedra of complexes of the families $[M(\text{tacn})L_3]$ (circles) and $[M(\text{ctha})L_3]$ (squares) represented in a shape map for the elongating trigonal twist distortion of the octahedron (continuous line).

particularly for some complexes with generalized coordinates along that pathway of up to 24–28%. Some structures, however, are little twisted but experience deviations from the octahedron due to a large size difference between the constrained and unconstrained triangular faces (22), as in two Y complexes.¹⁰⁹ It is worth noting that there are also examples of complexes of this family that are nearly perfectly

octahedral.^{110,111} The related $[M(\text{chta})L_3]$ complexes (chta = cyclohexanetriamine) present lesser degrees of distortion.

12. FAC-COORDINATED OPEN-CHAIN TRIDENTATE LIGANDS

The ligands with the tridentate diethylenetriamine (dien) skeleton 23 coordinate in a *fac* mode, different from the pincer ligands to be discussed later that span three *mer* coordination sites. In complexes with two such ligands, two different conformations can be found (24), depending on whether the central nitrogen atoms of the two ligands occupy *trans* or *cis* relative positions. In the *trans* complexes, an increase in the M–N distances is expected to induce a distortion of the type shown in 25 that could be extrapolated to a planar hexagonal coordination. A plot of the shape measures of complexes of that family relative to the octahedron and the planar hexagon (Figure 24a) shows them distributed at an early stage of that distortion pathway within a good approximation. The main deviations from the hexagonal path among the *trans* compounds come from Cu(II) complexes subject to Jahn–Teller distortions. The most extensive distortions along the path correspond to Cd(II)¹¹² and high-spin Mn(II)¹¹³ and Fe(II)¹¹⁴ complexes.



In the case of the *cis* complexes, the highly asymmetric distribution of the nonchelated edges results in a completely different distortion, as can be appreciated by large deviations from the hexagonal path (Figure 24a). The distortion experienced by the *cis* isomers is a combination of a twist toward an elongated prism with isosceles trigonal bases (26),

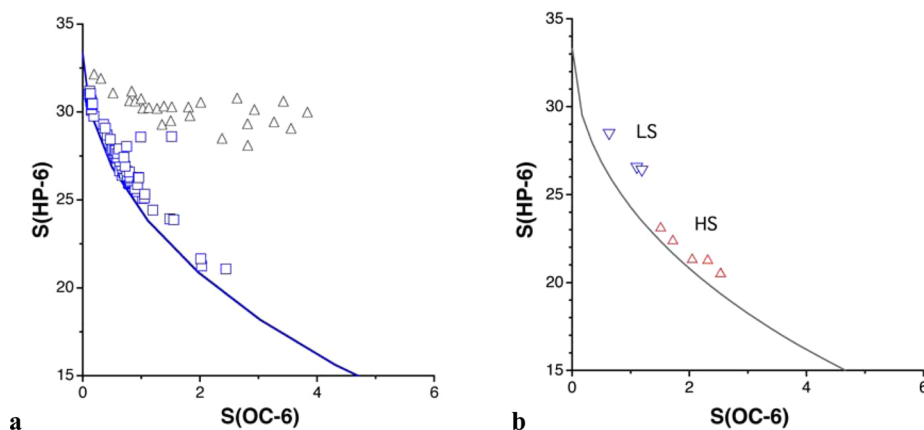
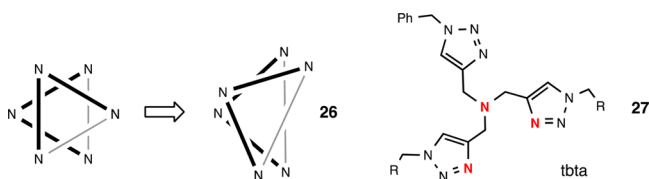


Figure 24. (a) Minimal distortion pathway from the octahedron to the planar hexagon (continuous line) and the structures of the *trans*- $[M(\text{dien})_2]$ (squares) and *cis*- $[M(\text{dien})_2]$ (triangles) complexes. (b) Normalized polyhedra of low-spin (downward triangles) and high-spin (upward triangles) $[M(\text{tbta})_2]$ complexes (27, M = Fe^{II}, Co^{II}) in the shape map relative to the octahedron (OC-6) and the planar hexagon (HP-6).

which explains the deviation of their structures from all four paths analyzed (canonical, elongated and flattened Bailar twists, and hexagonal planarization). As found in other families, the most distorted structures of cis complexes correspond to high-spin d⁵-Mn(II)^{115,116} or d¹⁰-Zn(II)³⁴ ions that seem to be better adapted electronically to the trigonal prismatic geometry.³²



The ligand tbta (tris[(1-benzyl-1*H*-1,2,3-triazol-4-yl)methyl]amine (27, R = benzyl) reported by Grimme, Sarkar, and co-workers,^{117–119} and similar ligands with other R groups, although potentially tetridentate tripod ligands, are found coordinated in an open-chain tridentate mode *trans*-24 through the pivotal amine nitrogen and two of the three triazole rings. This family of complexes appear distributed along the path from octahedron to planar hexagon, once we disregard bond-distance distortions by using the normalized coordination polyhedra.¹⁵ In the case of Fe(II) and Co(II) complexes, the low- and high-spin structures are nicely segregated along the path, with the high-spin versions showing a higher degree of distortion toward the hexagon (Figure 24b). One of those structures¹¹⁷ significantly distorted toward the hexagon is shown in Figure 25, to be compared with the idealized path 25.

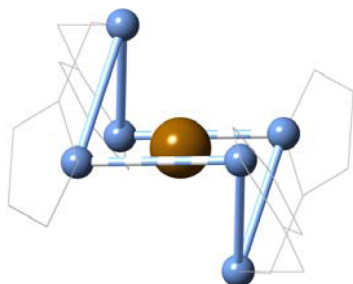


Figure 25. Coordination skeleton of a high-spin $[\text{Fe}^{\text{II}}(\text{tbta})_2]$ complex¹¹⁷ that presents a 26% distortion along the pathway from the octahedron to a planar hexagon. The cylinders do not represent chemical bonds but the bent hexagonal topology of the two facial tridentate ligands.

13. SCORPIONATES AND RELATED CLAW-TYPE LIGANDS

The trispyrazolylborate (TpB, Figure 26b, X = B), trispyrazolylmethane (TpM, Figure 26b, X = C), and triscarbeneborate anions (Figure 26c), often referred to as scorpionates, form part of the family of ligands with the same topology as the three finger claws (Figure 26a). For tridentate ligands of this type, a parameter analogous to the bite angle of a bidentate ligand is the sum of the three L–M–L bond angles, Σ .¹ This parameter is roughly constant for a given ligand and therefore may be responsible to some extent for the deviations of the coordination sphere from an ideal polyhedron, although there is some degree of flexibility in those ligands that can be calibrated by the standard deviation of the angular parameter. The angular parameters Σ that correspond to ideal octahedral

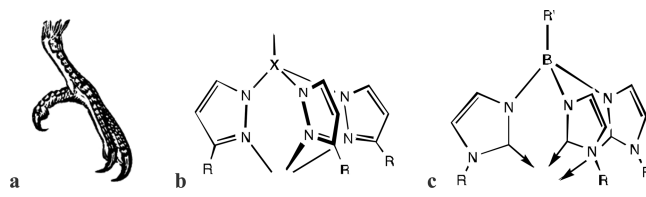
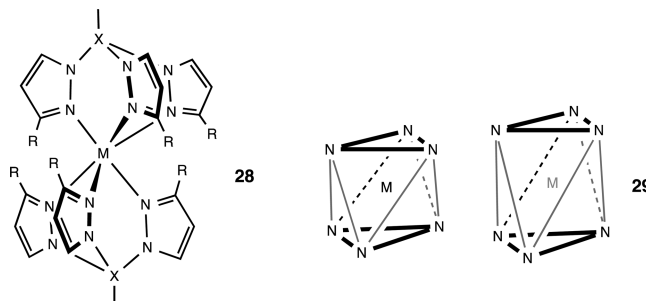


Figure 26. (a) Claw of a ceyx, a genus of kingfisher characterized by having three toes (clipart courtesy FCIT) and topologically analogous claw ligands: (b) trispyrazolylborate and trispyrazolylmethane (X = BR and CR, respectively) and (c) triscarbeneborate.

and tetrahedral geometries are 270 and 328° , respectively. The span of the claws analyzed earlier cover the range between 254 and 280° , with standard deviations varying between 1 and 12° . For the triscarbene ligands, not included in our earlier analysis, we find an average Σ of 273° (8). It thus seems clear that most such ligands adapt well to the octahedral geometry and also allow some degree of distortion from the ideal geometry if electronically or sterically required. In contrast, they force too-small bond angles for an ideal tetrahedral coordination (see below).



Focusing now on the six-coordinate complexes with two claw ligands 28, these have the same topology as the complexes with two cyclic tridentate ligands discussed earlier, and therefore, we expect them to follow the elongated Bailar twist 21. However, these compounds show significant deviations from that path and seem to undergo rather an elongation of the coordination octahedron 29 without a significant degree of Bailar twist (Figure 27). The compounds that deviate from the pure octahedron elongation pathway are mostly (a) the Cu(II) compounds in which a Jahn–Teller distortion makes the elongation of the octahedron quite asymmetric and (b) the complexes with ligands substituted at the α position (Figure 26, R = phenyl, benzyl, pyridyl, or naphthyl groups). The rest of the compounds present deviations from the elongation path of $<5\%$, including those with less bulky substituents at the α carbon of the pyrazol rings, such as methyl, *i*-propyl, *n*-pentyl, cyclopropyl, cyclobutyl, or trifluoromethyl.

Inspection of the structures with a degree of elongation greater than 20% reveals that they correspond to d⁰, d⁵, and d¹⁰ ions: Cd(II),^{120–129} Mn(II),^{130–133} Y(III),^{134,135} and Ag(I).^{136,137} An outlier found among the TpM complexes at S(O_{C-6}) ≈ 3.8 (Figure 27b) represents a Cd compound¹²⁰ in which the benzyl-1,8-naphthalimide groups hanging from the pivotal carbon atom of TpM introduce severe steric strain that may explain a different distortion mode. It undergoes an elongated Bailar twist of 41% instead, with a very small deviation from that distortion pathway (0.8%). Of the wide portion of the path covered by all complexes, the change in spin state in an Fe(II) spin-crossover system occurs with a small yet detectable shift,^{138,139} and all the TpM complexes with that ion

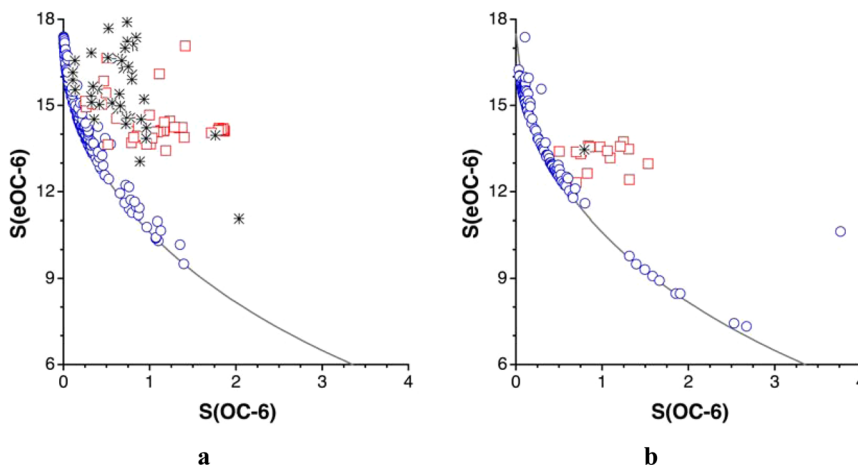


Figure 27. (a) Six-coordinate trispyrazolylborate ($X = B$) and (b) trispyrazolylmethane ($X = C$) complexes of type **28** in a shape map for the distortion of the octahedron to an elongated trigonal antiprism ($eOC-6$). Cu(II) complexes are represented by squares, complexes with $R =$ phenyl or related groups are represented by asterisks, the rest are represented by circles, and the continuous line represents the minimal distortion path.

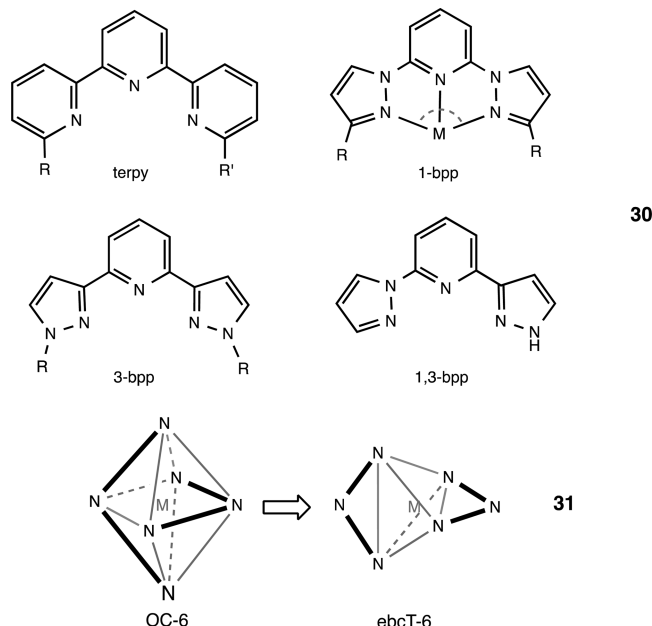
appear to be the least distorted ones from the octahedral geometry. Finally, a bird's-eye view of the two shape maps (Figure 27) shows that the complexes with TpM cover a wider range of elongation distortions than the TpB analogues. The fact that, on average, the C–N distances in TpM ligands are 0.1 shorter than the B–N distances in TpB analogues, and consequently the N–M–N bond angles are 2° smaller may, account for the enhanced elongation of the coordination octahedron seen in the TpM complexes (Figure 27b).

A handful of compounds with two related claw ligands in which the pyrazol rings of TpB are replaced by N-heterocyclic carbenes also present small distortions of the octahedron along the elongated trigonal prism path (between 3 and 7%) and right along the path (path deviations of 0.2% at most).^{140–144} Similarly, a few complexes with two tridentate $RC(CH_2PR_2)_3$ claw ligands present twist-elongated structures with up to 31% distortions toward the elongated trigonal prism.^{145–149}

14. CLAMP (OR PINCER) LIGANDS: TERPYRIDINE AND BIS(PYRAZOLYL)PYRIDINE

Tridentate ligands that coordinate in a *mer* mode in octahedral complexes include terpyridine (terpy) and the bpp (bpp = 2,6-di[pyrazolyl]pyridine) isomers 1-bpp, 3-bpp, and 1,3-bpp (**30**). Wider information on spin-crossover systems with ligands of this family can be found in recent reviews.^{150–152} By schematically representing the arrangement of the chelate rings along the edges of a coordination octahedron (**31**), we can have a visual perception of how the octahedral (OC-6) coordination sphere may be deformed toward an edge-bicapped tetrahedron (ebcT-6) as the M–N distances increase, e.g., upon transition from low- to high-spin states.¹⁵⁰

A remarkable structural behavior is observed for the $[Fe(terpy)_2]^{2+}$ complexes when their structural data is displayed in a shape map relative to those two reference shapes (Figure 28), where we see that two different stereochemical regimes exist, one for the low-spin complexes, which show similar degrees of distortion toward the edge-bicapped tetrahedron, and another for the high-spin complexes, which go from geometries much more distorted toward the capped tetrahedron to geometries that significantly deviate from that path, apparently following a well-defined track.



The vast majority of complexes in this family are unsubstituted at the α positions (i.e., $R = R' = H$ in **30**), and practically all of them are low-spin compounds. The only exception is $[Fe(terpy)_2]$, whose magnetic properties have been interpreted as due to an iron(II) ion coordinated by two terpyridine radical anions.¹⁵³ The two independent iron atoms of this compound fall right on the minimal distortion pathway between the octahedron and the bicapped tetrahedron, and so does the one in a compound with two methyl groups at the α positions.¹⁵⁴ The rest of the high-spin compounds have two characteristics in common: they bear substituents at the α positions, such as phenyl, *p*-tolyl, or pyridyl, and they deviate from the capped tetrahedron path. Our analysis shows that such deviation can be associated with the presence in all cases of additional weakly coordinating interactions from those substituents.

The high-spin structure that deviates most from the bicapped tetrahedron path in Figure 28 is that of the dinuclear complex cation¹⁵⁵ $[Fe_2(septpy)_2]^{4+}$, in which each bridging septipyridine ligand employs its outermost pyridyl groups to coordinate to the two iron atoms in a clamp mode, whereas the central

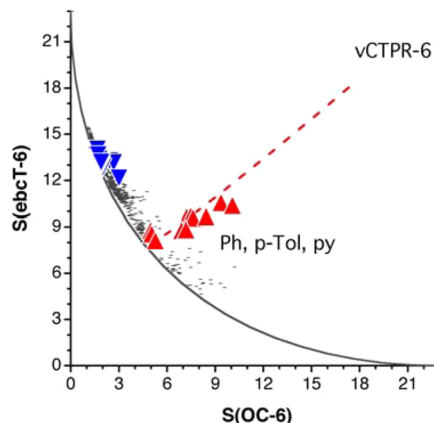


Figure 28. Shape map for metal complexes with two ligands having the terpyridine skeleton (dots), with the Fe^{II} low-spin complexes represented by downward triangles and the high-spin ones represented by upward triangles. The continuous line represents the minimal distortion path between the octahedron and the edge-bicapped tetrahedron (ebcT-6), and the dashed line corresponds to a projection of the minimal distortion path from an intermediate geometry to the vacant capped trigonal prism (vCTPR-6).

pyridyl remains uncoordinated but establishes a short contact to one of the iron atoms at 2.88 Å (Figure 29), much shorter

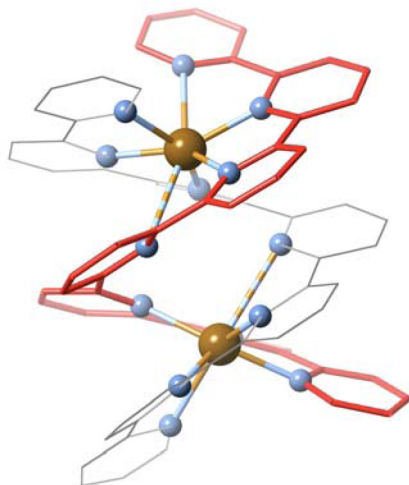
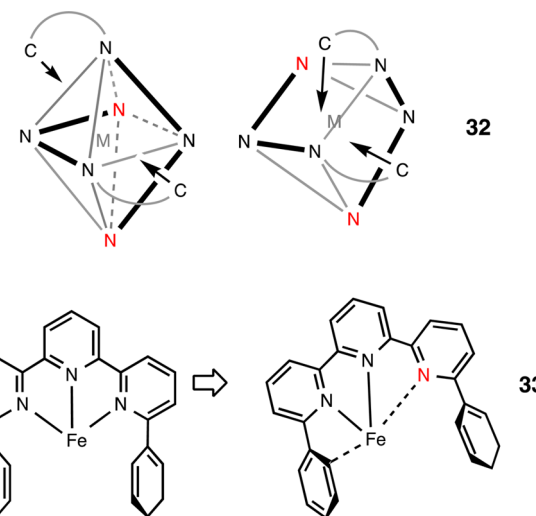


Figure 29. Molecular structure of the $[\text{Fe}_2(\text{septipyridine})_2]^{4+}$ complex,¹⁵⁵ in which incipient $\text{Fe}-\text{N}$ bonds from the central pyridyl group are indicated by multibar sticks.

than the sum of the van der Waals radii⁷⁶ (4.10 Å). A related situation appears in a mononuclear complex with the quaterpyridine ligand,¹⁵⁶ whose pending pyridyl rings establish short contacts with the Fe atom at 2.82 Å. In both cases the incipient coordination of pyridyl rings should account for the new distortion pathway toward a capped or a bicapped trigonal prism. This is shown in the shape map by plotting the position of the ideal structures that are distorted toward a capped trigonal prism starting from a geometry intermediate between the octahedron and the edge-bicapped tetrahedron, at a 43% distortion along that path (dashed line in Figure 28).

Another group of high-spin terpy complexes feature a phenyl or *para*-tolyl substituent at the α position of at least one of the external pyridyl groups.^{157–159} It must be noted that, in the case with only one phenyl substituent ($R = \text{H}$, $R' = \text{Ph}$), the

complex cation appears in its low-spin state at 193 K with perchlorate as a counterion but in its high-spin state at room temperature with hexafluorophosphate as a counterion.¹⁵⁸ In the low-spin case, the pending Ph group is oriented perpendicular to the terpyridine group, the *ipso* carbon atom is held at a distance of 3.44 Å from Fe, and the two α carbon atoms are at 3.86 and 4.11 Å. In the high-spin form, the phenyl group is rotated, approaching one of the α carbon atoms at 3.40 Å, which could be taken as indicative of an incipient η^2 coordination,¹⁶⁰ especially if we compare that distance with a van der Waals radii sum⁷⁶ of 4.21 Å. In the complexes with two α phenyl or *p*-tolyl substituents at the terpyridine framework,^{157,158} similar contacts between the pending phenyl rings and the iron atom are found, only in this case two of the $\text{Fe}-\text{N}$ bonds are significantly elongated, as if one were in a ligand-substitution pathway. The incipient coordination of the α carbon atoms is directed toward two edges of the idealized octahedron, or toward two square faces of the ideal trigonal prism, as illustrated in 32. Interestingly, the symmetric substitution in diphenylterpyridine and similar ligands induces an asymmetric coordination associated with its tilting (33), in such a way that one of the phenyl rings gets closer to Fe while the other gets farther away, avoiding steric repulsion and pulling away its neighboring donor atom. It seems clear that the extra distortion of these high-spin complexes is associated with the existence of such weak coordinating interactions, more likely than to the existence of π -stacking interactions.¹⁵⁷



A particularly interesting case is that of the sexipyridine binuclear complex,¹⁵⁵ in which one iron atom is in the high-spin state, the other is in the low-spin state at 253 K, and each of them appears in the corresponding regions of the shape map (Figure 28). Although the two Fe atoms present short η^2 contacts with neighboring pyridyl rings at similar distances, it must be considered that the covalent radii for the former is 0.2 Å longer,³ and one can hypothesize that the weak interaction is more effective in promoting a further distortion of the coordination polyhedron for the high-spin center.

It is particularly illustrative to try to correlate the stereochemistry and the existence of intermolecular $\text{Fe}\cdots\text{X}$ contacts in two compounds with spin-crossover behavior, $[\text{Fe}(1-\text{bpp})_2]\text{(BF}_4)_2$ and $[\text{Fe}(1-\text{bpp})_2]\text{(BF}_4)_2\text{-H}_2\text{O}$. A plot of the shortest intermolecular distance from Fe to a potential donor atom (F in these two cases) as a function of the average $\text{Fe}-\text{N}$ bond distance (Figure 30) shows clearly how the transition from the

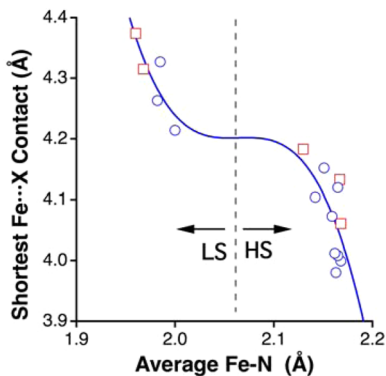


Figure 30. Shortest Fe...X intermolecular contact as a function of the average Fe–N bond distance in the structures of $[\text{Fe}(1\text{-bpp})_2](\text{BF}_4)_2$ (squares) and $[\text{Fe}(1\text{-bpp})_2](\text{BF}_4)_2 \cdot \text{H}_2\text{O}$ (circles) determined at different temperatures.⁷⁷

low- to the high-spin state significantly facilitates the approach of a weakly interacting species, at distances consistent with the sum of the corresponding van der Waals radii (3.9 Å). A similar behavior is found for a PF_6^- salt in its high-spin state¹⁶¹ ($\text{Fe}-\text{N} = 2.171$ Å, $\text{Fe}-\text{F} = 3.545$ Å). We can summarize the behavior of the iron(II) terpyridine and topologically related complexes by saying that the low-spin centers present moderate distortions from the octahedral geometry in the direction of the edge-bicapped tetrahedron while the high-spin centers present the same distortion mode to a higher degree. Moreover, the high-spin iron atoms experience additional distortions associated with the existence of weak coordinating interactions that are favored intramolecularly by the presence of phenyl or pyridyl groups at the α positions of terpy. Intermolecular interactions with counteranions are also found to be favored in the high-spin state.

The stereochemical trends of iron(II) complexes with the topologically analogous bpp ligands have been analyzed recently,¹⁵⁰ and the opening up of new coordination sites in the high-spin centers and the presence of weak coordinating interactions have been already discussed, although we had used at that time the less-precise Bailar path as the reference distortion mode. Thus, for the sake of consistency, we show here their behavior in a shape map relative to the octahedron and the edge-bicapped tetrahedron (Figure 31). In this family, two secondary coordination interactions are associated, in general, with the deviations from the bicapped tetrahedron path, and the geometries are intermediate between those leading to a bicapped trigonal prism (with the two extra donor atoms approaching the capping sites); those that tend to a hexagonal bipyramidal consistent with the torsion angle between the two ligand planes are discussed elsewhere.¹⁵⁰

A series of complexes recently synthesized by Cipressi and Brown with noninnocent clamp ligands containing the core shown in 34¹⁶² are also found to closely follow the ebcT-6 distortion pathway with degrees of distortion that range from 36% (Ni, Ru) to 52% (Mn). A trigonal distortion proposed by the authors is not supported by a shape analysis, which indicates deviations from that path of at least 23%, compared to deviations from the ebcT-6 path of 5% or less.

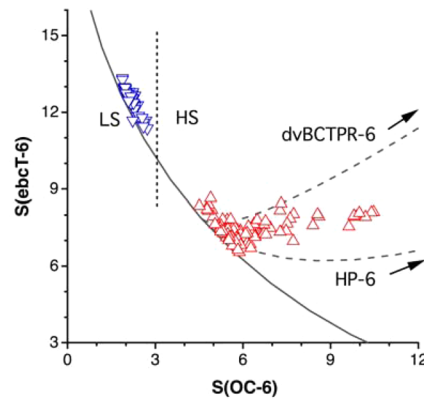
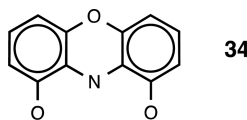
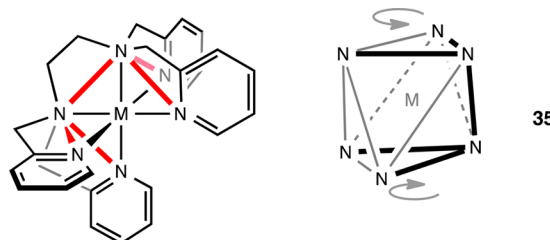


Figure 31. Shape map for iron(II) complexes with two 3-bpp ligands (30) in low-spin (downward triangles) and high-spin states (upward triangles). The continuous line represents the minimal distortion path between the octahedron and the edge-bicapped tetrahedron, and the dashed lines correspond to projections of the minimal distortion paths from an intermediate geometry to the divacant bicapped trigonal prism (dvBCTPR-6) and to the planar hexagon (HP-6).

15. SAWHORSE HEXADENTATE LIGANDS

In Fe complexes, the hexadentate ligands with the sawhorse topology shown in 35 have two chelated edges on parallel faces of the coordination octahedron, linked by another chelate unit that may act as a hinge. As the Fe–N bond distance increases, the torsion angle between the two chelated faces decreases, showing a good linear correlation (Figure 32a). The flattening of the coordination polyhedron produced by the shortening of the edge spanned by the ethylene linker is compensated by the shortening of the edges of the trigonal faces, therefore adjusting the distortions to a canonical Bailar path (Figure 32b).



16. EQUATORIALLY COORDINATED OPEN-CHAIN TETRADENTATE LIGANDS

Open-chain tetradentate ligands such as bis(salicylenealminato) 36a or triethylenetetraamine (36b) and topologically equivalent ligands constrain three of the four equatorial edges of the octahedron in the trans complexes. Depending on the ligand skeleton, the longer metal–ligand distances may favor a widening of the nonchelated equatorial edge, leading to an equatorially vacant pentagonal bipyramidal (vPBPY-6, 37a). A shape analysis of the salen complexes 36a confirms that their structures appear close to the minimal distortion pathway that goes from the octahedron to the vacant pentagonal bipyramidal (Figure 33a). As in other families, the low- and high-spin states of iron complexes occupy clearly separated zones along the path, with the low-spin ones being much less distorted and the high-spin ones with longer metal–ligand distances presenting much larger distortions from the octahedron. The structures that resemble most a vacant

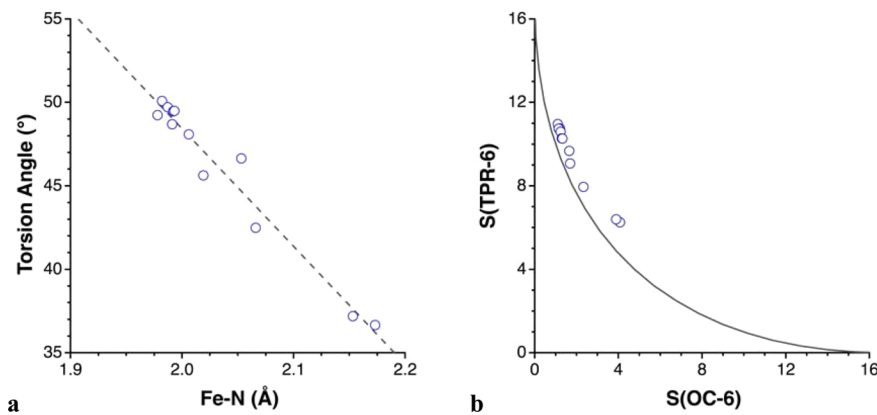


Figure 32. Correlation between the average Fe–N bond distance and the torsion angle of the two trigonal faces spanned by the two terminal chelate rings formed by sawhorse ligands **35** in Fe complexes (a) and position of their structures in a Bailar shape map (b).

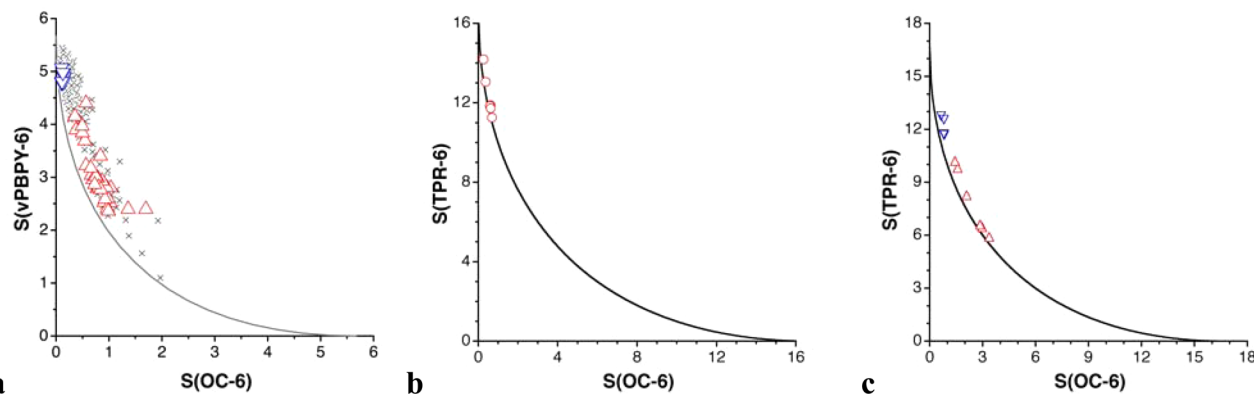


Figure 33. (a) Shape measures of six-coordinate iron *trans*-bis(salicylenealdiminato) complexes (**36a**) of low-spin (downward triangles) and high-spin (upward triangles) states and analogous complexes with other metal ions (crosses). (b) Bailar shape map for complexes with open-chain N₄-tetridentate ligands (squares) with a skeleton of type **36b**. (c) Bailar shape map for complexes **36d** in high-spin (upward triangles) and low-spin (downward triangles) states.

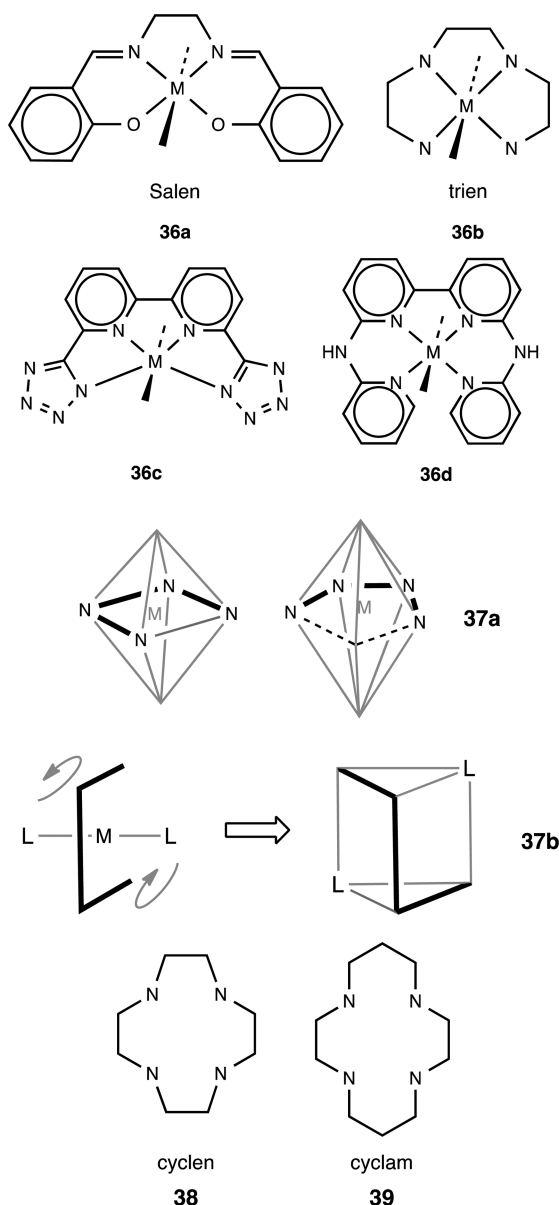
pentagonal bipyramidal belong to Ti and V complexes,^{163–166} for which we expect long metal–ligand distances according to their atomic radii (Figure 1). Even the heavier transition metals Ru and Os, with smaller atomic radii (Figure 1), consistently present less-distorted octahedral structures. An Fe(II) spin-crossover complex¹⁶⁷ with ligand **36c** also is well-described by the vacant pentagonal bipyramidal pathway, but now much closer to this ideal shape, especially in its high-spin version, with $S(vPBPy-6) = 0.20$, indicative of a nearly perfect vacant pentagonal bipyramidal.

It must be noted that the ethylenediamine linker that bridges the two salicyleneimine groups in **36a** has some degree of flexibility, and it can act, therefore, as a hinge while the salicyleneimine groups act as rigid panes in a torsion that induces a loss of planarity of the four donor atoms, therefore combining some degree of trigonal twist **37b** to the square-to-pentagonal distortion **37a** just discussed. Thus, while in the octahedral structures the two NNO planes of salen are coplanar, in those more twisted toward the trigonal prism the angle between them can be as large as 13°,^{163,168,169} still a small torsion angle, due to constraints imposed by an skeleton with double and aromatic bonds. Related tetradeinate ligands with an aliphatic backbone of type **36b** result in enhanced flexibility around the hinge and distortions from the octahedral geometry that correspond to a Bailar twist (Figure 33b). In contrast, analogous ligands with double-bonded skeletons are best described as distorted toward the vacant pentagonal bipyramidal,

with a Ru and a Ni complex^{170–172} being rather close to that shape. Another possibility is to add an sp^3 link to the two outer chelating units that provides enough flexibility as to respond to stretching of M–L bonds with a Bailar twist. This can be seen in the family of spin-crossover Fe(II) complexes with ligand **36d** (Figure 33c), which once again present different degrees of twisting (torsion angles around the central hinge of up to 21°) depending on their spin state.^{173–175}

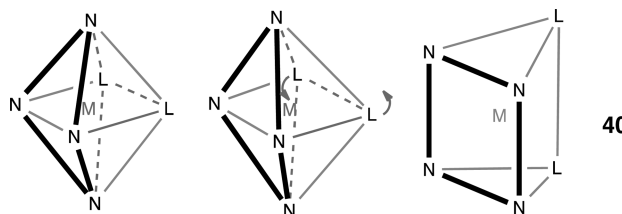
17. MACROCYCLIC TETRADENTATE LIGANDS

In an octahedron, a macrocyclic tetradentate ligand can occupy either four equatorial coordination sites in a *trans* isomer or two neighboring faces in a *cis* isomer. The degree of flexibility of the macrocycle has some say on this choice, and in the case of cyclen (38) only *cis* complexes are found, whereas the more flexible cyclam (39) can be found in both conformations. The rigid porphyrinato and phthalocyaninato ligands, on their side, always occupy equatorial positions in *trans*-octahedral complexes, but they can also be found in *cis*-trigonal prismatic complexes occupying a square face³² when the transition metal has a d^0 to d^2 electron configuration, for which the trigonal prism is a good stereochemical choice. Of interest to the present discussion, a variety of complexes with tetradentate macrocyclic ligands have been found to present spin crossover.¹⁷⁶



The inequality of the edge lengths associated with variations in the metal–ligand bond distances may induce a planarization of the macrocyclic cyclen and cyclam ligands in the cis

complexes that heads toward a slightly distorted trigonal prismatic geometry (40). This qualitative expectation is confirmed by the corresponding shape maps (Figure 34a). In the cyclen family, the structures that appear closer to the trigonal prism correspond to metal ions with a d⁰ configuration, Sc(III)¹⁷⁷ and Y(III).¹⁷⁸ The next most prismatic structure of this family (at S(TPR-6) ≈ 7) is that of a Cr(III) complex.¹⁷⁹ As for the *cis*-cyclam complexes, those structures that appear from the middle of the path to the trigonal prismatic end (Figure 34b) all correspond to Zr and Hf complexes.



Whereas no structures have been found of cyclen complexes in the trans conformation, there are a host of cyclam complexes with that stereochemistry. Interestingly, the cyclam ring can adapt to variations in size of the metal atom within, reflected by average M–N distances in the range 1.93–2.18 Å, which have a negligible effect on shifting the metal atom out of the N₄ plane. Given the existence of chelate rings of two different sizes, there is, however, a rectangular distortion of the equatorial plane. Therefore, we show the normalized polyhedra (to disregard the trivial axial elongation upon increasing M–L_{ax} bond distances) in the elongated rectangular bipyramidal shape map (Figure 35), which represents very closely the distortions found in this family of complexes. The compound that deviates most from that path is a tetramethylcyclam Cu(II) complex¹⁸⁰ in which the substituents force a significant deviation of the two weakly bound aqua ligands from the axial directions. Another outlier comes from a powder diffraction structure of a Mn complex.¹⁸¹

18. OPEN-CHAIN PENTADENTATE LIGANDS

The open-chain pentadentate ligands **41** seem to have enough flexibility thanks to their central propyl linkers. Therefore, in spite of the asymmetric distribution of the chelate rings in both the cis and trans arrangements of the two ends of the ligand (**42**), these structures are roughly aligned along the Bailar path (Figure 36a), even if with a somewhat higher dispersion than

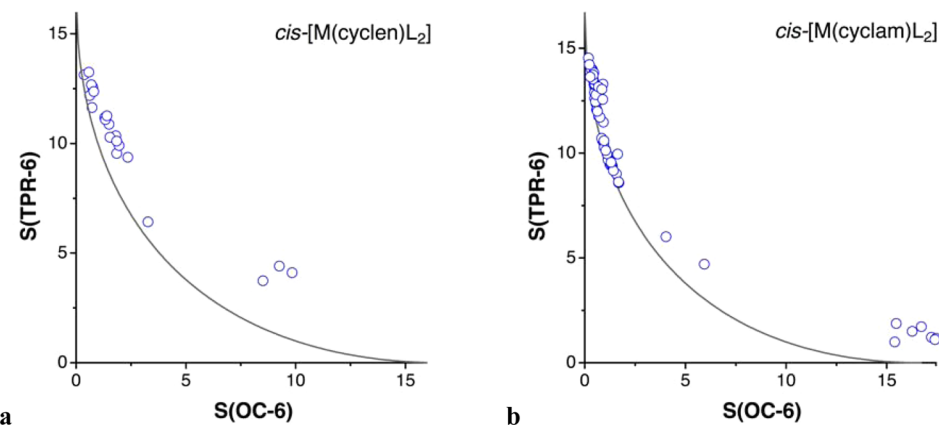


Figure 34. Shape map for the Bailar interconversion of the octahedron and the trigonal prism (continuous line) showing the stereochemistries of the *cis*-[M(cyclen)L₂] (a) and *cis*-[M(cyclam)L₂] (b) complexes.

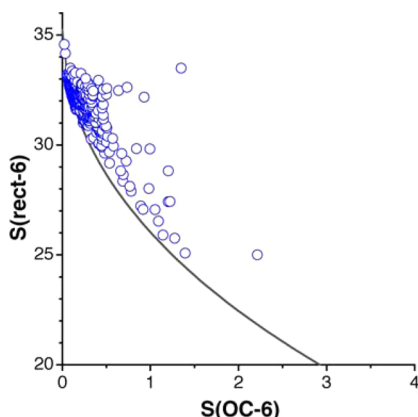
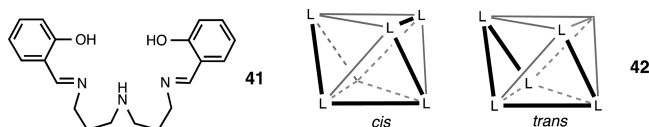


Figure 35. Shape map for the rectangular bipyramidal distortion path of the octahedron (continuous line) showing the stereochemistries of the normalized polyhedra of *trans*-[M(cyclam)L₂] complexes (circles).

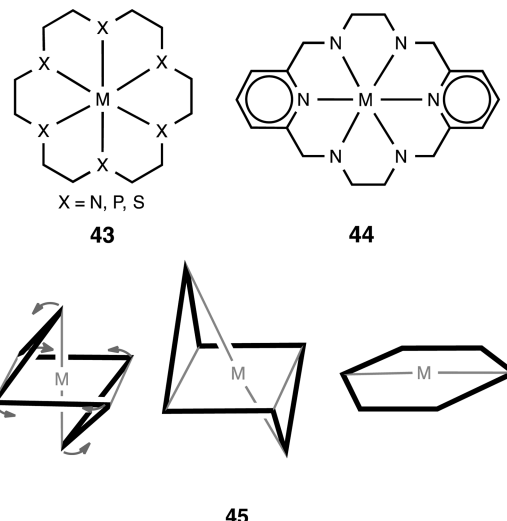
found for the bis- and tris(bidentate) systems. Within this family, some Fe(III) complexes present spin crossover,¹⁸² and the low- to high-spin transition is clearly reflected in the average Fe–N bond distances and in the degree of distortion toward a trigonal prism measured by the Bailar generalized coordinate (Figure 36b).



19. MACROCYCLIC HEXADENTATE LIGANDS

Shape analyses of complexes containing aliphatic hexadentate macrocyclic ligands such as hexaaazacyclooctadecane and hexathiacyclooctadecane (43) indicate (Figure 37a) that, with some exceptions, they follow the pathway from the octahedron to the planar hexagon (45). The structures that deviate most from that path belong to complexes with macrocycles containing X₄Y₂ mixed donor atom sets, such as S₄N₂ or P₄S₂, not only because of the different M–X and M–Y distances but especially because of the substantial differences in the bite angles corresponding to XX or YY chelate rings (i.e.,

different edge lengths). For that reason, the use of normalized coordination polyhedra does not indicate angular distortions consistent with the expected pathway. The compound that shows the most extreme distortion along the hexagonal path is a Cd(II) complex,¹⁸³ and the hexagonal distortion is clearly appreciated in the structure shown in Figure 38. It is remarkable that complexes with hexadentate macrocyclic ligands distort in much the same way as those with two open-chain tridentate ligands in a *trans* conformation (24 and Figure 24).



When the hexadentate macrocycle is composed of two pyridyl rings linked by two ethylenediamine backbones in the pyridylcoronands 44, the complexes present a different kind of distortion (Figure 37b), which goes from the octahedron to the edge-bicapped tetrahedron, similarly to what is found for complexes with two clamp ligands such as terpyridyne (31 and Figure 28), thus attesting to the flexibility of the ethyl bridges in comparison with the rigidity of the diaminopyridyl moieties.

20. OPEN-CHAIN HEXADENTATE LIGANDS

Open-chain hexadentate ligands of the types shown in 46 and 47 have been found to favor spin-crossover behavior in Fe(III) complexes.¹⁸² These two families of ligands differ in the length

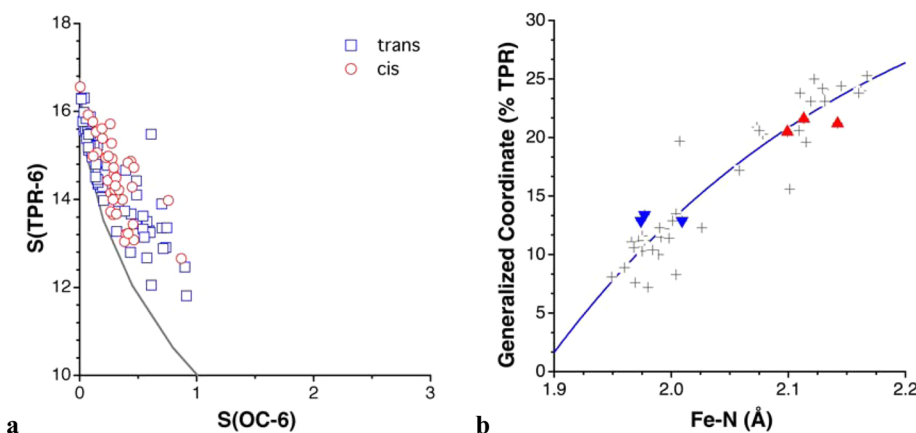


Figure 36. (a) Shape map for the Bailar distortion of the octahedron in a family of complexes with open-chain pentadentate ligands of type 41 in both *cis* (circles) and *trans* (squares) arrangements of the two ends of the ligand (42). (b) Generalized coordinate along the Bailar path as a function of the average Fe–N distance for *trans*-Fe complexes (crosses), highlighting those Fe(III) compounds that present spin crossover^{183,184} (downward triangles for the low-spin structures, upward triangles for the high-spin structures).

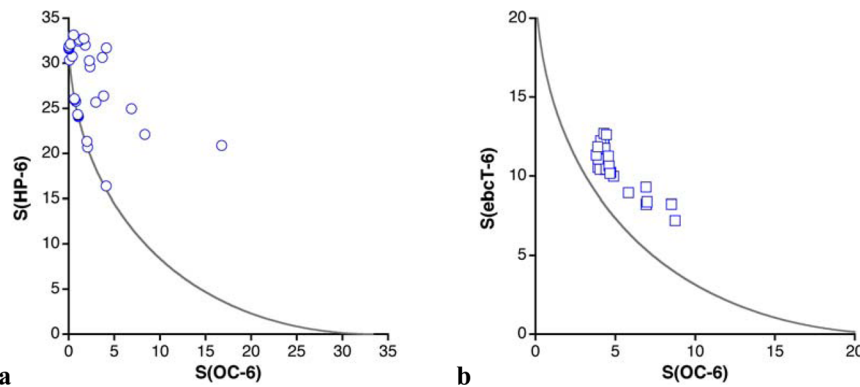


Figure 37. Shape maps for complexes with (a) aliphatic- and (b) bispyridyl-based hexadentate macrocyclic ligands of types 43 and 45, respectively.

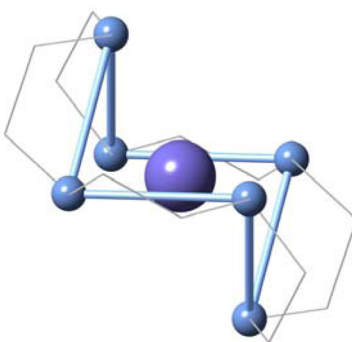
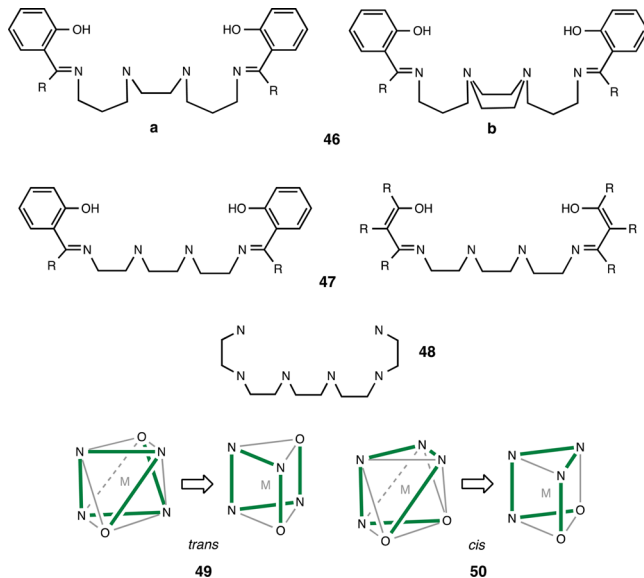


Figure 38. Cd(II) complex with an aliphatic hexadentate macrocyclic ligand¹⁸⁵ that presents the strongest distortion along the path from the octahedron to the planar hexagon.

of the chains holding the six donor atoms, to which we could add a third group of shorter chains with the topology shown in 48. A structural analysis of six-coordinate complexes of all transition metals with those ligands shows that the ones with the longest chains (46) present in practically all cases a trans conformation (49), with the only exception of a cis-Fe(III) compound.¹⁸⁶ In contrast, the intermediate-length chains 47 appear in all their complexes with the two end donor groups occupying cis coordination sites of the octahedron (50) and so do the shortest 16-atom chains 48, with the only exception of two Mn(II) compounds^{187,188} that have a nearly trigonal prismatic structure resulting from twisting an octahedral molecule with a trans conformation (49). It is interesting to point out that one of these cationic Mn complexes also



crystallizes in the alternative cis geometry with a different anion.¹⁸⁹

A shape analysis shows that the compounds with ligands of topology 46a are well-aligned along the Bailar path (Figure 39a), twisted up to 38% toward the trigonal prism, except for an Fe(III) complex that is nearly trigonal prismatic,¹⁹⁰ a geometry that is probably favored by the presence of a second ethyl strand linking the two central nitrogen atoms (46b). The compounds with the 18-atom chain ligands 47 also follow quite closely the Bailar path (Figure 39b) but going farther along that

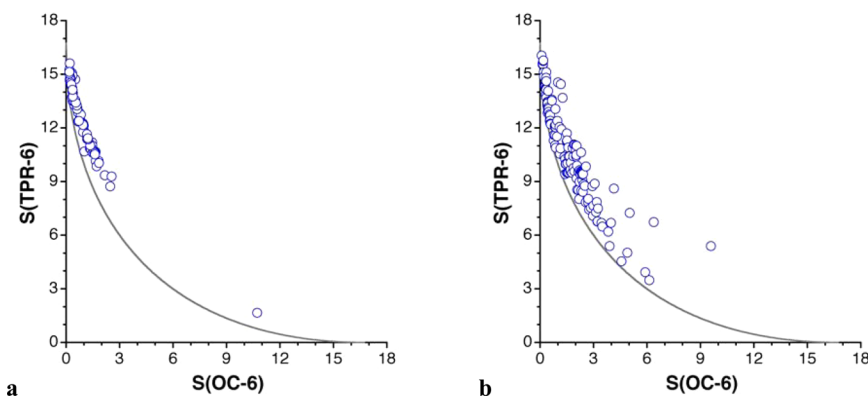


Figure 39. Complexes with open-chain hexadentate ligands 46 (a) and 47 (b) in Bailar shape maps.

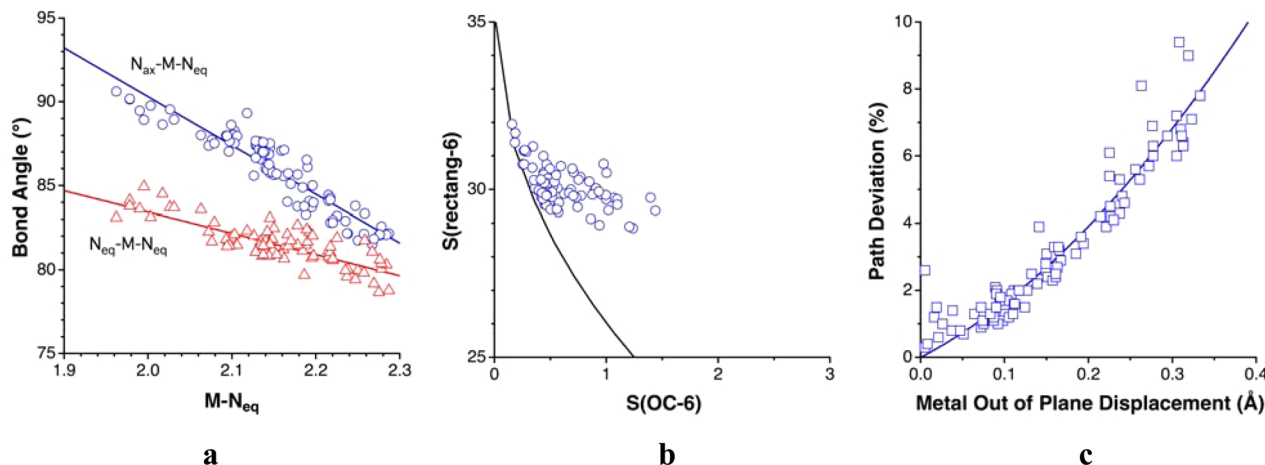
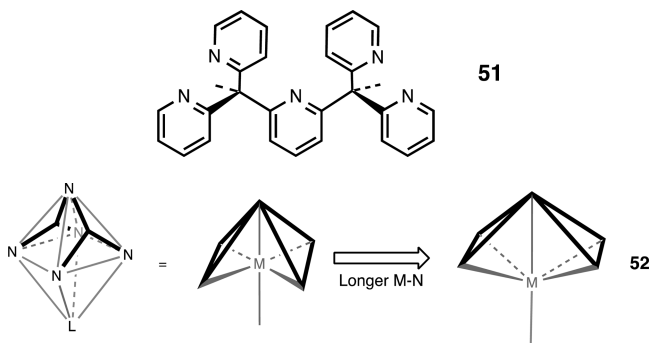


Figure 40. (a) Correlation between the bond angles subtended by the pentadentate ligand and the average $M-N_{eq}$ bond distance in complexes with paneling ligands **51**. (b) Position of the normalized coordination polyhedra of those complexes in a shape map relative to the octahedron and the rectangular bipyramid and (c) dependence of the path-deviation function on the out-of-plane displacement of the metal atom.

path, as illustrated by the two most twisted structures in two Fe(III) complexes^{181,191,192} that present nearly a 60% rotation toward the trigonal prism. Only four outliers are found among this family, corresponding to Mn(II) and Cd(II) complexes,^{193,194} precisely those with the longest average $M-N$ distances (2.6 Å or longer). Finally, the ligands with the shortest chains of type **48** present larger deviations from the Bailar pathway, because the shorter chelated edges result in a distortion of the coordination octahedra toward isosceles triangular prisms.

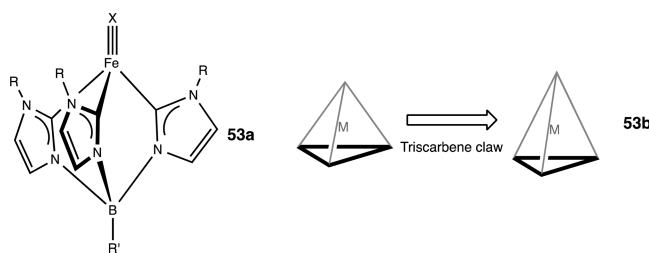
21. PANELING LIGANDS

The pentadentate ligands shown in **51** can panel two triangular faces of an octahedron. The distribution of the chelate rings is expected to result in an uncommon distortion of the coordination sphere with four N_{ax} -M- N_{eq} and two N_{eq} -M- N_{eq} bond angles smaller than 90°, which leads to a rectangular umbrella shape (**52**). The dependence of the bond angles affected by the chelate rings on the average $M-N$ distance can be clearly seen in Figure 40a: the longer the distance, the smaller those angles become. The octahedron–rectangular bipyramidal distortion path introduced earlier can reasonably describe those geometric changes, as seen by the many complexes that appear along the path or close to it (Figure 40b). A closer look at the structures tells us that the deviations from the rectangular bipyramidal pathway are essentially due to the displacement of the metal atom out of the equatorial plane formed by four pyridyl N atoms, which leads to a nice correlation between the shift of the metal atom from that plane and the path-deviation function (Figure 40c).



22. CLAW LIGANDS IN FOUR-COORDINATED COMPLEXES

Four-coordinate complexes featuring a triscarbene ligand **53a** have been prepared by Smith and co-workers,¹⁹⁵ and some of the Fe(II) members of this family have been found to present spin-crossover behavior. Because the $M-X$ bond to the monodentate ligand in many cases has multiple bond character (X can be, e.g., nitride, nitrosyl, or an imide), there are often large differences in bond distances between the $M-X$ and the $Fe-C$ bonds that result in a distortion of the coordination sphere from the tetrahedron. To discriminate the angular distortions associated with spin crossover from the intrinsic bond-length distortion, normalized coordination polyhedra¹⁵ have been used for the shape analysis of this family of complexes.



It has been noticed already that the triscarbene claw is quite closed (sum of C-Fe-C bond angles $\Sigma = 273^\circ$) compared to the angular requirements of the tetrahedron ($\Sigma = 328^\circ$). The outcome of such a geometric feature of this triscarbene ligand is that in four-coordinate complexes the coordination sphere is significantly distorted from the tetrahedron toward an elongated trigonal pyramidal geometry (**53b**), i.e., a closed claw (CL-4). Thus, the normalized coordination spheres of all complexes of this family are nicely displayed along the pyramidalization path that goes from the tetrahedron to a closed claw (Figure 41a). Elongation of $M-C$ bonds with a rigid ligand should result in a closing of the claw, or a decreased Σ value (**54a**), and, consequently, a greater distortion from the tetrahedron to an elongated trigonal pyramid. However, a poor correlation is found between the $M-C$ distance and Σ . Moreover, if we focus on the Fe(II) complexes, we note that

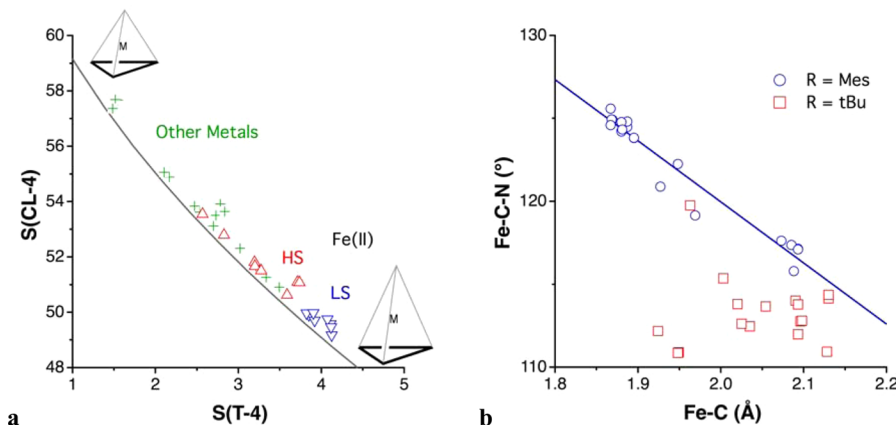
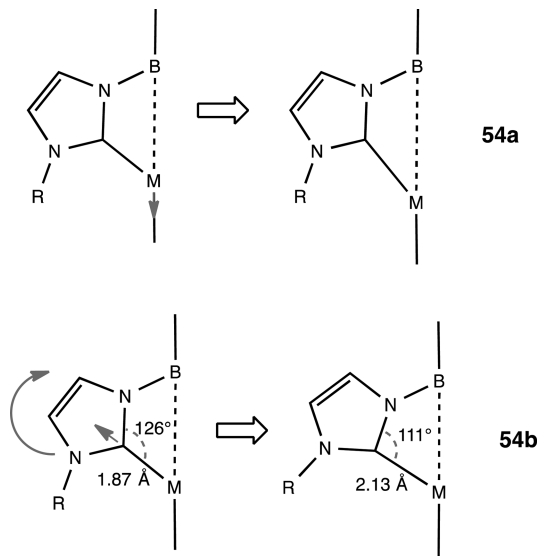


Figure 41. (a) Shape map for the four-coordinate triscarbene metal complexes relative to the ideal tetrahedron (T-4) and the closed claw (CL-4). (b) Behavior of the mesityl- (circles) and *t*-butyl-substituted (squares) triscarbene four-coordinate Fe(II) complexes regarding the dependence of the orientation of the carbene rings (measured by the M–C–N bond angle) on the metal–ligand bond distance.

they are more pyramidalized in the low-spin state, contrary to the expectations for rigid claws schematized in **54a**.



A closer look at the structures reveals that in this case the elongation of the M–C bonds induces a reorganization of the

claw that barely affects the bond angles around the metal. The most significant changes are found in the M–C–N and C–N–B bond angles, indicating that the elongation of the M–C bond induces a twist of the carbene rings, especially when the N-substituent is a mesityl group. The geometrical response of the claw to a bond elongation can be illustrated by comparing two Fe(II) complexes, one with a low-spin configuration¹⁹⁵ ($Fe-C = 1.87 \text{ \AA}$) and the other in a high-spin state¹⁹⁶ with much longer $Fe-C$ bond distances (2.13 \AA), whose different carbene ring orientations (**54b**) are evidenced by the quite different $Fe-C-N$ bond angles. In other words, in this family lengthening of the M–C bond distances is achieved at the expense of distorting the not-so-rigid triscarbene ligand (i.e., opening the claw) rather than by modifying the metal coordination sphere. Such behavior can be exemplified by the correlation between the M–C–N bond angle and the M–C distance in the mesityl-substituted complexes (Figure 41b). The *t*-Bu analogues, in contrast, seem to adapt to bond-distance differences by distorting both the claw and the metal coordination sphere, although the latter seems to predominate. Thus, a Co(III) complex shows the largest claw distortion of type **54b** within this family and appears well aligned with the Mes complexes,¹⁹⁷ whereas for the rest of the members the canonical behavior **54a** seems to predominate. In the low-spin state, the shorter M–C distances approach the bulky

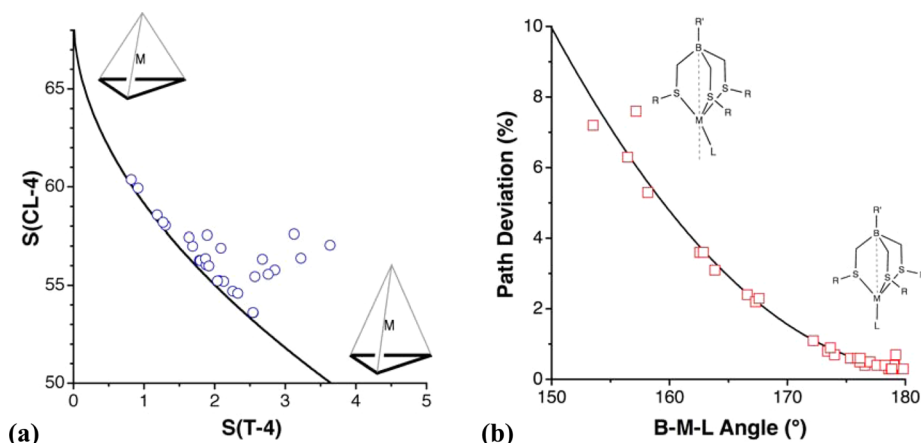
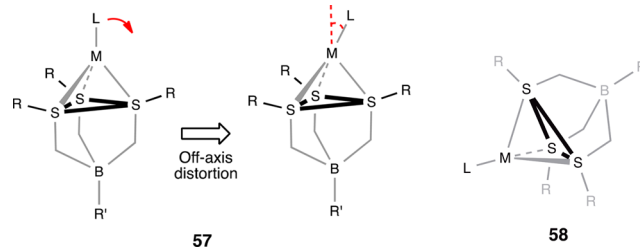
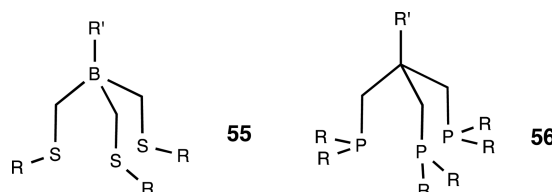


Figure 42. (a) Shape map for four-coordinate complexes with tris(thioether)borate tridentate ligands (**55**) relative to the ideal tetrahedron (T-4) and the closed claw (CL-4). (b) Dependence of the path-deviation function on the off-axis distortion of the monodentate ligand.

substituents at the carbene to the monodentate ligand, therefore enhancing the steric hindrance, which may be avoided by opening up the claw and explaining the counterintuitive behavior of the two spin states in this case.

Regardless of the distortion mechanism that operates to adapt the molecules to varying M–C distances, the distortion of the metal coordination sphere is excellently described by the tetrahedron–closed claw distortion pathway (Figure 41a), with a maximum path deviation of 1.5%. The generalized coordinates indicate that the analyzed structures present distortions from 12.5 to 20.9% along that path. It is noteworthy, for instance, that, while iron is found in this family of complexes in oxidation states from I to V, there seems to be no clear correlation between the deviation from the ideal tetrahedron and the oxidation state. What is clear, however, is that, for the same metal and oxidation state, the ligands with flanking *t*-Bu groups are more open (larger Σ) than those with mesityl. It can be concluded, therefore, that the steric bulk of the N-substituents has an important effect on the degree of distortion of the metal coordination sphere from the tetrahedron: the bulkier the substituent, the closer it is to the tetrahedron.

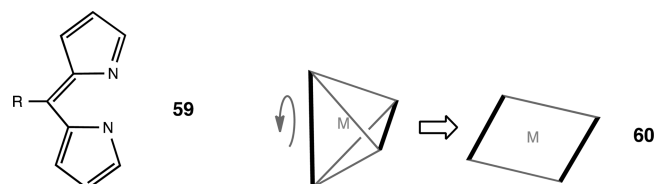
Other topologically related S- and P-donor ligands are those shown in **55** and **56**. The former (with R = *t*Bu in most cases) has similar geometric parameters to the triscarbene ligands just discussed (disregarding those structures in which the metal or sulfur atoms present disorder): $\Sigma_{av} = 285^\circ$ (6), with all values within the range 275–300°; S···S bite = 3.42 (9) Å. Because these claws are significantly more closed than required for a tetrahedral geometry (ideally $\Sigma = 328^\circ$), all those compounds present tetrahedral shape measures in excess of 0.8, with most of them following closely the claw distortion pathway (Figure 42a). A handful of them, however, deviate from the claw distortion path that preserves a trigonal symmetry axis, with the three S-donor atoms occupying the base of a more or less elongated trigonal pyramid path, with path-deviation functions in excess of 3%. A look at their structures shows that they present instead an off-axis distortion of the monodentate ligand (**57**), with the path-deviation function presenting a clear dependence on the B···M–L angle (Figure 42b). Alternatively, such a distortion can be viewed as a coordination mode through which one sulfur atom occupies the apical coordination site of the elongated trigonal pyramid (**58**), at which the constraints imposed by chelate rings result in an off-axis shift of that apical donor atom. We can further observe that all those complexes that deviate >3% from the claw path have Ni^{II} or Co^I, i.e., d⁸ metal ions,^{198,199} with B···M–L angles as small as 157°. As found for the triscarbene ligands, there is no clear correlation between the M–S bond length and the degree of distortion, because both the claw and the metal coordination sphere can adapt well to changes in bond distances. Instead, one can find that the sum of the average S–M–S and M–S–C bond angles presents a fair correlation with the M–S bond distance, and also that those two bond angles present an inverse correlation.



The complexes with the related tris(phosphine) ligand **56** behave similarly, appearing distributed along the claw pathway that distorts the tetrahedron to an elongated trigonal pyramid (Figure 43a), reaching the highest degree of elongation (S(T-4) > 3.5) for a silver(I) complex.²⁰⁰ Also the deviations from that path correspond mostly to off-axis distortions of the monodentate ligand, as seen by the nice correlation between the path-deviation function and the C···M–L angle (Figure 43b).

23. BIS(BIDENTATE) FOUR-COORDINATE COMPLEXES

The deviations of bischelate tetracoordinate complexes from the tetrahedral structure have been analyzed previously with regard to their chiral behavior,²⁰¹ and we show here two families to place their stereochemical variations in the wider context of this paper. Those families comprise the [M-(dipyrin)₂] and [M(bipy)₂] complexes, where dipyrin is the ligand shown in **59**. Although at first sight the topology of the chelate rings in those complexes could be expected to lead to elongated tetrahedra upon lengthening of the M–N bonds, we must remember that bond stretching favors smaller bite angles that may be best suited for a square planar coordination (**60**).



Interestingly enough, the dipyrin complexes show a variety of geometries along the interconversion path between the tetrahedral and the square planar (Figure 44a). Only one Ni(II) and several Pd(II) complexes, however, are truly square planar,^{202–206} whereas the rest show degrees of planarization of at most 62%, achieved by a Cd(II) compound.²⁰⁷

In contrast with the behavior of the dipyrin complexes, the bipyridine analogues (Figure 44b) deviate from the twist pathway as the structures approach the tetrahedron, without ever reaching the tetrahedral geometry. Such a difference can be attributed to the smaller bite of bipyridine (bite angle¹ 73° (2)) compared to that of dipyrin (91° (3)), which prevents its complexes to achieve tetrahedral angles. A breakdown of the structures by metal ions, however, reveals some differences that suggest that the d⁸ electron configuration favors geometries closer to square planar, whereas d¹⁰ ions are closer to the tetrahedron, although in many such compounds the attribution of an oxidation state to the metal is ambiguous because they crystallize with a polyoxometalate anion that has Mo or W in more than one oxidation state. Another ligand with a bite angle similar to dipyrin, bis(diphenylphosphino)butane (dppb), also forms a few four-coordinate complexes that follow closely the square-to-tetrahedron minimal distortion pathway, with Ni

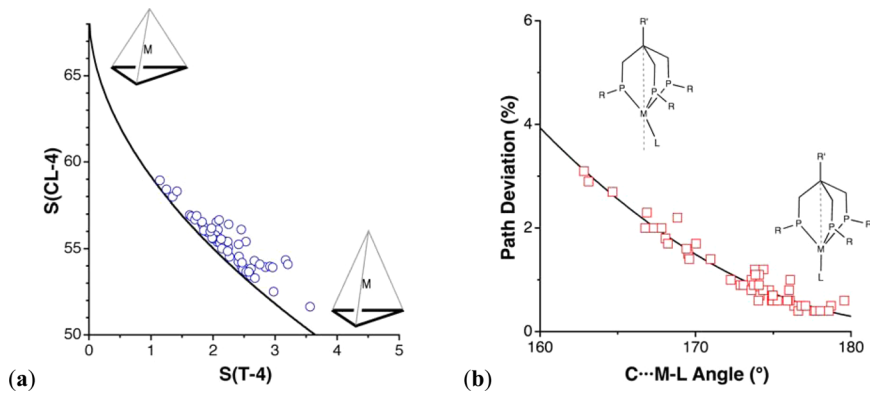


Figure 43. (a) Shape map for four-coordinate complexes with tris(phosphine) tridentate ligands (**S6**) relative to the ideal tetrahedron (T-4) and the closed claw (CL-4). (b) Dependence of the path-deviation function on the off-axis distortion of the monodentate ligand.

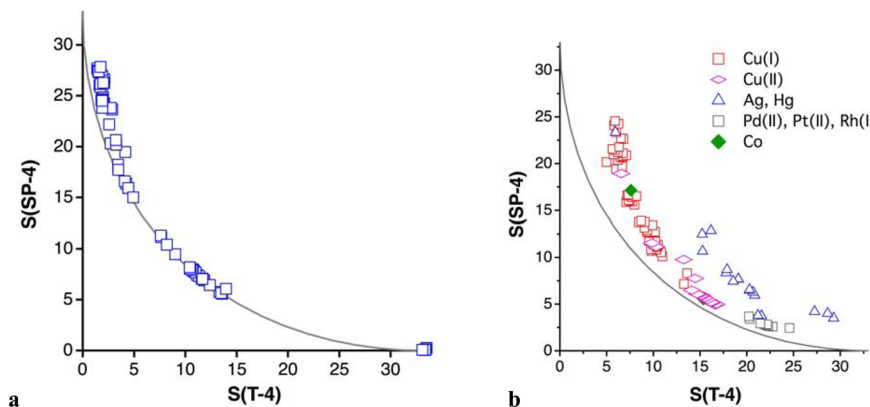


Figure 44. Structures of four-coordinate bischelate complexes with (a) dipyrin (**59**) and (b) bipyridine ligands plotted in a map relative to the square planar (SP-4) and tetrahedral (T-4) reference shapes.

forming practically tetrahedral complexes^{208–210} while Rh is present in an intermediate geometry,²¹¹ 62% along the tetrahedron-to-square path.

24. CONCLUSIONS

In this review I have shown how the combination of topological schemes and continuous shape measure analyses allows us to detect the specific distortion modes that result from metal-ligand bond-distance changes with different arrangements of chelate rings on the edges of a coordination polyhedron. Those distortion modes in most cases can be represented by minimal distortion pathways from a regular polyhedron (e.g., the octahedron or the tetrahedron) to less regular shapes used in this paper and summarized in Table 3 (see also the Methodological Aspects section). Complexes that deviate most from the expected distortion pathways are (a) those with substituents at the α position of a donor atom; (b) those that have both a significant distortion from the regular (e.g., octahedral) geometry and one or more contacts with neighboring donor atoms, often from solvents or counterions; and (c) Cu(II) complexes with significant Jahn-Teller distortion.

To give but a few examples of some trends that can be established from the present shape analysis, the following rules can be stated:

(1) The trischelate complexes follow the Bailar path with bidentate ligands of large bite angles ($81^\circ < \alpha \leq 97^\circ$) but undergo a twist toward a flattened trigonal prism for ligands with a small bite angle ($35^\circ < \alpha < 80^\circ$).

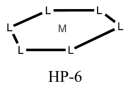
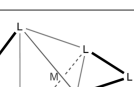
(2) The six-coordinate bischelate complexes present different distortions from the octahedron depending on whether the two monodentate ligands are in trans or cis conformation. While the former distort to a rectangular bipyramid, the latter approach the shape of a tetrahedron in which the two donor atoms of each bidentate ligand occupy a vertex of the tetrahedron, in what could be called a doubled-vertex tetrahedron. The monochelate complexes with four monodentate ligands, on the other hand, distort toward a trapezoidal bipyramid.

(3) The large distortions associated with long metal-ligand distances (e.g., in high-spin complexes) may open new coordination sites that favor the formation of intermolecular contacts with counteranions or solvent molecules. Such interactions are often accompanied by a clear deviation from the minimal distortion path followed by other compounds of the same family and can be intra- or intermolecular in nature. Examples of this intramolecular behavior can be found among the compounds with extended pyridyl tripod ligands that may incorporate a pivotal N atom of the ligand to the coordination sphere, as well as among complexes with two pincer ligands such as terpyridine. In the latter, the general distortive trend from the octahedron to an edge-bicapped tetrahedron is switched to a distortion toward a vacant capped trigonal prism in the presence of such intermolecular contacts. Another example is provided by the coordination (high spin) and decoordination (low spin) of one donor atom of pentadentate macrocyclic ligands upon spin crossover.

Table 3. Distortion Modes Associated to the Topology of Chelate Rings

Ligand set	Distortion pathway	Topology	Distorted Polyhedron
Trisbidentate, large bite Open chain hexadentate Open chain pentadentate	Bailar and anti-Bailar twists		
	Bailar twist		
	Bailar twist		
Tris(bidentate), small bite	Flattened trigonal prism		
<i>cis</i> -Bis(bidentate)	Double-vertex Tetrahedron		
<i>trans</i> -Bis(bidentate)	Rectangular bipyramid		
Mono(bidentate)	Double-vertex Trigonal bipyramid		
Extended tripods	Truncated trigonal pyramid		
Cyclic pentadentate	Pentagonal bipyramid		
Bis(cyclic tridentate)	Elongated trigonal prism		
Mono(cyclic tridentate)	Elongated trigonal prism		
<i>cis</i> -cyclic tetradentate	Distorted trigonal prism		
Bis(open chain tridentate)	Planar hexagon		

Table 3. continued

Ligand set	Distortion pathway	Topology	Distorted Polyhedron
Cyclic hexadentate	Hexagon		 HP-6
Bis(claw)	Elongated octahedron		 eOC-6
<i>mer</i> -Bis(clamp)	Edge-bicapped tetrahedron		 ebcT-6
Open chain tetradentate (rigid hinge)	Pentagonal bipyramid		 vPBPY-6
(flexible hinge)	Bailar twist		 TPR-6
Hexadentate sawhorse	Bailar twist		 TPR-6
Four coordinate complexes			
Tridentate	Trigonal pyramid		 CL-4
Bis(bidentate)	Planarization		 SP-4

(4) A case of intermolecular coordinative interactions triggered by the high-spin state has been identified in Fe(II) complexes with two tridentate clamp ligands.

(5) As the coordination sphere is contracted upon transition to the low-spin state, counterions that are hydrogen-bonded to the ligands may be significantly pulled toward the metal atom, as happens with the chlorides in $[\text{Fe}(\text{pycolylamine})_3]\text{Cl}_2$.

(6) If tridentate ligands that span a trigonal face of the coordination polyhedron are considered, they can either elongate the octahedron to form an elongated trigonal antiprism, as found for complexes with two TpB (trispyrazolylborate) ligands or combine a Bailar twist with an elongation distortion, thus describing a path toward the elongated trigonal prism, as in the case of the triazacyclononane complexes.

(7) Another type of distortion found is a bending away of two opposing trigonal faces of the octahedron, which can be

described by a minimal distortion path to the planar hexagon, presented by the families of *fac*-bis(tridentate) complexes, as well as by complexes with an hexadentate macrocyclic ligand.

(8) In some instances steric effects of substituents occupying α positions relative to the donor atoms can be held responsible for significant deviations from the minimal distortion paths followed by similar compounds lacking those steric effects.

(9) Tetracoordinate complexes with a claw tridentate ligand (e.g., a triscarbene) show evidence of ligand flexibility that results in a poor correlation between the metal–ligand bond distances and the degree of polyhedral distortion, because both the tridentate ligand and the metal coordination sphere present distortive responses to variations in metal–ligand bond lengths.

The relationships between ligand topology and distortion pathways associated with changes in metal–ligand distance are summarized in a graphical way in Table 3.

25. METHODOLOGICAL ASPECTS

All structures that fall along the minimal distortion pathway between two ideal shapes P and T must obey eq 2, where θ_{PT} is a constant that depends exclusively on the two extreme shapes defining the path, according to eq 3.¹³

$$\arcsin\left(\frac{\sqrt{S_{\text{path}}(T)}}{10}\right) + \arcsin\left(\frac{\sqrt{S_{\text{path}}(P)}}{10}\right) = \theta_{PT} \quad (2)$$

$$\theta_{PT} = \arcsin\left(\frac{\sqrt{S_p(T)}}{10}\right) = \arcsin\left(\frac{\sqrt{S_T(P)}}{10}\right) \quad (3)$$

Then, for an arbitrary structure X , we can define its absolute deviation from the minimal distortion path by eq 4, which has the units of an angle in the shape hypersphere of dimension $3N$ (where N is the number of points that define the shape). Alternatively, we can define a relative path-deviation function as a percentage of the total path length (eq 5), which is the path-deviation function implemented in the program SHAPE.

$$\Delta_X(P, T) = \arcsin\left(\frac{\sqrt{S_X(T)}}{10}\right) + \arcsin\left(\frac{\sqrt{S_X(P)}}{10}\right) - \theta_{PT} \quad (4)$$

$$\Delta_X^{\text{rel}}(P, T) = \frac{\Delta_X(P, T)}{\theta_{PT}} 100 \quad (5)$$

The relative path-deviation function used so far in all our stereochemical studies is very useful when one analyzes different structures that may appear all along a given path, as for the Bailar, Berry, and planarization pathways that relate the octahedron with the trigonal prism, the square pyramid with the trigonal bipyramidal, and the tetrahedron with the square, respectively. However, when we wish to compare different distortion modes of the same ideal polyhedron, which may have very different lengths (i.e., very different θ_{PT} values), comparison of the values for two paths may not give us correct information on which of the two paths best describes the deviation of our problem structure from shape T . This is especially true when one of the paths has an extreme shape D that is physically unachievable, and for which we may find molecular structures that cover at most the initial 30 or 40% of the path. In those cases, we should compare the absolute path deviations in the space of shape measures, which represent a normalized dimensionless sum of squared distances between the points in the ideal structure in a minimal distortion path and those in the real structure, eq 5.

All of the paths presented in the figures of this paper have been chosen after comparison of the mean absolute path deviation for that path with those of alternative paths. The path constants required for such an analysis are given in Table 4. For the sake of reproducibility, the coordinates of reference shapes used in this review and not included in the program SHAPE 2.1 are provided as Supporting Information. The program SHAPE 2.1 can be freely downloaded at <http://www.ee.ub.es>. Crystal structural data were retrieved from the Cambridge Structural Database (CSD).²¹²

Table 4. Constants for the Minimal Distortion Pathways between the Octahedron OC-6 (or the Tetrahedron T-4) and Other Ideal Structures D with Six (or Four) Vertices

octahedron D	$\theta_D(D, \text{OC-6})$
planar hexagon (HP-6)	35.264
trigonal prism (TPR-6)	24.149
flattened trigonal prism (fTPR-6)	31.004
elongated trigonal prism (eTPR-6)	27.274
rectangular bipyramidal (rect-6)	36.415
truncated pyramid (truncpyr-6)	29.044
edge-bicapped tetrahedron (ebcT-6)	28.637
tetrahedron with two doubled edges (t-6)	38.032
vacant capped octahedron (vCOC-6)	11.784
trapezoid-6	25.603
equatorially vacant pentagonal bipyramidal (vPBPY-6)	13.787
tetrahedron D	$\theta_D(D, \text{T-4})$
twist (SP-4)	35.264
pyramidalization (vTBPY-4)	10.896
claw-4 (CL-4)	56.012

ASSOCIATED CONTENT

S Supporting Information

The Supporting Information is available free of charge on the ACS Publications website at DOI: [10.1021/acs.chemrev.5b00537](https://doi.org/10.1021/acs.chemrev.5b00537).

Atomic coordinates for ideal reference shapes ([PDF](#))

AUTHOR INFORMATION

Corresponding Author

*E-mail: santiago@qi.ub.es.

Notes

The authors declare no competing financial interest.

Biography



Santiago Alvarez (Panamá, 1950) studied chemistry at the University of Barcelona, where he obtained a Ph.D. under the supervision of Prof. Jaume Casabó. After a postdoctoral stay with Roald Hoffmann at Cornell University in 1983–1984, he became Profesor Titular (Associate Professor) at the University of Barcelona in 1985 and full professor in 1987. He has developed theoretical research on bonding, stereochemistry, and magnetic properties of transition metal compounds. More recently he has made contributions to the application of continuous shape and symmetry measures to stereochemical studies and to the establishment of structure–properties correlations. He has also promoted encounters across the borders of science and humanities through essay articles and the biannual NoSIC

(Not Strictly Inorganic Chemistry) meetings. He has been a Generalitat de Catalunya Distinguished Professor from 2000 to 2006, is a Fellow of the Royal Society of Chemistry, is a corresponding member of the Spanish Academy of Sciences, is a member of the European Academy of Sciences, and is a Lifetime Honorary Member of the Israel Chemical Society. He has been awarded the prize for research in Inorganic Chemistry by the Real Sociedad Espanola de Química in 2003, the Solvay prize for research in Chemical Science in 2003, and the Catalan-Sabatier prize by the Société Chimique de France in 2012.

ACKNOWLEDGMENTS

Funding from the Spanish Ministerio de Economía y Competitividad (Project CTQ2011-23862-C02-01) is gratefully acknowledged.

REFERENCES

- (1) Aguilà, D.; Escribano, E.; Speed, S.; Talancón, D.; Yermán, L.; Alvarez, S. Calibrating the Coordination Chemistry Tool Chest: Metrics of Bi- and Tridentate Ligands. *Dalton Trans.* **2009**, 6610–6625.
- (2) Alvarez, S.; Ruiz, E. Self-Assembly of Coordination Compounds: Design Principles. In *Supramolecular Chemistry, From Molecules to Nanomaterials*; Steed, J. W., Gale, P. A., Eds.; John Wiley & Sons: Chichester, U.K., 2012; Vol. 5, pp 1993–2044.
- (3) Cordero, B.; Gómez, V.; Platero-Prats, A. E.; Revés, M.; Echeverría, J.; Cremades, E.; Barragán, F.; Alvarez, S. Covalent Radii Revisited. *Dalton Trans.* **2008**, 2832–2838.
- (4) Halcrow, M. A. *Spin-Crossover Materials: Properties and Applications*; John Wiley and Sons: Chichester, U.K., 2013.
- (5) Real, J. A.; Gaspar, A. B.; Muñoz, M. C. Thermal, pressure and light switchable spin-crossover materials. *Dalton Trans.* **2005**, 2062–2079.
- (6) Shatruk, M.; Phan, H.; Chrisostomo, B. A.; Suleimenova, A. Symmetry-breaking Structural Phase Transitions in Spin Crossover Complexes. *Coord. Chem. Rev.* **2015**, 289–290, 62–73.
- (7) Garcia, Y.; Gütlich, P. Thermal Spin Crossover in Mn(II), Mn(III), Cr(II) and Co(III) Coordination Compounds. In *Spin Crossover in Transition Metal Compounds II*; Gütlich, P., Goodwin, H. A., Eds.; Springer-Verlag: Heidelberg, 2004; pp 47–62.
- (8) Goodwin, H. A. Spin Crossover in Co(II) Systems. In *Spin Crossover in Transition Metal Compounds II*; Gütlich, P., Goodwin, H. A., Eds.; Springer-Verlag: Heidelberg, 2004; pp 23–47.
- (9) Gütlich, P. Spin Crossover – Quo Vadis? *Eur. J. Inorg. Chem.* **2013**, 2013, 581–591.
- (10) Alvarez, S.; Alemany, P.; Casanova, D.; Cirera, J.; Llunell, M.; Avnir, D. Shape Maps and Polyhedral Interconversion Paths. *Coord. Chem. Rev.* **2005**, 249, 1693–1708.
- (11) Alvarez, S.; Avnir, D.; Llunell, M.; Pinsky, M. Continuous Symmetry Maps and Shape Classification. The Case of Six-coordinated Metal Compounds. *New J. Chem.* **2002**, 26, 996–1009.
- (12) Zabrodsky, H.; Peleg, S.; Avnir, D. Continuous Symmetry Measures. *J. Am. Chem. Soc.* **1992**, 114, 7843–7851.
- (13) Casanova, D.; Cirera, J.; Llunell, M.; Alemany, P.; Avnir, D.; Alvarez, S. Minimal Distortion Pathways in Polyhedral Rearrangements. *J. Am. Chem. Soc.* **2004**, 126, 1755–1763.
- (14) Cirera, J.; Ruiz, E.; Alvarez, S. Shape and Spin State in Tetracoordinate Transition Metal Complexes. The Case of the d⁶ Configuration. *Chem. - Eur. J.* **2006**, 12, 3162–3167.
- (15) Alvarez, S.; Menjón, B.; Falceto, A.; Casanova, D.; Alemany, P. Stereochemistry of Complexes with Double and Triple Metal-Ligand Bonds: A Continuous Shape Measures Analysis. *Inorg. Chem.* **2014**, 53, 12151–12163.
- (16) Llunell, M.; Casanova, D.; Cirera, J.; Alemany, P.; Alvarez, S. *SHAPE (2.1)*; Universitat de Barcelona: Barcelona, Spain, 2013.
- (17) Bai, Y.-L.; Tao, J.; Huang, R.-B.; Zheng, L.-S.; Zheng, S.-L.; Oshida, K.; Einaga, Y. Pressure Effects and Mössbauer Spectroscopic Studies on a 3D Mixed-Valence Iron Spin-crossover Complex with NiAs Topology. *Chem. Commun.* **2008**, 1753–1755.
- (18) Chainok, K.; Neville, S. M.; Moubaraki, B.; Batten, S. R.; Murray, K. S.; Forsyth, C. M.; Cashion, J. D. Synthesis, Structures and Spin Crossover Properties of Infinite 3D Frameworks of Iron(II) Containing Organodinitrile Bridging Ligands. *Dalton Trans.* **2010**, 39, 10900–10909.
- (19) Bronisz, R. Tetrazol-2-yl as a Donor Group for Incorporation of a Spin-Crossover Function Based on Fe(II) Ions into a Coordination Network. *Inorg. Chem.* **2007**, 46, 6733–6739.
- (20) Ozarowski, A.; McGarvey, B. R. EPR study of manganese(II) and copper(II) in single crystals of the spin-crossover complex hexakis(1-propyltetrazole)iron(2+). *Inorg. Chem.* **1989**, 28, 2262–2266.
- (21) Wiehl, L. Structures of hexakis(1-propyltetrazole)iron(II) bis(tetrafluoroborate), [Fe(CHN₄C₃H₇)₆](BF₄)₂, hexakis(1-methyltetrazole)iron(II) bis(tetrafluoroborate), [Fe(CHN₄CH₃)₆](BF₄)₂, and the analogous perchlorates. Their relation to spin crossover behaviour and comparison of Debye-Waller factors from structure determination and Mössbauer. *Acta Crystallogr., Sect. B: Struct. Sci.* **1993**, 49, 289–303.
- (22) Kusz, J.; Spiering, H.; Gütlich, P. The deformation tensor ϵ of the spin transition in the mixed crystal [Fe_{0.46}Zn_{0.54}(ptz)₆](BF₄)₂. *J. Appl. Crystallogr.* **2004**, 37, 589–595.
- (23) Kusz, J.; Zubko, M.; Neder, R. B.; Gütlich, P. Structural phase transition to disorder low-temperature phase in [Fe(ptz)₆](BF₄)₂ spin-crossover compounds. *Acta Crystallogr., Sect. B: Struct. Sci.* **2012**, 68, 40–56.
- (24) Kusz, J.; Spiering, H.; Gütlich, P. X-ray structure study of the light-induced metastable states of the spin-crossover compound [Fe(mtz)₆](BF₄)₂. *J. Appl. Crystallogr.* **2001**, 34, 229–238.
- (25) Dova, E.; Stassen, A. F.; Driessens, R. A. J.; Sonneveld, E.; Goubitz, K.; Peschar, R.; Haasnoot, J. G.; Reedijk, J.; Schenk, H. Structure Determination of the [Fe(teec)₆](BF₄)₂ Metal Complex from Laboratory and Synchrotron X-ray Powder Diffraction Data with Grid-search Techniques. *Acta Crystallogr., Sect. B: Struct. Sci.* **2001**, 57, 531–538.
- (26) Dova, E.; Peschar, R.; Takata, M.; Nishibori, E.; Schenk, H.; Stassen, A. F.; Haasnoot, J. G. Low-Spin State Structure of [Fe(chloroethyltetrazole)₆](BF₄)₂ Obtained from Synchrotron Powder Diffraction Data. *Chem. - Eur. J.* **2005**, 11, 5855–5865.
- (27) Roubeau, O.; Evangelisti, M.; Natividad, E. A Spin Crossover Ferrous Complex with Ordered Magnetic Ferric Anions. *Chem. Commun.* **2012**, 48, 7604–7606.
- (28) Hibbs, W.; van Koningsbruggen, P. J.; Arif, A. M.; Shum, W. W.; Miller, J. S. One- and Two-Step Spin-Crossover Behavior of [Fe^{II}(isoxazole)₆]²⁺ and the Structure and Magnetic Properties of Triangular [Fe^{III}₃O(OAc)₆(isoxazole)₃][ClO₄]. *Inorg. Chem.* **2003**, 42, 5645–5653.
- (29) Bailar, J. C. Problems in the Stereochemistry of Coordination Compounds. *J. Inorg. Nucl. Chem.* **1958**, 8, 165–175.
- (30) Kepert, D. L. *Inorganic Stereochemistry*; Springer: New York, 1982.
- (31) Alvarez, S. Relationships Between Temperature, Magnetic Moment and Continuous Symmetry Measures in Spin Crossover Complexes. *J. Am. Chem. Soc.* **2003**, 125, 6795–6802.
- (32) Cremades, E.; Echeverría, J.; Alvarez, S. The Trigonal Prism in Coordination Chemistry. *Chem. - Eur. J.* **2010**, 16, 10380–10396.
- (33) Zhang, R.-H.; Hong, Q.-M.; Yang, J.-M.; Zhang, H.-L.; Blackburn, G. M.; Zhou, Z.-H. Syntheses, Spectroscopies and Structures of Zinc Complexes with Malate. *Inorg. Chim. Acta* **2009**, 362, 2643–2649.
- (34) Turner, D. L.; Stone, K. H.; Stephens, P. W.; Vaid, T. P. Cadmium and Zinc Thiolate and Selenolate Metal-organic Frameworks. *Dalton Trans.* **2010**, 39, 5070–5073.
- (35) Ma, G.; Fischer, A.; Nieuwendaal, R.; Ramaswamy, K.; Hayes, S. E. Cd(II)-ethylenediamine Mono- and Bimetallic Complexes – Synthesis and Characterization by ¹¹³Cd NMR Spectroscopy and

- Single Crystal X-ray Diffraction. *Inorg. Chim. Acta* **2005**, *358*, 3165–3173.
- (36) Zemskova, S. M.; Glinskaya, L. A.; Klevtsova, R. F.; Fedotov, M. A.; Larionov, S. V. Structure and Properties of Mono-and Heterometallic Cadmium, Zinc, and Nickel Complexes Containing Diethyldithiocarbamate ions and Ethylenediamine Molecules. *J. Struct. Chem.* **1999**, *40*, 284–292.
- (37) Glinskaya, L. A.; Zemskova, S. M.; Klevtsova, R. F.; Larionov, S. V.; Gromilov, S. A. The Preparation, Structures and Thermal Properties of $[MEn_3][Cd(S_2CNEt_2)_3]_2$ [$M = \text{zinc(II)}, \text{cadmium(II)}$] Complexes. *Polyhedron* **1992**, *11*, 2951–2956.
- (38) McCleverty, J. A.; Gill, S.; Kowalski, R. S. Z.; Bailey, N. A.; Adams, H.; Lombard, K. W.; Murphy, M. A. Aspects of the Inorganic Chemistry of Rubber Vulcanisation. Part 3. Anionic Cadmium Complexes Derived from Dialkylthiocarbamates, 2-mercaptopbenzo-thiazole and its Derivatives, and Dialkyl Dithiophosphates, and the Crystal and Molecular Structures of $[NBu^{\text{n}}_4][Cd(S_2CNEt_2)_3]$, $[NEt_4^-][Cd(C_7H_4NS_2)_3]$, and $[NMe_4][Cd\{S_2P(OPr')_2\}_3]$. *J. Chem. Soc., Dalton Trans.* **1982**, 493–503.
- (39) Fan, J.; Zhu, H.-F.; Okamura, T.-a.; Sun, W.-Y.; Tang, W.-X.; Ueyama, N. Discrete and Infinite Cage-Like Frameworks with Inclusion of Anionic and Neutral Species and with Interpenetration Phenomena. *Chem.—Eur. J.* **2003**, *9*, 4724–4731.
- (40) Gust, K. R.; Knox, J. E.; Heeg, M. J.; Schlegel, H. B.; Winter, C. H. Synthesis, Structure, and Molecular Orbital Calculations of Chromium(III) and Iron(III) Complexes Containing η^2 -Pyrazolato Ligands. *Angew. Chem., Int. Ed.* **2002**, *41*, 1591–1594.
- (41) Deacon, G. B.; Gitlits, A.; Roesky, P. W.; Burgstein, M. R.; Lim, K. C.; Skelton, B. W.; White, A. H. Simple Syntheses, Structural Diversity, and Tishchenko Reaction Catalysis of Neutral Homoleptic Rare Earth(II or III) 3,5-Di-tert-butylpyrazolates—The Structures of $[Sc(^{\text{t}}Bu_2pz)_3]$, $[Ln_2(^{\text{t}}Bu_2pz)_6]$ ($Ln = La, Nd, Yb, Lu$), and $[Eu_4(^{\text{t}}Bu_2pz)_8]$. *Chem.—Eur. J.* **2001**, *7*, 127–138.
- (42) Greaney, T. M.; Raston, C. L.; White, A. H.; Maslen, E. N. Crystal Structure of Potassium Tris(acetylacetonato)cadmite(II) Monohydrate. *J. Chem. Soc., Dalton Trans.* **1975**, 876–879.
- (43) Gromilov, S. A.; Baidina, I. A.; Prokhorova, S. A.; Stabnikov, P. A. Crystal and Molecular Structure of Monomeric Y(III) Dipivaloylmethanate. Arrangement of Adsorbed Layers. *J. Struct. Chem.* **1995**, *36*, 496–501.
- (44) Rosa, P.; Mézailles, N.; Ricard, L.; Mathey, F.; Le Floch, P. Dianionic Homoleptic Biphenophosphine Complexes of Group 4 Metals. *Angew. Chem., Int. Ed.* **2000**, *39*, 1823–1826.
- (45) Martin, J. L.; Takats, J. Crystal and Molecular Structure of Tetraphenylarsonium Tris(benzenedithiolato)tantalate(V). *Inorg. Chem.* **1975**, *14*, 1358–1364.
- (46) Tatsumi, K.; Matsubara, I.; Inoue, Y.; Nakamura, A.; Miki, K.; Kasai, N. Trigonal Versus Nontrigonal Deformation from Octahedral Geometry in d^0 Metal Six-coordination: Two Geometrical Isomers of [metal tris(norbornane-exo-2,3-dithiolate)]⁻ (metal = niobium, tantalum) and Their Interconversion. *J. Am. Chem. Soc.* **1989**, *111*, 7766–7777.
- (47) Welch, J. H.; Bereman, R. D.; Singh, P. Syntheses and Characterization of Three Tris Complexes of the Ligand 5,6-dihydro-1,4-dithiin-2,3-Dithiolate. Crystal Structure of $[(C_6H_5)_4As]_2[Ti(\text{DDDT})_3]$. *Inorg. Chem.* **1990**, *29*, 68–73.
- (48) Wang, D.-Q.; Fu, A.-Y.; Wei, X.-L. Tris(ethylenediamine-[κ^2 N,N']cadmium(II) bis(1,2-dicyanoethylenedithiolato-[κ^2 S,S'])cuprate(II). *Acta Crystallogr., Sect. E: Struct. Rep. Online* **2004**, *60*, m1872–m1874.
- (49) Chen, W.-T.; Wang, M.-S.; Cai, L.-Z.; Guo, G.-C.; Huang, J.-S. Syntheses, Structures, Properties, and Theoretical Studies of d^{10} Metal Complexes of Ethylenediamine. *Aust. J. Chem.* **2005**, *58*, 578–584.
- (50) Rây, P.; Dutt, N. K. Kinetics and Mechanism of Racemization of Optically Active Cobaltic Trisbiguanide Complex. *J. Indian Chem.* **1943**, *20*, 81–92.
- (51) Rzepa, H. S.; Cass, M. E. In Search of the Bailar and Rây–Dutt Twist Mechanisms That Racemize Chiral Trischelates: A Computational Study of Sc^{III} , Ti^{IV} , Co^{III} , Zn^{II} , Ga^{III} , and Ge^{IV} Complexes of a Ligand Analogue of Acetylacetone. *Inorg. Chem.* **2007**, *46*, 8024–8031.
- (52) Ahmed, M. A. K.; Fjellvag, H.; Kjekshus, A.; Birkedal, R. K.; Norby, P.; Gupta, N. S.; Wragg, D. S. Syntheses, Crystal Structures, and Thermal Stabilities of Polymorphs of $\text{Cr}(\text{thd})_3$. *Z. Anorg. Allg. Chem.* **2010**, *636*, 2422–2432.
- (53) Rius, J.; Galí, S. Tris(ethylenediamine)cobalt(III) arsenate trihydrate $[\text{Co}(\text{C}_2\text{H}_8\text{N}_2)_3]\text{AsO}_4 \cdot 3\text{H}_2\text{O}$. *Cryst. Struct. Commun.* **1982**, *11*, 829–834.
- (54) Maiti, R.; Shang, M.; Graham Lappin, A. A ruthenium(IV) Complex with Six Sulfur Donor Atoms. *Chem. Commun.* **1999**, 2349–2350.
- (55) Terzis, A.; Filippakis, S.; Mentzas, D.; Petrouleas, V.; Malliaris, A. Structure and Magnetic Behavior of Iron(III) Dithiocarbamate Complexes Exhibiting $S = 1/2 \rightleftharpoons S = 5/2$ Thermal Equilibrium. Study of the Tris(N-methyl-N-n-butylthiocarbamato)iron Homologue. *Inorg. Chem.* **1984**, *23*, 334–337.
- (56) Isfort, C. S.; Kreickmann, T.; Pape, T.; Frohlich, R.; Hahn, F. E. Helical Complexes Containing Diamide-Bridged Benzene-o-dithiolo-Catecholato Ligands. *Chem.—Eur. J.* **2007**, *13*, 2344–2357.
- (57) Hahn, F. E.; Offermann, M.; Isfort, C. S.; Pape, T.; Frohlich, R. Heterobimetallic Triple-Stranded Helicates with Directional Benzene-o-dithiol/Catechol Ligands. *Angew. Chem., Int. Ed.* **2008**, *47*, 6794–6797.
- (58) Wang, K.; McConnachie, J. M.; Stiefel, E. I. Syntheses of Metal Dithiolen Complexes from Thiometalates by Induced Internal Redox Reactions. *Inorg. Chem.* **1999**, *38*, 4334–4341.
- (59) Cowie, M.; Bennett, M. J. Trigonal-prismatic vs. Octahedral Coordination in a Series of Tris(benzene-1,2-dithiolato) Complexes. 2. Crystal and Molecular Structure of Tetraphenylarsonium Tris(benzene-1,2-dithiolato)niobate(V), $[(C_6H_5)_4As][Nb(S_2C_6H_4)_3]$. *Inorg. Chem.* **1976**, *15*, 1589–1595.
- (60) Huynh, H. V.; Lügger, T.; Hahn, F. E. Synthesis and X-ray Molecular Structure of $[\text{WVI}(\text{C}_6\text{H}_4\text{S}_2-1,2)_3]$ Completing the Structural Characterization of the Series $[\text{W}(\text{C}_6\text{H}_4\text{S}_2-1,2)_3]^{n-}$ ($n = 0, 1, 2$): Trigonal-Prismatic versus Octahedral Coordination in Tris(benzene-1,2-dithiolato) Complexes. *Eur. J. Inorg. Chem.* **2002**, *2002*, 3007–3009.
- (61) Chiu, W.-H.; Peng, S.-M.; Che, C.-M. Bis(amido)ruthenium(IV) Complexes with 2,3-Diamino-2,3-dimethylbutane. Crystal Structure and Reversible Ru(IV)–Amide/Ru(III)–Amine and Ru(IV)–Amide/Ru(II)–Amine Redox Couples in Aqueous Solution. *Inorg. Chem.* **1996**, *35*, 3369–3374.
- (62) Qi, Y.; Li, Y.-G.; Wang, E.; Zhang, Z.; Chang, S. Metal-controlled Self-assembly of Arsenic–vanadium-cluster Backbones with Organic Ligands. *Dalton Trans.* **2008**, 2335–2345.
- (63) Katz, B. A.; Strouse, C. E. Molecular Transformations in the Solid State. Crystallographic Resolution of the Spin Isomers of Tris(2-picolyamine)iron(II) Dichloride and the Structural Relationship Between the Methanol and Ethanol Solvates. *J. Am. Chem. Soc.* **1979**, *101*, 6214–6221.
- (64) Mikami, M.; Konno, M.; Saito, Y. The Structures of High-spin (298, 150 K) and Low-spin (90 K) States and the Spin Phase-transition Mechanism of a Spin Crossover Complex; Tris([alpha]-picolyamine)iron(II) Chloride-ethanol. *Acta Crystallogr., Sect. B: Struct. Crystallogr. Cryst. Chem.* **1980**, *36*, 275–287.
- (65) Chernyshov, D.; Hostettler, M.; Törnroos, K. W.; Bürgi, H.-B. Ordering Phenomena and Phase Transitions in a Spin-Crossover Compound—Uncovering the Nature of the Intermediate Phase of $[\text{Fe}(2-\text{pic})_3]\text{Cl}_2\text{EtOH}$. *Angew. Chem., Int. Ed.* **2003**, *42*, 3825–3830.
- (66) Kusz, J.; Schollmeyer, D.; Spiering, H.; Gütlich, P. The LIESST State of $[\text{Fe}(\text{pic})_3]\text{Cl}_2\text{EtOH}$ – The Superstructure Under Continuous Irradiation. *J. Appl. Crystallogr.* **2005**, *38*, 528–536.
- (67) Törnroos, K. W.; Hostettler, M.; Chernyshov, D.; Vangdal, B.; Bürgi, H.-B. Interplay of Spin Conversion and Structural Phase Transformations: Re-entrant Phase Transitions in the 2-Propanol Solvate of Tris(2-picolyamine)iron(II) Dichloride. *Chem. — Eur. J.* **2006**, *12*, 6207–6215.

- (68) Chernyshov, D.; Vangdal, B.; Tornroos, K. W.; Bürgi, H.-B. Chemical Disorder and Spin Crossover in a Mixed Ethanol–2-propanol Solvate of Fe^{II} tris(2-picolyamine) Dichloride. *New J. Chem.* **2009**, *33*, 1277–1282.
- (69) Greenaway, A. M.; Sinn, E. High-spin and Low-spin α -picolyamine Iron(II) Complexes. Effect of Ligand Reversal on Spin State. *J. Am. Chem. Soc.* **1978**, *100*, 8080–8084.
- (70) Greenaway, A. M.; O'Connor, C. J.; Schrock, A.; Sinn, E. High- and Low-Spin Interconversion in a Series of (α -picolyamine)iron(II) Complexes. *Inorg. Chem.* **1979**, *18*, 2692–2695.
- (71) Hostettler, M.; Tornroos, K. W.; Chernyshov, D.; Vangdal, B.; Bürgi, H.-B. Challenges in Engineering Spin Crossover: Structures and Magnetic Properties of Six Alcohol Solvates of Iron(II) Tris(2-picolyamine) Dichloride. *Angew. Chem., Int. Ed.* **2004**, *43*, 4589–4594.
- (72) Jahro, I. S.; Onggo, D.; Ismunandar; Rahayu, S. I.; Muñoz, M. C.; Gaspar, A. B.; Seredyuk, M.; Gütlich, P.; Real, J. A. Synthesis, Crystal Structure and Magnetic Properties of the Spin Crossover System [Fe(pq)₃]²⁺. *Inorg. Chim. Acta* **2008**, *361*, 4047–4054.
- (73) Li, M.-X.; Niu, H.-Y.; Wang, W.; Wang, J.-P. A Keggin-type Arsenotungstate Anion-supported Transition Metal Complex: Hydrothermal Synthesis and Characterization of [Fe(2,2'-bipy)₃]1.5-[AsW^{VI}₁₀W^V₂O₄₀Fe(2,2'-bipy)₂(H₂O)] · 0.25H₂O. *Z. Naturforsch., B: J. Chem. Sci.* **2008**, *63*, 183–186.
- (74) Xie, J.; Gilbert-Wilson, R.; Moubaraki, B.; Murray, K. S.; Wedd, A. G. A Fe(bipy)₂ Unit Fused to a Keggin Polyoxotungstate Anion. *Aust. J. Chem.* **2010**, *63*, 252–256.
- (75) Wang, J.-P.; Guo, G.-L.; Niu, J.-Y. Hydrothermal Syntheses, Crystal Structures of Three New Organic–inorganic Hybrids Constructed from Keggin-type [BW₁₂O₄₀]⁵⁻ Clusters and Transition Metal Complexes. *J. Mol. Struct.* **2008**, *885*, 161–167.
- (76) Alvarez, S. A Cartography of the van der Waals Territory. *Dalton Trans.* **2013**, *42*, 8617–8636.
- (77) Money, V. A.; Carbonera, C.; Elhaik, J.; Halcrow, M. A.; Howard, J. A. K.; Letard, J.-F. Interplay Between Kinetically Slow Thermal Spin-Crossover and Metastable High-Spin State Relaxation in an Iron(II) Complex with Similar T_{1/2} and T(LIESST). *Chem. - Eur. J.* **2007**, *13*, 5503–5514.
- (78) Martak, F.; Onggo, D.; Ismunandar; Nugroho, A. A.; Meetsma, A. 2009. Accessible from the Cambridge Structural Database (refcode UDUYOJ). <https://summary.ccdc.cam.ac.uk/structure-summary-form> (accessed September 14, 2015).
- (79) Halepoto, D. M.; Holt, D. G. L.; Larkworthy, L. F.; Leigh, G. J.; Povey, D. C.; Smith, G. W. Spin Crossover in Chromium(II) Complexes and the Crystal and Molecular Structure of the High Spin Form of Bis[1,2-bis(diethylphosphino)ethane]di-iodochromium(II). *J. Chem. Soc., Chem. Commun.* **1989**, 1322–1323.
- (80) Karunadasa, H. I.; Arquero, K. D.; Berben, L. A.; Long, J. R. Enhancing the Magnetic Anisotropy of Cyano-Ligated Chromium(II) and Chromium(III) Complexes via Heavy Halide Ligand Effects. *Inorg. Chem.* **2010**, *49*, 4738–4740.
- (81) Moliner, N.; Muñoz, M. C.; Létard, S.; Létard, J.-F.; Solans, X.; Burriel, R.; Castro, M.; Kahn, O.; Real, J. A. Spin-crossover in the [Fe(abpt)₂(NCX)₂] (X = S, Se) System: Structural, Magnetic, Calorimetric and Photomagnetic Studies. *Inorg. Chim. Acta* **1999**, *291*, 279–288.
- (82) Tao, J.-Q.; Gu, Z.-G.; Wang, T.-W.; Yang, Q.-F.; Zuo, J.-L.; You, X.-Z. Spin-crossover Iron(II) Complexes [Fe(Medpq)(py)₂(NCS)₂] and [Fe(Medpq)(py)₂(NCSe)₂]: Syntheses, Characterization and Magnetic Properties. *Inorg. Chim. Acta* **2007**, *360*, 4125–4132.
- (83) Yamada, M.; Hagiwara, H.; Torigoe, H.; Matsumoto, N.; Kojima, M.; Dahan, f.; Tuchagues, J.-P.; Re, N.; Iijima, S. A Variety of Spin-Crossover Behaviors Depending on the Counter-Ion. *Chem. - Eur. J.* **2006**, *12*, 4536–4549.
- (84) Guionneau, P.; Marchivie, M.; Garcia, Y.; Howard, J. A. K.; Chasseau, D. Spin Crossover in [Mn^{III}(pyrol)₃tren] Probed by High-pressure and Low-temperature X-ray Diffraction. *Phys. Rev. B: Condens. Matter Mater. Phys.* **2005**, *72*, 214408.
- (85) Seredyuk, M.; Gaspar, A. B.; Kusz, J.; Bednarek, G.; Gütlich, P. Variable-temperature X-ray Crystal Structure Determinations of {Fe[tren(6-Mepy)₃])(ClO₄)₂ and {Zn[tren(6-Mepy)₃])(ClO₄)₂ Compounds: Correlation of the Structural Data with Magnetic and Mössbauer Spectroscopy Data. *J. Appl. Crystallogr.* **2007**, *40*, 1135–1144.
- (86) McDaniel, A. M.; Rappe, A. K.; Shores, M. P. Structural and Electronic Comparison of 1st Row Transition Metal Complexes of a Tripodal Iminopyridine Ligand. *Inorg. Chem.* **2012**, *51*, 12493–12502.
- (87) Kirchner, R. M.; Mealli, C.; Bailey, M.; Howe, N.; Torre, L. P.; Wilson, L. J.; Andrews, L. C.; Rose, N. J.; Lingafelter, E. C. The Variable Coordination Chemistry of a Potentially Heptadentate Ligand with a Series of 3d Transition Metal Ions. The Chemistry and Structures of [M(py₃tren)]²⁺, where M(II) = Mn, Fe, Co, Ni, Cu, and Zn and (py₃tren) = N{CH₂CH₂N=C(H)(C₅H₄N)}₃. *Coord. Chem. Rev.* **1987**, *77*, 89–163.
- (88) Li, S.-N.; Ren, Y.-W.; Li, J.; Zhang, F.-X.; Hu, M.-C. {Tris[2-(2-pyridylmethyleneimino)ethyl]amine}manganese(II) bis(perchlorate). *Acta Crystallogr., Sect. E: Struct. Rep. Online* **2006**, *62*, m498–m499.
- (89) He, H.-S. {Tris[2-(2-pyridylmethyleneamino- κ^2 N,N')ethyl]amine}cadmium(II) bis(perchlorate). *Acta Crystallogr., Sect. E: Struct. Rep. Online* **2007**, *63*, m346–m347.
- (90) Qian, M.; Gou, S.-H.; He, L.; Zhou, Y.-M.; Duan, C.-Y. [Tris(2-pyridyl- κ N-methyleneamino- κ N-ethyl)amine- κ N]manganese(II) di-perchlorate. *Acta Crystallogr., Sect. C: Cryst. Struct. Commun.* **1999**, *55*, 742–744.
- (91) Park, G.; Przyborowska, A. M.; Ye, N.; Tsoupas, N. M.; Bauer, C. B.; Broker, G. A.; Rogers, R. D.; Brechbiel, M. W.; Planalp, R. P. Steric Effects Caused by N-alkylation of the Tripodal Chelator N,N',N"-tris(2-pyridylmethyl)-cis,cis-1,3,5-triaminocyclohexane (tachypy): Structural and Electronic Properties of the Mn(II), Co(II), Ni(II), Cu(II) and Zn(II) Complexes. *Dalton Trans.* **2003**, 318–324.
- (92) Childers, M. L.; Su, F.; Przyborowska, A. M.; Bishwokarma, B.; Park, G.; Brechbiel, M. W.; Torti, S. V.; Torti, F. M.; Broker, G.; Alexander, J. S.; Rogers, R. D.; Ruhlandt-Senge, K.; Planalp, R. P. Pyridine-Ring Alkylation of Cytotoxic r-1,c-3,c-5-Tris[(2-pyridylmethyl)amino]cyclohexane Chelators: Structural and Electronic Properties of the Mn^{II}, Fe^{II}, Ni^{II}, Cu^{II} and Zn^{II} Complexes. *Eur. J. Inorg. Chem.* **2005**, *2005*, 3971–3982.
- (93) Monteiro, B.; Roitershtein, D.; Ferreira, H.; Ascenso, J. R.; Martins, A. M.; Domingos, A.; Marques, N. Triamidotriazacyclonane Complexes of Group 3 Metals. Synthesis and Crystal Structures. *Inorg. Chem.* **2003**, *42*, 4223–4231.
- (94) Schlager, O.; Wieghardt, K.; Grondéy, H.; Rufinska, A.; Nuber, B. The Hexadentate Ligand 1,4,7-Tris(o-aminobenzyl)-1,4,7-triazacyclonane and Its Complexes with Zinc(II), Cadmium(II), and Mercury(II) in Solution and in the Solid State. *Inorg. Chem.* **1995**, *34*, 6440–6448.
- (95) Byriel, K. A.; Dunster, K. R.; Gahan, L. R.; Kennard, C. H. L.; Latte, J. L. Mercury Macrocyclic Complexes: Synthesis and Crystal Structures of {[HgCl(μ -Cl)(L¹)][Hg(μ -Cl)₂]}_n (L¹ = 1,4,7,10-tetraoxa-13-azacyclooctadecane), [Hg(L²)Cl₂] (L² = 1,4,7,10,13-pentaoxa-16-azacyclooctadecane) and [Hg(L³)Cl₂] (L³ = 16-methyl-1,4,7,10,13-pentaoxa-16-azacyclooctadecane). *Inorg. Chim. Acta* **1992**, *196*, 35–41.
- (96) Minacheva, L. K.; Tul'chinskii, M. L.; Bocharov, S. V.; Sakhrova, V. G.; Tsividze, A. Y.; Porai-Koshits, M. A. Preparation, IR Spectra and Crystal Structure of Cadmium Thiocyanate Complexes with 1,7-diaza-15-crown-5, Cd(C₁₀H₁₂N₂O₃) (NCS)₂, Containing 7-coordinate Cadmium. *Koord. Khim.* **1989**, *15*, 1629–1635.
- (97) Ruiz-Martínez, A.; Casanova, D.; Alvarez, S. Association/Dissociation Paths and Ill-defined Coordination Numbers. *Chem. - Eur. J.* **2010**, *16*, 6567–6581.
- (98) Ababei, R.; Pichon, C.; Roubeau, O.; Li, Y.-G.; Brefuel, N.; Buisson, L.; Guionneau, P.; Mathonière, C.; Clérac, R. Rational Design of a Photomagnetic Chain: Bridging Single-Molecule Magnets with a Spin-Crossover Complex. *J. Am. Chem. Soc.* **2013**, *135*, 14840–14853.
- (99) Guionneau, P.; Sánchez Costa, J.; Létard, J.-F. Revisited Crystal Symmetry of the High-spin Form of the Iron(II) Spin-crossover Complex Dicyano[2,13-dimethyl-6,9-dioxa-3,12,18-triazabicyclo[12.3.1]octadeca-1(18),2,12,14,16-pentaene]iron(II)

- Monohydrate. *Acta Crystallogr., Sect. C: Cryst. Struct. Commun.* **2004**, *60*, m587–m589.
- (100) Guionneau, P.; Le Gac, F.; Kaiba, A.; Costa, J. S.; Chasseau, D.; Létard, J.-F. A Reversible Metal–Ligand Bond Break Associated to a Spin-crossover. *Chem. Commun.* **2007**, 3723–3725.
- (101) Hayami, S.; Gu, Z.-Z.; Einaga, Y.; Kobayashi, Y.; Ishikawa, Y.; Yamada, Y.; Fujishima, A.; Sato, O. A Novel LIESST Iron(II) Complex Exhibiting a High Relaxation Temperature. *Inorg. Chem.* **2001**, *40*, 3240–3242.
- (102) Létard, J.-F.; Costa, J. S.; Guionneau, P.; Marcen, S. 2009. Accessible from the Cambridge Structural Database (refcode XEZMEU03). <https://summary.ccdc.cam.ac.uk/structure-summary-form> (accessed September 14, 2015).
- (103) Wang, Q.; Venneri, S.; Zarrabi, N.; Wang, H.; Desplanches, C.; Létard, J.-F.; Seda, T.; Pilkington, M. Stereochemistry for Engineering Spin Crossover: Structures and Magnetic Properties of a Homochiral vs. Racemic $[Fe(N_3O_2)(CN)_2]$ Complex. *Dalton Trans.* **2015**, *44*, 6711–6714.
- (104) Helm, M. L.; Helton, G. P.; VanDerveer, D. G.; Grant, G. J. Mercury-199 NMR Studies of Thiacrown and Related Macrocyclic Complexes: The Crystal Structures of $[Hg(18S6)](PF_6)_2$ and $[Hg(9N_3)_2](ClO_4)_2$. *Inorg. Chem.* **2005**, *44*, 5696–5705.
- (105) Stockholm, C.; Wieghardt, K.; Nuber, B.; Weiss, J.; Flörke, U.; Haupt, H.-J. Co-ordination Chemistry of 1,4,7-triazacyclonane (L) and its N-methylated Derivative (L') with Silver(I) and Mercury(II). The Crystal Structures of $[AgL'_2]PF_6$ and $[AgL'(SCN)]$. *J. Chem. Soc., Dalton Trans.* **1991**, 1487–1490.
- (106) Haselhorst, G.; Stoetzel, S.; Strassburger, A.; Walz, W.; Wieghardt, K.; Nuber, B. Synthesis and Co-ordination Chemistry of the Macrocycle 1,4,7-trisopropyl-1,4,7-triazacyclonane. *J. Chem. Soc., Dalton Trans.* **1993**, 83–90.
- (107) Baker, M. V.; Brown, D. H.; Skelton, B. W.; White, A. H. An Investigation of 1,4,7-tri(4-alkynyl)-1,4,7-triazacyclonanes: Ligand Synthesis and Metal Coordination Chemistry. *J. Chem. Soc., Dalton Trans.* **2000**, 4607–4616.
- (108) Zobi, F.; Blacque, O.; Steyl, G.; Spingler, B.; Alberto, R. Formation and Reactivity of $[(tacn)-N-CO-Re^{III}Br(CO)_2]^+$ in Water: A Theoretical and Experimental Study. *Inorg. Chem.* **2009**, *48*, 4963–4970.
- (109) Bambirra, S.; van Leusen, D.; Tazelaar, C. G. J.; Meetsma, A.; Hessen, B. Rare Earth Metal Alkyl Complexes with Methyl-Substituted Triazacyclonane-amide Ligands: Ligand Variation and Ethylene Polymerization Catalysis. *Organometallics* **2007**, *26*, 1014–1023.
- (110) Yang, Y.-S.; Gu, W.; Qian, J.; Gao, F.-X.; Yan, S.-P. Syntheses, Structures, and Spectroscopic Properties of Copper(II) and Cobalt(III) Complexes Containing 1,4,7-tribenzyl-1,4,7-triazacyclonane Ligand. *J. Coord. Chem.* **2007**, *60*, 1681–1690.
- (111) Searle, G. H.; Wang, D.-N.; Larsen, S.; Larsen, E. The Structure of a Novel Complex of Cobalt(III) with a Tridentate Macrocyclic Ligand with Tertiary Amine Donors, $[CoL(NCCH_3)_2Cl]_nCoCl_4$ ($L = 1,4,7$ -Trimethyl-1,4,7-triazacyclonane). *Acta Chem. Scand.* **1992**, *46*, 38–42.
- (112) Lian, Z.-X.; Li, H.-H. Bis(N,N',N'' -diethylenetriamine-[κ^3N]cadmium(II) naphthalene-1,5-disulfonate. *Acta Crystallogr., Sect. E: Struct. Rep. Online* **2007**, *63*, m939–m941.
- (113) Fu, M.-L.; Guo, G.-C.; Liu, X.; Liu, B.; Cai, L.-Z.; Huang, J.-S. Syntheses, Structures and Properties of Three Selenoarsenates Templated by Transition Metal Complexes. *Inorg. Chem. Commun.* **2005**, *8*, 18–21.
- (114) Kiebach, R.; Bensch, W.; Hoffmann, R.-D.; Pöttgen, R. Solvothermal Synthesis and Characterization of the New Iron Thioantimonates(III) $[Fe(C_6H_{18}N_4)]FeSb_4$ and $[Fe(C_4H_{13}N_3)_2]_2Fe_2Sb_4S_{10}$ Containing Fe^{II} and Fe^{III} and Protein-Analogous $[2Fe^{III}-2S]^{2+}$ Clusters. *Z. Anorg. Allg. Chem.* **2003**, *629*, 532–538.
- (115) Fu, M.-L.; Guo, G.-C.; Liu, B.; Wu, A.-Q.; Huang, J.-S. Two New Thiostannates Templated by Transition Metal Complexes. *Wuji Huaxue Xuebao (Chin. J. Inorg. Chem.)* **2005**, *21*, 25–29.
- (116) Nather, C.; Herzberg, N.; Bensch, W. Infinite Anionic Chains Formed by Alternating Bidentately Acting $[SbS_4]^{3-}$ Anions and $[Mn(dien)]^{2+}$ Complexes in the Compound $[Mn(dien)]_2[Mn(dien)-SbS_4]_2$. *Z. Naturforsch., B: J. Chem. Sci.* **2013**, *68*, 605–610.
- (117) Schweinfurth, D.; Demeshko, S.; Hohloch, S.; Steinmetz, M.; Brandenburg, J. G.; Dechert, S.; Meyer, F.; Grimme, S.; Sarkar, B. Spin Crossover in Fe(II) and Co(II) Complexes with the Same Click-Derived Tripodal Ligand. *Inorg. Chem.* **2014**, *53*, 8203–8212.
- (118) Schweinfurth, D.; Krzystek, J.; Schapiro, I.; Demeshko, S.; Klein, J.; Telser, J.; Ozarowski, A.; Su, C.-Y.; Meyer, F.; Atanasov, M.; Neese, F.; Sarkar, B. Electronic Structures of Octahedral Ni(II) Complexes with “Click” Derived Triazole Ligands: A Combined Structural, Magnetometric, Spectroscopic, and Theoretical Study. *Inorg. Chem.* **2013**, *52*, 6880–6882.
- (119) Schweinfurth, D.; Weisser, F.; Bubrin, D.; Bogani, L.; Sarkar, B. Cobalt Complexes with “Click”-Derived Functional Tripodal Ligands: Spin Crossover and Coordination Ambivalence. *Inorg. Chem.* **2011**, *50*, 6114–6121.
- (120) Reger, D. L.; Sirianni, E.; Horger, J. J.; Smith, M. D.; Semeniuc, R. F. Supramolecular Architectures of Metal Complexes Controlled by a Strong $\pi \cdots \pi$ Stacking, 1,8-Naphthalimide Functionalized Third Generation Tris(pyrazolyl)methane Ligand. *Cryst. Growth Des.* **2010**, *10*, 386–393.
- (121) Reger, D. L.; Mason, S. S.; Rheingold, A. L.; Ostrander, R. L. Syntheses, Structures, ^{113}Cd Solution NMR Chemical Shifts, and Investigations of Fluxional Processes of Bis[poly(pyrazolyl)borato]-cadmium Complexes. *Inorg. Chem.* **1993**, *32*, 5216–5222.
- (122) Kitano, T.; Sohrin, Y.; Hata, Y.; Wada, H.; Hori, T.; Ueda, K. Improved Selectivity for Cu(II) of Methyl-Substituted Poly(pyrazolyl)borates, $[HB(3-Mepz)_3]^-$ and $[B(3-Mepz)_4]^-$, through Steric Contact. *Bull. Chem. Soc. Jpn.* **2003**, *76*, 1365–1373.
- (123) Lobbia, G. G.; Bovio, B.; Santini, C.; Cecchi, P.; Pettinari, C.; Marchetti, F. Tris(4-bromo-1H-pyrazol-1-yl)borato Derivatives of First-row Transition and Group 12 and 14 Metals. X-ray Crystal Structure of $[HB(4-Brpz)_3]_2Cd$. ^{113}Cd Solution NMR Study of Bis[poly(pyrazolyl)borato]cadmium Complexes. *Polyhedron* **1998**, *17*, 17–26.
- (124) Reger, D. L.; Myers, S. M.; Mason, S. S.; Dahrenbourg, D. J.; Holtcamp, M. W.; Reibenspies, J.; Lipton, A. S.; Ellis, P. D. ^{113}Cd Shielding Tensors of Monomeric Cadmium Compounds Containing Nitrogen Donor Atoms. 3. Syntheses, Crystal Structure, and ^{113}Cd NMR Spectroscopy of the Six-Coordinate Complexes $[HB(pz)_3]_2Cd$, $[HB(3-Phpz)_3]_2Cd$, and $[B(pz)_4]Cd[HB(3-Phpz)_3]$ (pz = pyrazolyl). *J. Am. Chem. Soc.* **1995**, *117*, 10998–11005.
- (125) McWhinnie, W. R.; Monsef-Mirza, Z.; Perry, M. C.; Shaikh, N.; Hamor, T. A. Some Hydridotris(3,5-dimethylpyrazolyl)borate Complexes of Zinc, Cadmium and Mercury—Synthetic, Structural and NMR Investigations. *Polyhedron* **1993**, *12*, 1193–1199.
- (126) Yoon, J. H.; Ryu, D. W.; Choi, S. Y.; Kim, H. C.; Koh, E. K.; Tao, J.; Hong, C. S. Spin Crossover in the Cyanide-bridged $Mo^V Mn^{III}$ Single-chain Magnet Containing Fe^{II} Cations. *Chem. Commun.* **2011**, *47*, 10416–10418.
- (127) Reger, D. L.; Collins, J. E.; Myers, S. M.; Rheingold, A. L.; Liable-Sands, L. M. Syntheses of Cationic, Six-Coordinate Cadmium(II) Complexes Containing Tris(pyrazolyl)methane Ligands. Influence of Charge on Cadmium-113 NMR Chemical Shifts. *Inorg. Chem.* **1996**, *35*, 4904–4909.
- (128) Cingolani, A.; Martini, D.; Marchetti, F.; Pettinari, C.; Ricciutelli, M.; Skelton, B. W.; White, A. H. Synthesis, Spectroscopic and Structural Characterisation of Cd(II) and Zn(II) Derivatives of Tris(3,4,5-trimethylpyrazol-1-yl)methane. *Inorg. Chim. Acta* **2003**, *350*, 641–650.
- (129) Reger, D. L.; Wright, T. D.; Semeniuc, R. F.; Grattan, T. C.; Smith, M. D. Supramolecular Structures of Cadmium(II) Coordination Polymers: A New Class of Ligands Formed by Linking Tripodal Tris(pyrazolyl)methane Units. *Inorg. Chem.* **2001**, *40*, 6212–6219.
- (130) Xing, Y. H.; Aoki, K.; Bai, F. Y. Synthesis and Structure of the Mn(II) Complexes with Tripyrazolylborate Ligands: $Mn[HB(pz)_3]_2$ and $Mn[HB(3,5-Me_2-pz)_3]_2$. *Synth. React. Inorg. Met.-Org. Chem.* **2004**, *34*, 1149–1163.

- (131) Kitano, T.; Sohrin, Y.; Hata, Y.; Kawakami, H.; Hori, T.; Ueda, K. Selectivity of Sterically Efficient $[\text{HB}(\text{pz})_3]^-$ and Crowded $[\text{B}(\text{pz})_4]^-$ for First-series Transition Metals and Cd. *J. Chem. Soc., Dalton Trans.* **2001**, 3564–3571.
- (132) Kunz, K.; Bolte, M.; Lerner, H.-W.; Wagner, M. Photochemistry of Cymanthrenyl Scorpionates: Formation of a Novel Tritopic Cyclopentadienyl/Scorpionate Hybrid Ligand. *Organometallics* **2009**, 28, 3079–3087.
- (133) Wang, J.; Xu, Y.-L.; Zhou, H.-B.; Wang, H.-S.; Song, X.-J.; Song, Y.; You, X.-Z. Octacyanotungstate(V)-based Square W_2M_2 ($\text{M} = \text{Co}, \text{Mn}$) Complexes: Synthesis, Structure and Magnetic Properties. *Dalton Trans.* **2010**, 39, 3489–3494.
- (134) Han, F.; Zhang, J.; Yi, W.; Zhang, Z.; Yu, J.; Weng, L.; Zhou, X. γ -Deprotonation of Anionic Bis(trimethylsilyl)amidolanthanide Complexes with a Countered $[(\text{Tp}^{\text{Me}^2})_2\text{Ln}]^+$ Cation. *Inorg. Chem.* **2010**, 49, 2793–2798.
- (135) Yi, W.; Zhang, J.; Zhang, F.; Zhang, Y.; Chen, Z.; Zhou, X. Versatile Reactivity of Scorpionate-Anchored Yttrium – Dialkyl Complexes towards Unsaturated Substrates. *Chem. - Eur. J.* **2013**, 19, 11975–11983.
- (136) Reger, D. L.; Collins, J. E.; Rheingold, A. L.; Liable-Sands, L. M.; Yap, G. P. A. Syntheses and Characterization of Cationic (Tris(pyrazolyl)methane)silver(I) Complexes. Solid-State Structures of $\{[\text{HC}(3,5-\text{Me}_2\text{pz})_3]_2\text{Ag}\}(\text{O}_3\text{SCF}_3)$, $\{[\text{HC}(3-\text{Butpz})_3]\text{Ag}\}(\text{O}_3\text{SCF}_3)$, and $\{[\text{HC}(3-\text{Butpz})_3]\text{Ag}(\text{CNBu}^t)\}(\text{O}_3\text{SCF}_3)$. *Organometallics* **1997**, 16, 349–353.
- (137) Cingolani, A.; Effendy; Martini, D.; Pellei, M.; Pettinari, C.; Skelton, B. W.; White, A. H. Silver Derivatives of Tris(pyrazol-1-yl)methanes. A Silver(I) Nitrate Complex Containing a Tris(pyrazolyl)methane Coordinated in a Bridging Mode. *Inorg. Chim. Acta* **2002**, 328, 87–95.
- (138) Reger, D. L.; Little, C. A.; Rheingold, A. L.; Lam, M.; Concolino, T.; Mohan, A.; Long, G. J. Structural, Electronic, and Magnetic Properties of $\{\text{Fe}[\text{HC}(3,5-\text{Me}_2\text{pz})_3]\}_2(\text{BF}_4)_2$ ($\text{pz} = \text{Pyrazolyl}$): Observation of Unusual Spin-Crossover Behavior. *Inorg. Chem.* **2000**, 39, 4674–4675.
- (139) Reger, D. L.; Little, C. A.; Young, V. G., Jr; Pink, M. Variable-Temperature X-ray Structural Investigation of $\{\text{Fe}[\text{HC}(3,5-\text{Me}_2\text{pz})_3]\}_2(\text{BF}_4)_2$ ($\text{pz} = \text{Pyrazolyl Ring}$): Observation of a Thermally Induced Spin State Change from All High Spin to an Equal High Spin-Low Spin Mixture, Concomitant with the Onset of Nonmerohedral Twinning. *Inorg. Chem.* **2001**, 40, 2870–2874.
- (140) Forshaw, A. P.; Smith, J. M.; Ozarowski, A.; Krzystek, J.; Smirnov, D.; Zvyagin, S. A.; Harris, T. D.; Karunadasa, H. I.; Zadrozny, J. M.; Schnegg, A.; Holldack, K.; Jackson, T. A.; Alamiri, A.; Barnes, D. M.; Telser, J. Low-Spin Hexacoordinate Mn(III): Synthesis and Spectroscopic Investigation of Homoleptic Tris(pyrazolyl)borate and Tris(carbene)borate Complexes. *Inorg. Chem.* **2013**, 52, 144–159.
- (141) Forshaw, A. P.; Bontchev, R. P.; Smith, J. M. Oxidation of the Tris(carbene)borate Complex $\text{PhB}(\text{MeIm})_3\text{Mn}^{\text{IV}}(\text{CO})_3$ to $\text{Mn}^{\text{IV}}[\text{PhB}(\text{MeIm})_3]_2(\text{OTf})_2$. *Inorg. Chem.* **2007**, 46, 3792–3794.
- (142) Chen, F.; Wang, G.-F.; Li, Y.-Z.; Chen, X.-T.; Xue, Z.-L. Syntheses, Structures and Electrochemical Properties of Homoleptic Ruthenium(III) and Osmium(III) Complexes Bearing Two Tris(carbene)borate Ligands. *Inorg. Chem. Commun.* **2012**, 21, 88–91.
- (143) Frankel, R.; Kernbach, U.; Bakola-Christianopoulou, M.; Plaia, U.; Suter, M.; Ponikwar, W.; Noth, H.; Moinet, C.; Fehlhammer, W. P. Homoleptic Carbene Complexes: Part VIII. Hexacarbene Complexes. *J. Organomet. Chem.* **2001**, 617–618, 530–545.
- (144) Kernbach, U.; Ramm, M.; Luger, P.; Fehlhammer, W. P. A Chelating Triscarbene Ligand and Its Hexacarbene Iron Complex. *Angew. Chem., Int. Ed. Engl.* **1996**, 35, 310–312.
- (145) Arif, A. M.; Hefner, J. G.; Jones, R. A.; Whittlesey, B. R. Mononuclear Chromium Complexes of the Tripod Ligand (tripod = 1,1,1-[tris((dimethylphosphino)methyl)ethane]. *Inorg. Chem.* **1986**, 25, 1080–1084.
- (146) Suzuki, T.; Tsukuda, T.; Kiki, M.; Kaizaki, S.; Isobe, K.; Takagi, H. D.; Kashiwabara, K. Preparation, Crystal Structures and Spectroscopic Properties of Novel $[\text{M}^{\text{III}}\text{Cl}_3 - n(\text{P})_{3+n}]^{n+}$ ($\text{M} = \text{Co}, \text{Rh}; n = 0, 1, 2$ or 3) Series of Complexes Containing Tripodal Tridentate Phosphine, 1,1,1-tris(dimethylphosphinomethyl)ethane. *Inorg. Chim. Acta* **2005**, 358, 2501–2512.
- (147) Ando, T.; Kita, M.; Kashiwabara, K.; Fujita, J.; Kurachi, S.; Ohba, S. Preparation and Characterization of Cobalt(III) Complexes Containing 1,1,1-Tris(dimethylphosphinomethyl)ethane (mmtp), and the Crystal Structure of $[\text{Co}(\text{mmtp})_2][\text{Co}(\text{CN})_6] \cdot 2.25\text{H}_2\text{O}$. *Bull. Chem. Soc. Jpn.* **1992**, 65, 2748–2755.
- (148) Iwatsuki, S.; Obeyama, K.; Koshino, K.; Funahashi, S.; Kashiwabara, K.; Suzuki, T.; Takagi, H. D. New Low-spin Co(II) Complexes with Novel Tripodal 1,1,1-tris(dimethylphosphinomethyl)ethane Ligand: Electron Transfer Kinetics and Spectroscopic Characterization of $\text{Co}(\text{II})\text{P}_6$ and $\text{Co}(\text{II})\text{P}_3\text{S}_3$ Ions in Aqueous Solution. *Can. J. Chem.* **2001**, 79, 1344–1351.
- (149) Kashiwabara, K.; Ozeki, Y.; Kita, M.; Fujita, J.; Nakajima, K. Synthesis and Crystal Structure of Bis(1,1,1-tris(dimethylphosphinomethyl)ethane)iron(II) Tetrafluoroborate Dihydrate. *Bull. Chem. Soc. Jpn.* **1995**, 68, 3453–3457.
- (150) Kershaw Cook, L. J.; Mohammed, R.; Sherborne, G.; Roberts, T. D.; Alvarez, S.; Halcrow, M. Spin-state Behaviour of Iron(II)-Dipyrazolylpyridine Complexes. New Insights from Crystallographic and Solution Measurements. *Coord. Chem. Rev.* **2015**, 289–290, 2–12.
- (151) Hayami, S.; Komatsu, Y.; Shimizu, T.; Kamihata, H.; Lee, Y. H. Spin-crossover in Cobalt(II) Compounds Containing Terpyridine and its Derivatives. *Coord. Chem. Rev.* **2011**, 255, 1981–1990.
- (152) Craig, G. A.; Roubeau, O.; Aromí, G. Spin State Switching in 2,6-bis(pyrazol-3-yl)pyridine (3-bpp) Based Fe(II) Complexes. *Coord. Chem. Rev.* **2014**, 269, 13–31.
- (153) England, J.; Scarborough, C. C.; Weyhermuller, T.; Sproules, S.; Wieghardt, K. Electronic Structures of the Electron Transfer Series $[\text{M}(\text{bpy})_3]^n$, $[\text{M}(\text{tpy})_2]^n$, and $[\text{Fe}(\text{tbpy})_3]^n$ ($\text{M} = \text{Fe}, \text{Ru}; n = 3+, 2+, 1+, 0, 1-$): A Mössbauer Spectroscopic and DFT Study. *Eur. J. Inorg. Chem.* **2012**, 2012, 4605–4621.
- (154) Hu, L.; Liu, W.; Li, C.-H.; Zhou, X.-H.; Zuo, J.-L. Iron(II) Complexes Based on π -Conjugated Terpyridine Ligands with Tetrathiafulvalene or Its Radical Analogue. *Eur. J. Inorg. Chem.* **2013**, 2013, 6037–6048.
- (155) Liu, P.; Liu, Y.; Wong, E. L.-M.; Xiang, S.; Che, C.-M. Iron Oligopyridine Complexes as Efficient Catalysts for Practical Oxidation of Arenes, Alkanes, Tertiary Amines and N-acyl Cyclic Amines with Oxone. *Chem. Sci.* **2011**, 2, 2187–2195.
- (156) Dell'Amico, D. B.; Calderazzo, F.; Englert, U.; Labella, L.; Marchetti, F. The First Crystallographically Established Bis-qtpy (qtpy = 2,2':6':2":6":2"-quaterpyridine) Metal Complex. *J. Chem. Soc., Dalton Trans.* **2001**, 357–358.
- (157) Brauchli, S. Y.; Constable, E. C.; Harris, K.; Häussinger, D.; Housecroft, C. E.; Rösel, P. J.; Zampese, J. A. Towards Catenanes Using π -stacking Interactions and Their Influence on the Spin-State of a Bis(2,2':6':2"-terpyridine)iron(II) Domain. *Dalton Trans.* **2010**, 39, 10739–10748.
- (158) Constable, E. C.; Baum, G.; Bill, E.; Dyson, R.; van Eldik, R.; Fenske, D.; Kaderli, S.; Morris, D.; Neubrand, A.; Neuburger, M.; Smith, D. R.; Wieghardt, K.; Zehnder, M.; Zuberbühler, A. D. Control of Iron(II) Spin States in 2,2':6':2"-Terpyridine Complexes through Ligand Substitution. *Chem.—Eur. J.* **1999**, 5, 498–508.
- (159) Pelascini, F.; Wesolek, M.; Peruch, F.; De Cian, A.; Kyritsakas, N.; Lutz, P. J.; Kress, J. Iron Complexes of Terdentate Nitrogen Ligands: Formation and X-ray Structure of Three New Dicationic Complexes. *Polyhedron* **2004**, 23, 3193–3199.
- (160) Falceto, A.; Carmona, E.; Alvarez, S. Electronic and Structural Effects of Low Hapticity Coordination of Arene Rings to Transition Metals. *Organometallics* **2014**, 33, 6660–6668.
- (161) Kershaw Cook, L. J.; Thorp-Greenwood, F. L.; Comyn, T. P.; Cespedes, O.; Chastanet, G.; Halcrow, M. A. Unexpected Spin-Crossover and a Low-Pressure Phase Change in an Iron(II)/Dipyrazolylpyridine Complex Exhibiting a High-spin Jahn-Teller Distortion. *Inorg. Chem.* **2015**, 54, 6319–6330.
- (162) Cipressi, J.; Brown, S. N. Octahedral to Trigonal Prismatic Distortion Driven by Subjacent Orbital π Antibonding Interactions

- and Modulated by Ligand Redox Noninnocence. *Chem. Commun.* **2014**, *50*, 7956–7959.
- (163) Hills, A.; Hughes, D. L.; Leigh, G. J.; Sanders, J. R. Reactions of Vanadium(IV) Halide Complexes Containing Schiff-base Ligands with Hydrazines; Preparation and Structure of [N,N'-ethylenebis(salicylideneiminato)]bis-(phenylhydrazine)vanadium(III) Iodide. *J. Chem. Soc., Dalton Trans.* **1991**, 325–329.
- (164) Zhang, S.; Lai, L.; Shao, M.; Tang, Y. Preparation and Structure of Chloro[N,N'-ethylenebis(salicylideneiminato)]tetrahydrofuranTitanium(III). *Acta Phys.-Chim. Sin.* **1985**, *1*, 335–339.
- (165) Pasquali, M.; Marchetti, F.; Landi, A.; Floriani, C. Preparations and structures of NN'-ethylenebis(salicylideneiminato)-titanium(III) Derivatives. *J. Chem. Soc., Dalton Trans.* **1978**, 545–549.
- (166) Chen, H.; White, P. S.; Gagné, M. R. Synthesis and Reactivity of Titanium(IV)–Salen Complexes Containing Oxygen and Chloride Ligands. *Organometallics* **1998**, *17*, 5358–5366.
- (167) Seredyuk, M.; Piñeiro-López, L.; Muñoz, M. C.; Martínez-Casado, F. J.; Molnár, G.; Rodriguez-Velamazán, J. A.; Bousseksou, A.; Real, J. A. Homoleptic Iron(II) Complexes with the Ionogenic Ligand 6,6'-Bis(1H-tetrazol-5-yl)-2,2'-bipyridine: Spin Crossover Behavior in a Singular 2D Spin Crossover Coordination Polymer. *Inorg. Chem.* **2015**, *S4*, 7424–7432.
- (168) Herchel, R.; Sindelar, Z.; Travnický, Z.; Zboril, R.; Vanco, J. Novel 1D Chain Fe(III)-salen-like Complexes Involving Anionic Heterocyclic N-donor Ligands. Synthesis, X-ray Structure, Magnetic, ^{57}Fe Mössbauer, and Biological Activity Studies. *Dalton Trans.* **2009**, 9870–9880.
- (169) Guo, J.-F.; Wang, X.-T.; Wang, B.-W.; Xu, G.-C.; Gao, S.; Szeto, L.; Wong, W.-T.; Wong, W.-Y.; Lau, T.-C. One-Dimensional Ferromagnetically Coupled Bimetallic Chains Constructed with trans-[Ru(acac)₂(CN)]⁻: Syntheses, Structures, Magnetic Properties, and Density Functional Theoretical Study. *Chem. - Eur. J.* **2010**, *16*, 3524–3535.
- (170) Booysen, I. N.; Maikoo, S.; Akerman, M. P.; Xulu, B. Novel Ruthenium(II) and (III) Compounds with Multidentate Schiff Base Chelates Bearing Biologically Significant Moieties. *Polyhedron* **2014**, *79*, 250–257.
- (171) Griffith, G. A.; Al-Khatib, M. J.; Patel, K.; Singh, K.; Solan, G. A. Solid and Solution State Flexibility of Sterically Congested Bis(imino)bipyridine Complexes of Zinc(II) and Nickel(II). *Dalton Trans.* **2009**, 185–196.
- (172) Wang, Z.; Reibenspies, J.; Motekaitis, R. J.; Martell, A. E. Unusual Stabilities of 6,6'-bis(aminomethyl)-2,2'-bipyridyl Chelates of Transition-metal Ions and Crystal Structures of the Ligand and its Copper(II) and Nickel(II) Complexes. *J. Chem. Soc., Dalton Trans.* **1995**, 1511–1518.
- (173) Bonnet, S.; Molnar, G.; Sánchez Costa, J.; Siegler, M. A.; Spek, A. L.; Bousseksou, A.; Fu, W.-T.; Gamez, P.; Reedijk, J. Influence of Sample Preparation, Temperature, Light, and Pressure on the Two-Step Spin Crossover Mononuclear Compound [Fe(bapbpy)(NCS)₂]. *Chem. Mater.* **2009**, *21*, 1123–1136.
- (174) Bonnet, S.; Siegler, M. A.; Costa, J. S.; Molnar, G.; Bousseksou, A.; Spek, A. L.; Gamez, P.; Reedijk, J. A Two-step Spin Crossover Mononuclear Iron(II) Complex with a [HS–LS–LS] Intermediate Phase. *Chem. Commun.* **2008**, 5619–5621.
- (175) Arcis-Castillo, Z.; Zheng, S.; Siegler, M. A.; Roubeau, O.; Bedoui, S.; Bonnet, S. Tuning the Transition Temperature and Cooperativity of bapbpy-Based Mononuclear Spin-Crossover Compounds: Interplay between Molecular and Crystal Engineering. *Chem. - Eur. J.* **2011**, *17*, 14826–14836.
- (176) Krüger, H.-J. Spin Transition in Octahedral Metal Complexes Containing Tetrazamacrocyclic Ligands. *Coord. Chem. Rev.* **2009**, 253, 2450–2459.
- (177) Buffet, J.-C.; Okuda, J. Scandium Alkyl and Amide Complexes containing a Cyclen-derived (NNNN) Macroyclic Ligand: Synthesis, Structure and Ring-opening Polymerization Activity Toward Lactide Monomers. *Dalton Trans.* **2011**, *40*, 7748–7754.
- (178) Ohashi, M.; Konkol, M.; Del Rosal, I.; Poteau, R.; Maron, L.; Okuda, J. Rare-Earth Metal Alkyl and Hydride Complexes Stabilized by a Cyclen-Derived [NNNN] Macroyclic Ancillary Ligand. *J. Am. Chem. Soc.* **2008**, *130*, 6920–6921.
- (179) Yokoyama, A.; Han, J. E.; Cho, J.; Kubo, M.; Ogura, T.; Siegler, M. A.; Karlin, K. D.; Nam, W. Chromium(IV)–Peroxo Complex Formation and Its Nitric Oxide Dioxygenase Reactivity. *J. Am. Chem. Soc.* **2012**, *134*, 15269–15272.
- (180) Hazari, S. K.; Roy, T. G.; Dey, B. K.; Das, S. C.; Tiekkink, E. R. T. Synthesis, Characterisation and Antifungal Activities of Some New Copper(II) Complexes of Isomeric 3,5,7,7,10,12,14,14-Octamethyl-1,4,8,11-Tetraazacyclotetradecanes. *Met.-Based Drugs* **1997**, *4*, 255–265.
- (181) Sen, R.; Bhattacharya, A.; Mal, D.; Bhattacharjee, A.; Gütlich, P.; Mukherjee, A. K.; Solzi, M.; Pernechele, C.; Koner, S. A Cyanobridged Bimetallic Ferrimagnet: Synthesis, X-ray Structure and Magnetic Study. *Polyhedron* **2010**, *29*, 2762–2768.
- (182) Koningsbruggen, P. J. v.; Maeda, Y.; Oshio, H. Iron(III) Spin Crossover Compounds. In *Topics in Current Chemistry*; Gütlich, P., Goodwin, H. A., Eds.; Springer: Berlin/Heidelberg, **2004**; Vol. 233, pp 259–324.10.1007/b95409
- (183) Tanimura, K.; Kitashima, R.; Bréfuel, N.; Nakamura, N.; Matsumoto, N.; Shova, S.; Tuchagues, J.-P. Infinite Chain Structure and Steep Spin Crossover of a Fe^{III} Complex with a N₃O₂ Pentadentate Schiff-Base Ligand and 4-Aminopyridine. *Bull. Chem. Soc. Jpn.* **2005**, *78*, 1279–1282.
- (184) Imatomi, S.; Sato, T.; Hamamatsu, T.; Kitashima, R.; Matsumoto, N. Spin-Crossover Behavior of Isomorphous Bi- and Mononuclear Iron(III) Complexes. *Bull. Chem. Soc. Jpn.* **2007**, *80*, 2375–2377.
- (185) Lloris, J. M.; Martínez-Máñez, R.; Pardo, T.; Soto, J.; Padilla-Tosta, M. E. Binding, Electrochemical and Metal Extraction Properties of the New Redox-active Polyazacycloalkane 1,4,7,10,13,16-hexa(ferroenylmethyl)-1,4,7,10,13,16-hexaaazacyclooctadecane. *J. Chem. Soc., Dalton Trans.* **1998**, 2635–2642.
- (186) Assey, G.; Butcher, R. J.; Gultneh, Y.; Yisgedu, T. [2,2'-(2,6,9,13-Tetraazatetradecane-1,14-diyl)diphenolato]iron(III) Iodide. *Acta Crystallogr., Sect. E: Struct. Rep. Online* **2010**, *66*, m711–m712.
- (187) Arulsamy, N.; Glerup, J.; Hodgson, D. J. Mononuclear Iron(II), Manganese(II), and Nickel(II) and Tetrานuclear Iron(III) Complexes of a New Hexadentate Ligand. *Inorg. Chem.* **1994**, *33*, 3043–3050.
- (188) Zhang, H.-X.; Zheng, S.-T.; Yang, G.-Y. Pentaethylenehexaminemanganese(II) Pentaborate. *Acta Crystallogr., Sect. C: Cryst. Struct. Commun.* **2004**, *60*, m241–m243.
- (189) Xu, G.-H.; Wang, C.; Guo, P. Poly[(pentaethylenehexamine)-manganese(II)] [hepta- μ -selenido-tritin(IV)]: a Tin-selenium Net with Remarkable Flexibility. *Acta Crystallogr., Sect. C: Cryst. Struct. Commun.* **2009**, *65*, m171–m173.
- (190) Butcher, R. J.; Pourian, M.; Jasinski, J. P. {1,4-Bis[3-(3-methoxy-2-oxidobenzylideneamino)propyl]piperazine}iron(III) Tetrafluoridoborate. *Acta Crystallogr., Sect. E: Struct. Rep. Online* **2007**, *63*, m1913–m1914.
- (191) Bera, M.; Mukhopadhyay, U.; Ray, D. Iron(III) induced 2-phenyl Imidazolidine Ring Hydrolysis of a New Binucleating Schiff Base Ligand: X-Ray Structure of the Mononuclear Fe^{III}(NNO)₂ End Product. *Inorg. Chim. Acta* **2005**, *358*, 437–443.
- (192) Clemente-León, M.; Coronado, E.; López-Jordá, M. 2D and 3D Bimetallic Oxalate-based Ferromagnets Prepared by Insertion of Different Fe^{III} Spin Crossover Complexes. *Dalton Trans.* **2010**, *39*, 4903–4910.
- (193) Mondal, S.; Adak, P.; Das, C.; Naskar, S.; Pakhira, B.; Rheingold, A. L.; Sinn, E.; Eribal, C. S.; Chattopadhyay, S. K. Synthesis, X-ray Crystal Structures, Spectroscopic and Electrochemical Studies of Zn(II), Cd(II), Ni(II) and Mn(II) Complexes of N¹,N⁴-bis(pyridoxylidene)triethylenetetramine. *Polyhedron* **2014**, *81*, 428–435.
- (194) Sarkar, S.; Biswas, S.; Liao, M.-S.; Kar, T.; Aydogdu, Y.; Dagdelen, F.; Mostafa, G.; Chattopadhyay, A. P.; Yap, G. P. A.; Xie, R.-H.; Khan, A. T.; Dey, K. An Attempt Towards Coordination Supramoleculararity from Mn(II), Ni(II) and Cd(II) with a New

Hexadentate $[N_4O_2]$ Symmetrical Schiff Base Ligand: Syntheses, Crystal Structures, Electrical Conductivity and Optical Properties. *Polyhedron* **2008**, *27*, 3359–3370.

(195) Lin, H.-J.; Siretanu, D.; Dickie, D. A.; Subedi, D.; Scepaniak, J. J.; Mitcov, D.; Clérac, R.; Smith, J. M. Steric and Electronic Control of the Spin State in Three-Fold Symmetric, Four-Coordinate Iron(II) Complexes. *J. Am. Chem. Soc.* **2014**, *136*, 13326–13332.

(196) Nieto, I.; Cervantes-Lee, F.; Smith, J. M. A new synthetic route to bulky “second generation” tris(imidazol-2-ylidene)borate ligands: synthesis of a four coordinate iron(II) complex. *Chem. Commun.* **2005**, 3811–3813.

(197) Cowley, R. E.; Bontchev, R. P.; Sorrell, J.; Sarracino, O.; Feng, Y.; Wang, H.; Smith, J. M. Formation of a Cobalt(III) Imido from a Cobalt(II) Amido Complex. Evidence for Proton-Coupled Electron Transfer. *J. Am. Chem. Soc.* **2007**, *129*, 2424–2425.

(198) Cho, J.; Yap, G. P. A.; Riordan, C. G. Structural, Spectroscopic, and Electrochemical Properties of a Series of High-Spin Thiolatonicke(II) Complexes. *Inorg. Chem.* **2007**, *46*, 11308–11315.

(199) DuPont, J. A.; Yap, G. P. A.; Riordan, C. G. Influence of Ligand Electronic Effects on the Structure of Monovalent Cobalt Complexes. *Inorg. Chem.* **2008**, *47*, 10700–10707.

(200) Camalli, M.; Caruso, F. P NMR Study on the Ag(triphos)X Series (triphos = 1,1,1-tris(diphenylphosphinomethyl)ethane, X = anion). Crystal and Molecular Structure of Ag(triphos)I. *Inorg. Chim. Acta* **1990**, *169*, 189–194.

(201) Alvarez, S.; Avnir, D. Continuous Chirality Measures of Tetracoordinate Bis-chelate Metal Complexes. *Dalton Trans.* **2003**, 562–569.

(202) Hall, J. D.; McLean, T. M.; Smalley, S. J.; Waterland, M.; Telfer, S. G. Chromophoric Dipyrrin Complexes Capable of Binding to TiO₂: Synthesis, Structure and Spectroscopy. *Dalton Trans.* **2010**, *39*, 437–445.

(203) Pogozhev, D.; Baudron, S. A.; Hosseini, M. W. Combination of Hydrogen and Coordination Bonding for the Construction of One-dimensional Networks Based on a 7-azaindole Appended Dipyrrin. *CrystEngComm* **2010**, *12*, 2238–2244.

(204) Béziau, A.; Baudron, S. A.; Fluck, A.; Hosseini, M. W. From Sequential to One-Pot Synthesis of Dipyrrin Based Grid-Type Mixed Metal–Organic Frameworks. *Inorg. Chem.* **2013**, *52*, 14439–14448.

(205) March, F. C.; Couch, D. A.; Emerson, K.; Ferguson, J. E.; Robinson, W. T. Dipyrrromethene Complexes of Transition Metals. Part II. Stereochemistry of Complexes of Cobalt(II), Nickel(II), Copper(II), Zinc(II), Cadmium(II), Mercury(II), and Palladium(II) and Crystal Structure Analysis of the Palladium Complex. *J. Chem. Soc. A* **1971**, 440–448.

(206) Kido, H.; Shin, J.-Y.; Shinokubo, H. Selective Synthesis of a [32]Octaphyrin(1.0.1.0.1.0.1.0) Bis(palladium) Complex by a Metal-Templated Strategy. *Angew. Chem., Int. Ed.* **2013**, *52*, 13727–13730.

(207) Béziau, A.; Baudron, S. A.; Guenet, A.; Hosseini, M. W. Luminescent Coordination Polymers Based on Self-Assembled Cadmium Dipyrrin Complexes. *Chem.—Eur. J.* **2013**, *19*, 3215–3223.

(208) Irrgang, T.; Schareina, T.; Kempe, R. The Development of an Enantioselective Nickel Hydrosilylation Catalyst System via Multi-substrate Screening. *J. Mol. Catal. A: Chem.* **2006**, *257*, 48–52.

(209) Edwards, A. J.; Retboll, M.; Wenger, E. The Tetrahedral Tetrakis(phosphine) Complex [bis(diphenylphosphino)butane- κ P,P]-nickel(0)-benzene (1/2.5). *Acta Crystallogr., Sect. E: Struct. Rep. Online* **2002**, *58*, m375–m377.

(210) Fischer, R. A.; Langer, J.; Malassa, A.; Walther, D.; Gorls, H.; Vaughan, G. A Key Step in the Formation of Acrylic Acid from CO₂ and Ethylene: The Transformation of a Nickelalactone into a Nickel-acrylate Complex. *Chem. Commun.* **2006**, 2510–2512.

(211) Anderson, M. P.; Pignolet, L. H. Rhodium Complexes of 1,4-Bis(diphenylphosphino)butane. Crystal and Molecular Structures of $[Rh(dppb)_2]BF_4 \cdot C_4H_{10}O$ and $[Rh(cod)(dppb)]BF_4$. *Inorg. Chem.* **1981**, *20*, 4101–4107.

(212) Allen, F. H. The Cambridge Structural Database: A Quarter of a Million Crystal Structures and Rising. *Acta Crystallogr., Sect. B: Struct. Sci.* **2002**, *58*, 380–388.